THE UNIVERSITY OF CALGARY

Investigation of Rag Layers from Oil Sands Froth

by

Mehrrad Saadatmand

A THESIS

SUBMITTED TO THE FACULTY OF GRADUATE STUDIES

IN PARTIAL FULFILMENT OF THE REQUIREMENTS FOR THE

DEGREE OF MASTER OF SCIENCE IN ENGINEERING

DEPARTMENT OF CHEMICAL AND PETROLEUM ENGINEERING

CALGARY, ALBERTA

January, 2008

UNIVERSITY OF CALGARY

FACULTY OF GRADUATE STUDIES

The underdesigned certify that they have read and recommend to the faculty of Graduate Studies for acceptance a thesis entitled “Investigation of Rag Layers from Oil Sands Froth” submitted by Mehrrad Saadatmand in partial fulfillment of the requirement for the degree of Master of Science in Chemical Engineering.

_____

Dr. H.W.Yarranton, Supervisor
Department of Chemical and Petroleum Engineering

_____

Dr. B. Maini
Department of Chemical and Petroleum Engineering

_____

Dr. W.Y. Svrcek
Department of Chemical and Petroleum Engineering

_____

Dr. W. Shaw
Department of Mechanical and Manufacturing Engineering

_____

Date

Abstract

During the settling stages in some oil sands froth treatments, a rag layer (an undesirable mixture of dispersed oil, water and solids) can form at the water-oil interface. If the rag layer expands, water and solids may contaminate the produced oil and/or oil may be lost to the tailings stream. The objective of this thesis is to identify the mechanisms that lead to rag layer formation and to assess the effect of processing conditions on the rag layer.

Oil sand froths were diluted with mixtures of toluene and heptane and the diluted froths were centrifuged in steps of increasing rpm. The volumes of oil phase, rag layer, free water, and sediment were measured after each step. The force required to break the rag layers provided a measure of the relative strength of them. The data obtained from the experiments was used for material balances to determine the composition of the rag layers. Samples of the rag layer materials have also been tested to determine the size and properties of the rag layer solids. The possible mechanisms of rag formation were investigated through a series of experiments.

Three mechanisms appear to influence rag layer formation. At low centrifuge force and residence time, the rag layer volume depends on the hindered settling rate. Above 1500 rpm, a more compact rag layer forms and its volume appears to be controlled by the rate of water droplet coalescence. By 6000 rpm, most of the water is resolved and the rag layer consists primarily of fine solids. These solids are fine intermediate to oil-wet solids that do not readily pass through the water-oil interface.

The main process factors affecting rag formation appear to be the oil sand quality, the type of diluent, and the asphaltene precipitation. The higher quality oil sand produced much smaller rag layers. Also the initial rag layer volume in the aromatic solvent was larger than in the paraffinic solvents. The final volumes were similar in all solvents. Asphaltene precipitation significantly increased the initial rag layer volume but decreased the final volume.

Acknowledgements

I would like to express my sincere gratitude and thanks to my supervisor, Dr. Harvey W. Yarranton, for his continious support, encouragement and guidance throughout this research.

I am thankful to all members of the asphaltene research group for their cooperation and help during the course of this project, and also all my friends who have contributed in some way to this thesis. Elaine Baydak's help throughout this research was of great value and is appreciated.

I am also grateful to the Department of Chemical and Petroleum Engineering, the Department of Graduate Studies, Syncrude Canada Ltd., DBR-Schlumberger, Royal Dutch Shell, and Petrobras for financial support through my Masters program.

Finally, I would like to express my sincere thanks to my parents for their encouagement and understanding.

Dedicated to my Parents

Table of Contents

List of Tables

List of Figures

List of Symbols

a	Particle acceleration
C_D	Drag coefficient
d	Diameter of a spherical particle
D	Diameter of the settling vessel
d_p	Droplet/particle diameter
d_s	Particle diameter
g	Gravity acceleration
n	Richardson-Zaki's coefficient
n	Number of repeat measurements
P	Pressure
r	Radius of path of particle
Re	Reynolds Number
s	Standard deviation
T	Temperature
t	t-distribution
u	Hindered settling rate
u_0	Free settling rate of the aggregates
u_t	Terminal velocity
v_f	Fluid velocity
v_s	Velocity of the particles
v_t	Terminal velocity of a single particle in an infinite medium
x_i	Measured value

Greek Symbols

α_f	Volume fraction of fluid or suspension voidage
γ_C	Critical surface tension of wetting
γ_{LV}	Surface tension between liquid and vapor
γ_{SL}	Surface tension between solid and liquid
γ_{SV}	Surface tension between solid and vapor
θ	Contact angle
μ	Viscosity
ρ	Density
ω	Angular velocity

Subscripts

f	Fluid
i	i^{th} particle species in the suspension
m	Medium
p	Droplet or particle
s	Solids or particles
susp	Suspension

Chapter 1

Introduction

Although recent technological progress has increased conventional oil production, since 1985 less conventional oil has been discovered than has been consumed (Wells, 2005). This fact strongly suggests a need to focus more on alternative oil sources, such as oil sands. The Canadian oil sands resource of 1.7 trillion barrels is the world's largest single petroleum resource (Alberta's Energy Reserves 2006 and Supply/Demand Outlook 2007-2016, 2007). The recoverable reserves in the Athabasca oil sands are approximately 175 billion barrels (Scales, 2007). However, this resource is energy and water intensive and there is a constant effort to optimize existing oil sands processes and to develop new and more efficient processes.

Oil sand is a dark viscous mixture of bitumen, sand, clays, water, and some natural surfactants, Figure 1.1. It has a loose structure and can be broken easily into small clumps. The only industrial process for the separation of bitumen from oil sands is the Clark hot water extraction process, Figure 1.2. In the most recent version of the hot water extraction process, oil sand is first introduced into a hydrotransport line. At the mine site, oil sand is mixed with a 1:4 mass ratio of water-to-oil sand at approximately 80°C and the slurry is then pipelined to the extraction and upgrading plant site. Sodium hydroxide and steam are at times added to the system hot water. During hydrotransport, the hot water and sodium hydroxide liberate some natural surfactants and begin the process of separating bitumen from the sand grains.

At the plant site, oversized stones are removed by wet screening. After mixing with more hot water, the slurry is fed to the primary separation vessel. The additional hot water brings the water-to-oil sand ratio to approximately 1:1. In the primary separation vessel, the bitumen completely separates from the sand grains. However, the density of the bitumen is almost the same as the surrounding water and it will not separate from the

water. Therefore, the vessel is aerated so that the bitumen droplets attach to the air bubbles, float to the surface, and form a froth (the primary froth). The coarse solids settle to the bottom of the separation vessel and rest of the mixture is removed as a 'middlings' stream which is sent to sub aeration cells to produce a secondary froth (Schramm and Smith, 1989).

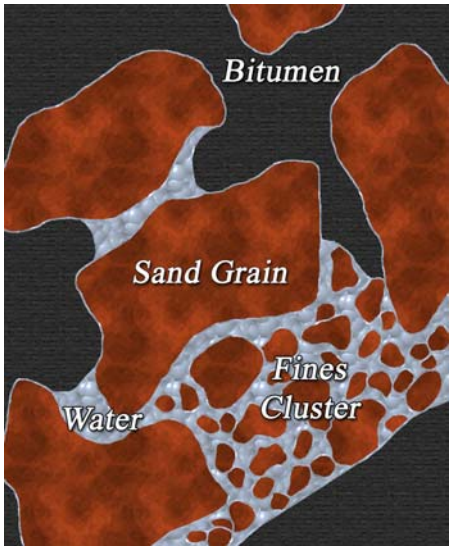

Figure 1.1 Illustration of the arrangement of bitumen, water, sand, and fine minerals in a typical sample of Athabasca oil sand (Hepler, 1994).

The product of the hot water process is the combined primary and secondary froth, which is a mixture of bitumen, water, fine solids, and natural surfactants. The froth must be further treated to separate the bitumen. In the Syncrude and Suncor processes, the froth is diluted with naphtha to reduce the density and viscosity of the continuous oil phase and then centrifuged to accelerate the separation. In the Albian process, the froth is diluted with a paraffinic solvent and separated with gravity settling. The product of froth treatment is diluted bitumen which is sent to upgrading for solvent recovery and bitumen separation.

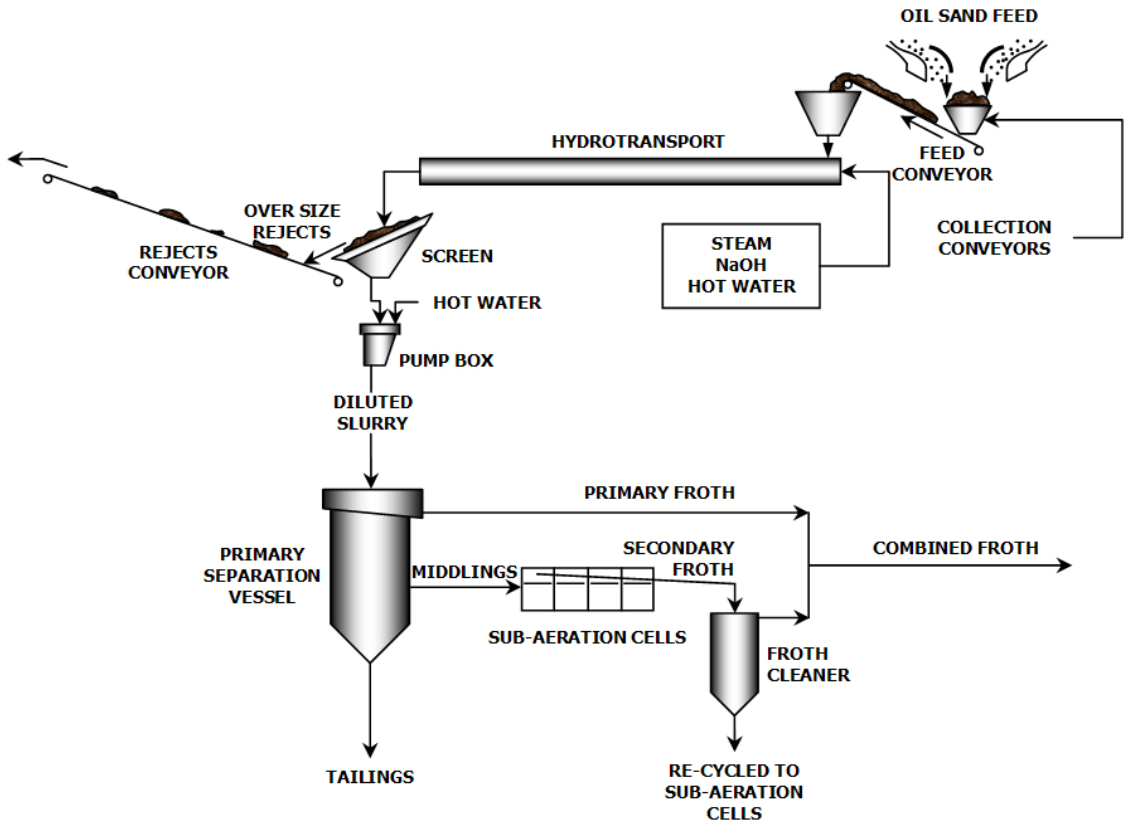

Figure 1.2 Simplified process sequence of hot water extraction process (Schramm and Smith, 1989).

One issue in froth treatment is the build up of material at the water-oil interface. This layer of "rag" material typically consists of water droplets and solids suspended in a continuous oil phase. In poor processing conditions, this rag layer can grow thick enough to overflow into the oil or water outlet streams. If the rag material enters the oil stream, it introduces water and fine solids which may cause corrosion and fouling in downstream processes. If it enters the water stream, some oil is lost to the water stream, reducing oil recovery or necessitating further treatment. Note, the same problems can occur in conventional and heavy oil separation processes.

The mechanisms that determine rag layer build up are not yet well understood. Consequently, the response of rag layers to changes in process conditions or chemical

additives is at times unpredictable. Since rag layers can ultimately shut down a process, there is an incentive to determine the factors that control rag layer growth.

1.1 Objectives

There are two main objectives to this research:

1. To understand the mechanisms that cause the rag layer to grow in oil sands froth treatment.
2. To understand how operating conditions and oil sand quality affect rag layer formation. In other words, to analyze some of the factors that may contribute to rag layer formation.

1.2 Thesis Structure

This thesis is comprised of seven more chapters.

- Chapter 2 is a review of bitumen extraction and froth treatment processes. The roles of asphaltenes, clays and natural surfactants such as naphthenic acids in the bitumen recovery process are discussed. Possible mechanisms of rag layer formation are reviewed.
- In Chapter 3, the experimental methods are detailed, including the materials used in the experiments, and the experimental methods themselves, extraction, step-wise centrifuge settling tests, microscopy, and size distribution measurements.
- In Chapter 4, a computer model of the hindered settling of mixtures of particles is outlined. The model was developed to aid in the interpretation of the step-wise settling tests.
- In Chapter 5, the rag layer composition is explained. Some properties of these compositions are also discussed.
- In Chapter 6, the mechanisms causing rag layer formation are discussed. The model of Chapter 4 is used here to explain some of the results.
- Chapter 7 summaries the experimental results of operating conditions, choice of diluent, and oil sands quality on rag layer formation.
- In Chapter 8, conclusions and recommendations are presented.

Chapter 2

Literature Review

In this chapter, oil sand composition, extraction and froth treatment are reviewed. Rag layers in general and in froth treatment are discussed. Possible mechanisms for rag layer accumulation, including hindered settling, slow coalescence, and oil-wet solids accumulation, are examined in more detail.

2.1 Oil Sands Composition

Oilsands are complex mixtures of sand, fine clays, connate water and bitumen (Dai and Chung, 1996). In Canada, oil sand is surface mined mainly in the Athabasca area in Alberta. The Athabasca oil sand deposits consist of approximately 83 wt% sands (including fine solids), 13 wt% bitumen and 4 wt% water (Peach, 1974). The quality of the oil sand deposit varies widely. The highest grade of Athabasca oil sand contains approximately 18 wt% bitumen and 2 wt% water. A rich oil sand has more than 10 wt% bitumen, a moderate oil sand has between 6 to 10 wt% bitumen, and every oil sand with lower than 6 wt% bitumen is considered lean (Takamura, 1982). Figure 2.1 shows an oil sand sample.

Figure 2.1 An oil sand sample

The mineral composition of Athabasca oil sand is approximately 90% quartz with minor amounts of potash feldspar, chert, muscovite, and the rest of the minerals are clays. Clays in oil sands are mostly kaolinite, illite, and montmorillonite. Montmorillonite only appears in the fines fraction which is defined as particles smaller than 44 μm in diameter (Takamura, 1982; Schramm, 1989).

Figure 2.2 shows a structural model of Athabasca oil sand (Hepler, 1994). In this model, water appears in three forms: as pendular rings at grain-to-grain contact points, as a roughly 10 nm thick film on the sand surfaces, and as water retained in fine clusters. The thin water film covers about 70% of the sand surface and pendular rings cover the rest of it. This water layer is stable because of the double layer repulsive forces acting between the sand and the bitumen surface. The clay minerals in the oil sands are also believed to be covered by the thin water film (Takamura, 1982). However, there is also evidence that the clays have adsorbed hydrocarbons and may be of mixed wettability (Kotlyar *et al*., 1998).

In lower grade oil sands, clusters of fine particles exist within the oil sand matrix. These fine clusters are saturated with water. Thus the amount of connate water in oil sands increases approximately linearly with increasing fines content. Fine clusters can form from either aggregates of small sand grains or booklets of clay minerals (Takamura, 1982).

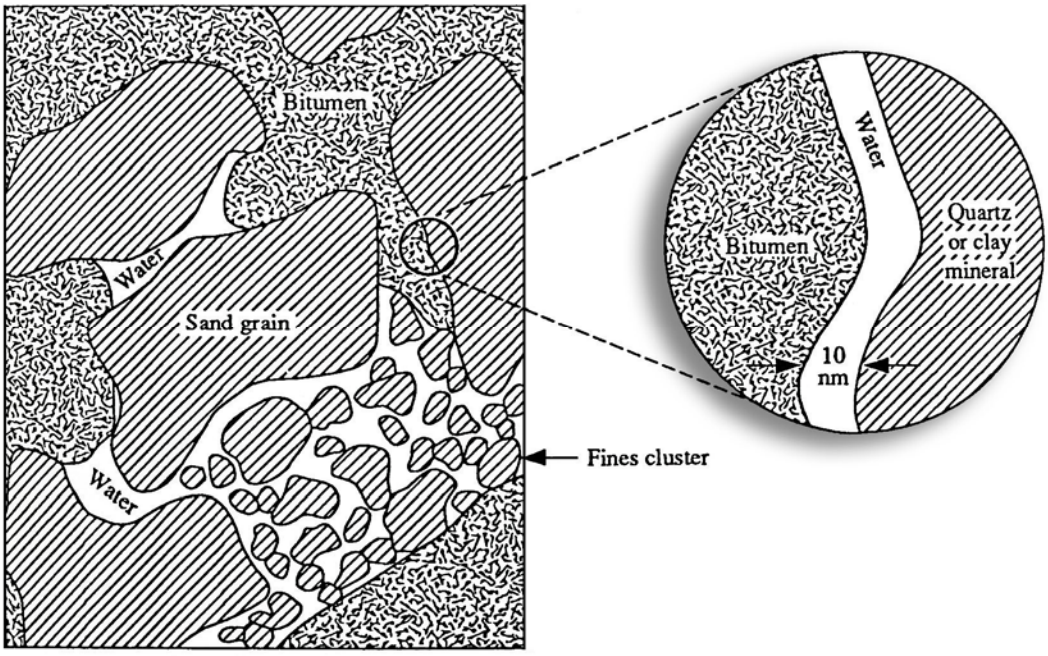

Figure 2.2 Structure of oil sands matrix (Hepler, 1994)

2.2. Bitumen Extraction from Oilsands

Among several processes developed for bitumen extraction from oil sands, the only large scale industrial process is hot water extraction process. The objective of the hot water extraction process is to separate bitumen in oil sands from the water and solids. The hot water extraction process was originally developed by Clark *et al.* (1932) for Athabasca oil sands. Syncrude, Suncor, and Albian Sands are using this process with some modifications.

Figure 1.2 shows one example of a simplified continuous hot water extraction process. The mined oil sand is screened to remove large rocks, mixed with hot water and steam and fed to a hydrotransport system. The mixture forms a slurry of some 7% bitumen and 70% solids. In the pipeline, the water forms an annulus which minimizes drag and allows transport of the oil sand slurry. The oil sand is also conditioned in the pipeline. Natural surfactants are liberated which aid in separating bitumen from the sand grains. Sometimes, sodium hydroxide is added to poorly processing oil sands to aid in the liberation of the surfactants (Schramm and Smith, 1989).

At the outlet of the pipeline, the slurry undergoes more screening to remove rocks and lumps of unconditioned oil sand. After diluting the slurry with more hot water, it is fed to a floatation vessel, the 'primary separation vessel'. The vessel contents are held under nearly quiescent conditions. Here, the bitumen completely separates from the sand grains. However, since its density is very close to water, it will not separate from the water medium. Therefore, the vessel is aerated so that bitumen droplets can attach to the air bubbles and float on the surface. At the same time coarse sands settle to the bottom of the vessel.

The bitumen froth is skimmed from the top of the vessel (primary froth), while the sand slurry is also withdrawn from the bottom (tailings). In the middle part of the separation vessel, there is always a hold-up of bitumen droplets and fine solids. The middlings stream is drawn off from this region and is fed to secondary floatation (Schramm, 1989).

The product of hot water extraction process is a combined froth which is a mixture of bitumen, water, fine solids, natural surfactants, and sometimes sodium hydroxide. The froth must be further treated to separate the bitumen. In the Syncrude and Suncor processes, the froth is diluted with naphtha to reduce the density and viscosity of the continuous oil phase and centrifuged to accelerate the separation. In the Albian process, the froth is diluted with a paraffinic solvent and separated with gravity settling. Froth treatment is discussed in Section 2.3.

2.2.1 Bitumen Liberation from Sand Grains

The key to bitumen extraction is bitumen liberation from sand grains in the hot water extraction process. Bitumen liberation involves several steps as shown in Figure 2.3.

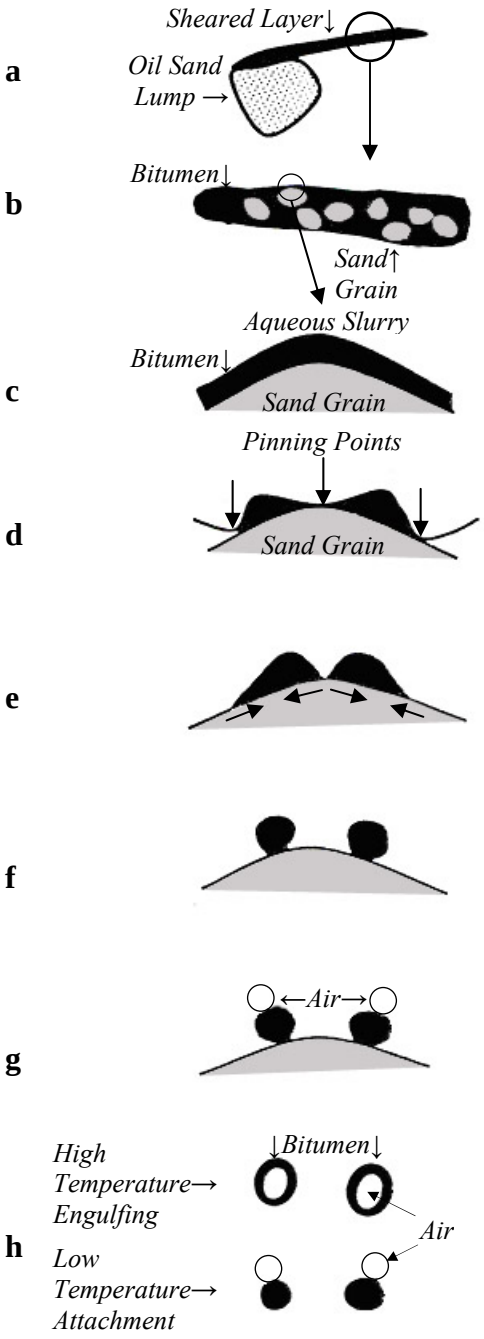

Figure 2.3 Bitumen liberation steps (Adopted from Masliyah *et al*., 2004)

Bitumen acts as a glue that holds a lump of oil sand together. Upon mixing oil sand lumps with hot water, their outer layer is heated and the bitumen viscosity is reduced. If the hot oil sand lump is exposed to turbulent conditions, the outer layer is sheared off. Fresh surface is then exposed to the warm water environment (Figure 2.3 a and b) and the same process is repeated until the whole lump is melted and separated (Masliyah *et al*., 2004).

Following the lump size reduction step, bitumen is liberated from exposed sand grains. This liberation involves bitumen thinning at the sand grain surface (Figure 2.3 c), followed by formation of pin holes in the bitumen layer coating the sand surface (Figure 2.3 d), bitumen recession on the sand grain (Figure 2.3 e), and finally formation of bitumen droplets (Figure 2.3 f). Bitumen droplets at this step attach to the air bubbles (Figure 2.3 g and h). These steps may occur in sequence or simultaneously (Masliyah *et al*., 2004).

Role of Surfactants in Bitumen Liberation from Oil Sands:

Sanford and Seyer (1979) studied the natural surfactants which are present in bitumen, and showed that they are the primary agents responsible for improved bitumen recovery. They also showed that NaOH, which is used as a process aid for some oil sands, reacts with components of bitumen to form these surfactants. Bowman and co-workers (1968, 1969, and 1976) showed that the surfactants active in the hot water extraction process are primarily water soluble salts of naphthenic acids having carboxylic functional groups (Schramm *et al*., 1984), Figure 2.4.

The carboxylate surfactants which are generated in hot water extraction process play a critical role in the maximum oil recovery. There is a single equilibrium concentration of carboxylate surfactant which leads to maximum oil recovery for all grades of oil sands irrespective of contamination or aging (Schramm *et al*., 1984). Below this optimum concentration, some of the bitumen is not recovered due to incomplete sand detachment from aerated bitumen droplets. At concentrations above the optimum value, the formation of micro sized oil-in-water emulsions in the middling phase results in poor bitumen-water

separation. It has been reported that at extremely high concentrations of surfactant, all of the bitumen emulsifies in the middling phase which results in zero oil recovery (Dai and Chung, 1996). This concentration is about 0.12 meq/L of carboxylate surfactant and is termed the 'critical concentration' (Hepler, 1994).

The carboxylic surfactants are at times available in the structure of oil sand, but in many cases they are produced in the hot water process by the reaction of added sodium hydroxide with naturally present acids in the bitumen (Schramm *et al*., 1984). Generally, rich oil sands already possess the critical concentration of carboxylate surfactant; hence do not require the addition of sodium hydroxide. Average grade oil sands require 0.02 to 0.04 wt% sodium hydroxide to produce the critical concentration, and low grade oil sands might need from 0.04 to 0.20 wt% sodium hydroxide (Hepler, 1994).

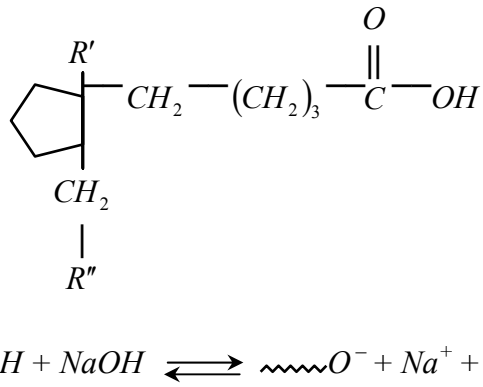

Figure 2.4 Simplified representation of the structure of the naphthenic acids and their conversion to surface active sodium salts in the hot water process (Adopted from Schramm *et al*., 1984).

Role of Fine Clays in Bitumen Liberation from Oil Sands:

Clay minerals such as montmorillonite and kaolinite present in oil sands can adversely affect bitumen liberation from oil sands (Liu *et al*., 2004). Montmorillonite clays have a plate-like structure which has unique properties such as a high specific surface area, interlayer swelling, and a large adsorption capacity for ions from a solution. Kaolinite, in contrast, is a non-expanding layer structured clay mineral, and it does not have room for

interlayer cations; a result, kaolinite swells little in water and its cation exchange capacity is low (Liu *et al*., 2004).

The adverse effect of montmorillonite on bitumen recovery is exacerbated by calcium ions. Montmorillonite clay particles attach weakly to the bitumen surface in the absence of calcium ions. However, in the presence of calcium ions, the adhesion force of montmorillonite clay particles to the bitumen surface increases dramatically. This is primarily due to dual adsorption of calcium ions both on the montmorillonite clay and the bitumen surface, which causes bridging between bitumen and montmorillonite clay particles. This process results in a slime coating of montmorillonite clay particles on the bitumen surface, which is a barrier for bitumen-air attachment and bitumen-bitumen coagulation, which leads to poor bitumen recovery (Liu *et al*., 2004).

The adhesion force between bitumen and kaolinite is considerably lower than the force between bitumen and montmorillonite. Moreover, calcium ions can not enhance the forces between bitumen and kaolinite clay. Therefore, the attachment of kaolinite clays to bitumen surface is weak compared to montmorillonite clays (Liu *et al*., 2004).

Since low quality ores usually have an abundance of fine clays and divalent cations concentration in the process water, the fines content combined with cations can reduce the processibility of these oil sands and their bitumen production (Liu *et al*., 2004). These fines are also carried to the froth and can impact froth treatment performance.

2.2.2 Oil Sand Aging

For a long time it has been known that the processing curves (plots of bitumen recovery versus weight percent of sodium hydroxide) change as oil sands are stored in the presence of air. This phenomenon has been termed ‘aging’. Aging increases the amount of sodium hydroxide needed to obtain maximum recovery, and also decreases the maximum recovery (Hepler, 1994).

Several mechanisms have been proposed in the literature to explain the oil sand aging. Among them, one which is widely accepted is proposed by Schramm and Smith (1987b). Based on their work the aging effect is a strong function of storage conditions. These conditions are sample size, sample environment and storage time. They suggest that during aging, reactions occur that either affect the source of carboxylic surfactant or produce chemical species which consume sodium hydroxide in the hot water extraction process. This results an increase in the amount of sodium hydroxide needed to achieve the critical concentration of carboxylate surfactant (Schramm and Smith, 1987a).

The aging mechanism of the oil sands involves mineral oxidations, specifically pyrite. These oxidations start by the exposure of oil sand to a higher potential partial pressure of oxygen which occurs during mixing of the oil sand from the deposit. These oxidations are possibly assisted by micro organisms. The suggested reactions result in the generation of polyvalent metal species, which can reduce the bitumen produced from the oil sand in two ways. They can either react with sodium hydroxide during the hot water extraction process and prevent the reaction that produces carboxylate surfactants, or they can react with carboxylate surfactants directly and immobilize them (Schramm and Smith, 1987b).

To reduce the effects of aging, Schramm and Smith (1987a) suggest storing the oil sand samples in “fairly large samples (20kg) in sealed, inert, gas-tight, full containers at low temperatures (-30 °C) in a carbon dioxide atmosphere”.

2.3 Froth Treatment

The froth skimmed from the top of the settler vessel in the hot water extraction process is a mixture of approximately 60 to 65 wt% bitumen, 28 to 34 wt% water, and 6 to 7 wt% solids (Hepler, 1994). There are two continuous phases in the froth: an aqueous phase with dispersed droplets of bitumen; and a bitumen phase which is aerated and contains dispersed water droplets. The bitumen droplets are small and remain in the aqueous phase probably because their surface is covered by a small amount of bi-wetted material that prevents coalescence with other bitumen droplets (Shelfantook, 2004). This part of

bitumen in froth accounts for less than one percent of the oil in the froth. The emulsified water present in the froth introduces impurities into bitumen. These impurities are typically dissolved salts and suspended solid particles which cause problems during froth treatment (Shelfantook, 2004). The dissolved salts contribute to corrosion in downstream distillation columns unless the water is removed from the bitumen.

The purpose of froth treatment is to separate bitumen from the water and solids in the froth. Bitumen has almost the same density as water and hence there is little driving force to separate it from the froth. Bitumen is also highly viscous (8.4×10^5 mPa.s at 25°C, (Schramm and Kwak, 1988)). The high viscosity negates any separation and results in high pressure drops during transport; therefore, diluents are added to the froth in order to reduce the viscosity and the density of the oil phase.

Currently, there are two commercialized froth treatment processes in Alberta: a naphtha based process used by Syncrude and Suncor and a paraffinic solvent based process used by Albian Sands Energy. In the Syncrude and Suncor processes, the froth is diluted with an aromatic solvent (naphtha), which promotes the settling and coalescence of the emulsified water. Note, some surfactants are also added to the froth. The diluted bitumen at this stage contains approximately 2% water and 0.5% fine solids. In the next recovery stage, the mixture is centrifuged, followed by distillation to recover the naphtha. The product of distillation is coker feed bitumen and contains approximately 1% fine solids (Romanova *et al*., 2004).

The Albian process uses a paraffinic diluent. This solvent also promotes flocculation of the emulsified water and suspended solids. The Albian process also results in some asphaltene precipitation, which makes the bitumen suitable for conventional hydro-treat refining. In this process, water and solids are separated from the solution in three counter current stage gravity settling stages. The bitumen produced from Albian process contains less water and solids (less than 0.2% water and virtually solids-free) compared to the process hat uses an aromatic diluent (Romanova *et al*., 2004, Shelfantook, 2004).

The factors that affect froth treatment have not been investigated as extensively as those for extraction. Romanova *et al*. (2004; 2006) investigated the effect of a number of processing conditions on froth treatment performance based on the amount of dilution required to achieve a given bitumen product quality; that is, less than 0.5 vol% water in the bitumen product. They found that the aromatic solvent based process was not sensitive to extraction temperature, the amount of sodium hydroxide added during extraction, or froth treatment temperature. Higher dilution ratios were required for poorer quality oil sands and for froths produced in high shear extractions possibly because these froths contained more solids. They found that the paraffinic process was more sensitive to extraction conditions with higher dilutions required for poor quality oil sands, extraction performed with non-optimum amounts of sodium hydroxide, and for higher shear extractions. The bitumen recovery was higher at higher froth treatment temperatures possibly because more compact rag layers were formed.

Romanova *et al.* (2004; 2006) did not focus on the accumulation of water and solids at the water-oil interface; that is, rag layer formation. Rag layers have been observed in froth treatment processes (Moran, 2006) and in the separation of water from conventional crude oils. These crude oils are typically produced from reservoirs that contain some emulsified water. In water-oil separators, rag layers often form as an intermediate layer at the crude oil-water interface. The rag layers also can form in refinery desalters when water is added to wash out water-soluble salts prior to refining. In crude oil separation processes, the failure to separate rag layers from crude oil-water mixtures leads to oil loss and water contamination of the product oil. This is particularly problematic in heavy crude oils with an American Petroleum Institute (API) gravity of less than 20 (Varadaraj and Brons, 2007).

Rag layers occur when the coalescence rate of the water droplets is slower than the accumulation rate (Frising *et al*. 2006) or when the fine oil-wet solids are held at the interface by interfacial tension forces. The accumulating solids may also present a barrier to material settling. Settling, coalescence, and wettability are discussed in more detail in the following thesis sections.

2.4 Hindered Settling

The separation process in froth treatment is based on either gravity settling or centrifugation and, in either case, can be described in terms of Stokes' law:

$$u_t = \frac{d_p^2(\rho_p - \rho_m)g}{18\mu_m} \qquad (\mathrm{Re} < 1) \qquad \textbf{(2.1)}$$

where u_t is the terminal velocity, ρ is the density, μ is the viscosity, d_p is the droplet/particle diameter and g is the gravity acceleration. Subscripts p and m denote droplet/particle and medium respectively. In centrifuge separation, g is substituted by the angular acceleration:

$$a = \omega^2 r \qquad \textbf{(2.2)}$$

where ω is the angular velocity and r is the radius of centrifugation (Shelfantook, 2004).

Stokes' law is applicable for an isolated particle settling in an infinitely dilute medium. However, diluted froth is a concentrated multi-species particle system. In this case, settling is hindered. In hindered settling, the velocity gradients around each particle in the system are affected by the presence of nearby particles. Furthermore, the particles in settling displace liquid, which flows upward and makes the particle velocity relative to the fluid greater than the absolute settling velocity (McCabe *et al*., 1985). In a uniform suspension, the settling velocity can be estimated from Equation 2.3 (Richardson and Zaki, 1954):

$$u = u_t \alpha_f^n \qquad \textbf{(2.3)}$$

where u is the hindered settling rate and u_t is the terminal velocity of an isolated particle, α_f is the volume fraction of fluid or suspension voidage, and n is the Richardson-Zaki's coefficient which can be determined either experimentally or by using the equations given by Richardson and Zaki, Table 2.1.

The usual form of hindered settling, Equation 2.4 is for a mono-dispersed system in the low Reynolds numbers is given by (Masliyah, 1979):

$$v_s - v_f = \frac{g d_s^2 (\rho_s - \rho_f)}{18 \mu_f} \alpha_f F(\alpha_f) \quad \textbf{(2.4)}$$

where v_s is the velocity of the particles, v_f is the fluid velocity and d_s is the particle diameter. ρ_s and ρ_f are the particle and fluid densities respectively, and μ_f is the fluid's viscosity. The term $F(\alpha_f)$ is a function that accounts for particles' concentration. When $\alpha_f \to 1$, $F(\alpha_f) \to 1$ and Equation 2.4 becomes Stokes' equation. $F(\alpha_f)$ can be determined either experimentally or from the equations found in Table 2.1. In Table 2.1, D is the inner diameter of the settling vessel, and Reynolds numbers are calculated for terminal velocity of an isolated particle.

In a multi-species particle system, particles of different density and diameter co-exist and Equation 2.4 is modified to Equation 2.5 for an N particle species system:

For $i = 1, 2, 3, \ldots, N$

$$v_i - v_f = \frac{g d_i^2}{18 \mu_f} F(\alpha_f)(\rho_i - \rho_{susp}) \quad \textbf{(2.5)}$$

the subscript i in this equation is substituted with subscript s in Equation 2.4, and is the i^{th} particle species in the suspension. ρ_{susp} is defined by Equation 2.6:

For $k = 1, 2, 3, \ldots, N$

$$\rho_{susp} = \rho_f \alpha_f + \sum_{k=1}^{N} \rho_k \alpha_k \quad \textbf{(2.6)}$$

Equation 2.5 is the generalized form of the slip velocity for the i^{th} particle species in a multi-species system (Masliyah, 1979). Note, in a centrifuge, the angular acceleration is used instead of gravitational acceleration and both the settling velocity and the Reynolds number must be determined accordingly.

Table 2.1 Some functional forms for $F(\alpha_f)$ (Adopted from Yan and Masliyah, 1993)

Source	Relation	Validity
Richardson and Zaki (1954):		
	$F(\alpha_f) = \alpha_f^n$	
where		
	$n = 4.65 + 19.5 d_s / D$	$\mathrm{Re} < 0.2$
	$n = (4.35 + 17.5 d_s / D)\,\mathrm{Re}^{-0.03}$	$0.2 < \mathrm{Re} < 1$
	$n = (4.45 + 18 d_s / D)\,\mathrm{Re}^{-0.1}$	$1 < \mathrm{Re} < 200$
	$n = 4.45\,\mathrm{Re}^{-0.1}$	$200 < \mathrm{Re} < 500$
	$n = 2.39$	$\mathrm{Re} \geq 500$
Barnea and Mizrahi (1973):		
	$F(\alpha_f) = \dfrac{\alpha_f^2}{\left(1 + (1-\alpha_f)^{1/3}\right)\exp\left[\dfrac{5(1-\alpha_f)}{3\alpha_f}\right]}$	all Re
Garside and Al-Dibouni (1977):		
	$F(\alpha_f) = \alpha_f^n$	
where		
	$\dfrac{5.1-n}{n-2.7} = 0.1\,\mathrm{Re}^{0.9}$	all Re

2.5 Emulsions

Emulsions are dispersions of one immiscible fluid in another. Emulsions are stabilized in the presence of surface active agents, which adsorb on the interface and present a barrier to flocculation and/or coalescence. Emulsion droplets show all usual behaviors of metastable colloids; namely, Brownian motion, reversible structural transitions due to droplet interactions that may be strongly modified, and irreversible transitions that commonly involve their destruction.

Emulsions are produced by shearing two immiscible fluids, which causes the fragmentation of one phase in the other. The volume fraction of droplets in the emulsion varies from zero to almost one. Oil-in-water emulsions are composed of oil droplets dispersed in water. Water-in-oil emulsions are composed of water droplets dispersed in an oil continuous phase. Emulsion droplets may also contain smaller droplets of the continuous phase dispersed within them. Such systems are labeled double emulsions or multiple emulsions (Bibette *et al*., 1999).

In the production stages of bitumen from oil sands, emulsions form by dispersion of the water in the oil phase. In the Syncrude and Suncor processes, the diluted bitumen product from the froth treatment process contains 2–3% water in the form of emulsions after the centrifuge step, even though demulsifying agents have been used. The emulsified water is usually in the form of 1–5 μm water droplets dispersed in the oil phase. These water-in-diluted bitumen emulsions are very stable, and are the source of several problems in the oil sands industry. The chloride salts that are present in the emulsified water create serious corrosion problems in the downstream processes (Gu *et al*., 2002). Furthermore, the emulsified water is likely a contributor to rag layer formation in froth treatment.

Even though water-in-oil emulsions are thermodynamically unstable, they can be kinetically very stable over long periods of time. Generally, the smaller the dispersed droplets, the more stable the emulsion. To separate the two initially mixed phases, the dispersed droplets must grow in size, a process called coalescence. It is widely accepted in the literature that coalescence takes place in three steps (Frising *et al*., 2006;

Sztukowski, 2005; Barnea and Mizrahi, 1975; Bazhlekov *et al*., 2000; Chesters, 1991; Fang *et al*., 2001; Klaseboer *et al*., 2000; Lobo *et al*., 1993; Palermo, 1991; Rommel *et al*., 1992; Saboni *et al*., 2002; Tobin *et al*., 1990; Tsouris and Tavlarides, 1994):

1. Approach of two droplets to within molecular separation distances (Figure 2.5 a).
2. Dimpling or creation of a planar interface between the droplets, following by the drainage of the continuous phase between the droplets (Figure 2.5 b).
3. Film rupture and bridging of the dispersed phase fluid which is the consequence of Van der Waals and other intermolecular forces and results in coalescence (Figure 2.5 c)..

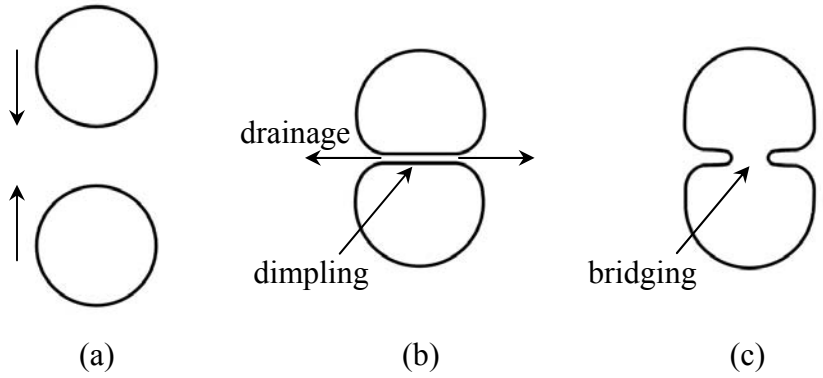

Figure 2.5 Coalescence steps; (a) droplets approach, (b) dimpling and drainage, (c) film rupture and bridging (Adopted from Sztukowski, 2005).

2.5.1 Stabilization of Oilfield Water-in-Oil Emulsions

Several factors have been reported to contribute to formation and stabilization of water-in-oil emulsions. Some of these factors include fine solids (Ali and Alqam, 2000), asphaltenes, resins, and natural surfactants (Durand and Poirier, 2000).

Role of Asphaltenes and Resins:

Asphaltenes and resins are the principal components of the polar fraction of bitumen and crude oils (Gu *et al*., 2002). They are polynuclear aromatics with some heteroatom functional groups. Asphaltenes are known to self-associate into aggregates of 6-10

molecules per aggregate on average (approximately 8000 g/mol). Some aggregates may be much larger with apparent molar masses in the order of 100,000 g/mol (Yarranton, 2005). Both asphaltenes and resin molecules contain hydrophobic and hydrophilic components and therefore are surface active and tend to adsorb on the surface of other materials.

When asphaltenes adsorb on the oil/water interface, they form stable films, which strongly contribute to the formation of stable emulsions (Khadim and Sarbar, 1999). Over time, the films become irreversibly adsorbed (Freer and Radke, 2004;). The compressibility of the films reduces with aging and as the film contracts. Emulsion stability has been correlated to the compressibility of the films (Yarranton *et al*., 2007). Resins tend to destabilize water-in-oil emulsions (McLean and Kilpatrick, 1997; Spiecker *et al*., 2003; Gafonova and Yarranton, 2001), and they may reduce asphaltene self-association and prevent irreversible film formation at the interface.

Role of Clays:

Yan *et al*., (1999) compared the ability of the different components of bitumen to stabilize water-in-diluted bitumen emulsions. They found that asphaltenes and fine solids were the main stabilizing agents and that the stability of water-in-oil emulsions was very high when both asphaltenes and fine solids were present in the system. Furthermore, they found that emulsions that form in deasphalted bitumen have a lower stability compared to those formed in bitumen with asphaltenes.

Sztukowski and Yarranton (2004) studied interfacial behavior and characterization of oil sands solids. They confirmed that a combination of fine solids and asphaltenes adsorbed on the surface of emulsified water created more stable emulsions than asphaltenes or solids alone. They also showed that at least some of the solids adsorb directly on the water/oil interface and that there is a competitive adsorption between the asphaltenes and solids.

Figure 2.6 shows the possible effect of fine solids on emulsion stability. The asphaltene layer formed at water/oil interface is about 2 nm thick (Sztukowski *et al*., 2003). The fine solids have an average thickness of less than 10 nm but have an irregular morphology that can make the thickness of their layer more than 10 nm (Figure 2.6 b). Therefore, solids may prevent emulsion droplets from close contact. Solids also occupy surface area and may reduce the probability of bridging between droplets thus preventing coalescence (Figure 2.6 a). In addition, the presence of trapped solids between the approaching interfaces of the droplets might lower the probability of close contact between the droplets (Figure 2.6 c).

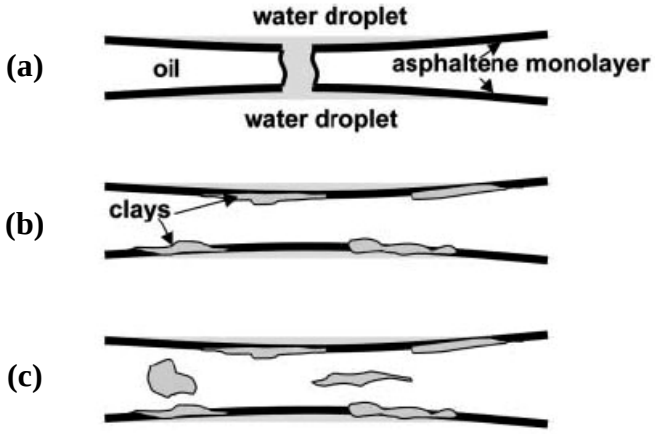

Figure 2.6 (a) Bridging of asphaltene film between two water droplets; (b) adsorbed solids prevent bridging; (c) trapped solids prevent close contact between droplets (From Sztukowski and Yarranton, 2004).

The asphaltenes that adsorb on the water/oil interface of the emulsions have a low hydrogen-to-carbon and a high oxygen-to-carbon ratios, compared to the rest of the asphaltenes present in the bitumen. This fraction of asphaltenes is the key stabilizer for water-in-oil emulsions. When these asphaltenes combine with fine solids (mainly clays contaminated by hydrocarbons), the emulsion stability is significantly increased (Gu *et al*., 2002).

Sztukowski and Yarranton (2004) also showed that coarse solids could destabilize water-in-oil emulsions at low concentrations. They speculated that the coarse likely water-wet solids acted as bridges between the droplets promoting coalescence. They noted that at very high concentrations, the coarse solids created very stable emulsions probably by packing the continuous phase between the droplets and preventing contact between the droplets.

Role of Surfactants:

Gu *et al*., (2002), studied the effect of water-soluble surface active components present in bitumen on emulsion stability. These components composed of basic, amphoteric and acidic agents. They found that these components act as destabilizers for the water-in-oil emulsions formed in bitumen. The complete removal of the water-soluble surface active components resulted in an increase in emulsion stability. They also reported that the addition of the extracted water soluble surface active components to the system decreased the emulsion stability.

Role of Solvents:

The stability of water-in-crude oil emulsions is also affected by the type of diluent. Paraffinic diluents tend to produce more stable emulsions than aromatic solvent unless asphaltene precipitation occurs (McLean and Kilpatrick, 1997). Paraffinic solvents are poorer solvents for asphaltenes than aromatics solvents and likely promote rapid stronger adsorption of asphaltenes on the interface and more rapid irreversible film formation. If asphaltenes are precipitated before emulsion formation, the emulsions formed are less stable because the concentration of asphaltene molecules in solution is reduced (Gafonova and Yarranton, 2001).

2.5.2 Emulsion Breaking

Since emulsions do contribute to the formation of undesirable dense packed layers, methods used to treat them in the conventional oil industry will be discussed. These dense packed layers which also are called ‘rag layers’ are similar to rag layers observed

in heavy oil and bitumen processing. Some emulsion breaking requires contact between droplets followed by coalescence which is achieved through gravity settling or centrifugation sometimes aided by chemical flocculants. Understanding coalescence aids in the understanding of rag layers. The main methods used to increase coalescence are thermal, electrostatic, and chemical. The methods used to treat oil sands froths are heating and chemical demulsification.

Thermal:

Heating an emulsion can be very beneficial to demulsification of water-in-oil emulsions, although the effectiveness of this method depends largely on the oil characteristics (Petrolite Corporation, 1973; Strøm-Kristiansen *et al*., 1995). The demulsification in thermal process is the result of changes in interfacial tension, modifications of the adsorption of emulsifiers on the interface, and reduction of viscosity (Chen and Tao, 2005). The disadvantages of this method are fuel cost and environmental friendliness (Frising *et al*., 2006), nevertheless, heating is used in most industrial emulsion breaking applications.

Thermal technologies like freeze-thaw methods (Boysen *et al*., 1999; Lorain *et al*., 2001) are based on the different solidification temperatures of oil and water. When the water droplets in the emulsion are frozen, they could be separated by any solid liquid separation process. Due to high energy costs, use of these techniques is limited (Frising *et al*., 2006).

Electrostatic:

Applying a high electric field to the flowing emulsion can affect flocculation and coalescence. The electrostatic field induces a charge on the droplets and causes them to align and stretch along field lines. This alignment promotes contact and the stretching weakens the interface which promotes coalescence (Eow, and Ghadiri, 2002). Electrostatic treaters are commonly used in refinery desalters. This method is not cost effective for most small-scale oilfield emulsion treaters and it is not effective for high solid content materials such as oil sand froths.

Chemical:

Some surfactants promote flocculation of the water droplets and others facilitate coalescence by replacing the existing emulsifiers and weakening the interfacial film (Angle, 2001; Balson, 2003). Although this technique can effectively break water-in-oil emulsions, chemical costs can be high. As well, the best choice of demulsifier is specific to each crude oil and can change as the water composition or solids content changes. These changes may occur slowly over the life of a project or rapidly over a few minutes or hours. In fact the wrong demulsifiers or wrong dosages can result in very stable emulsions. Even reasonably effective demulsifiers may not completely break the emulsion. For example, demulsifying agents are used in the froth treatment process, but the diluted bitumen after the centrifuge step still contains about 2–3 % water.

Czarnecki *et al*., (2007) investigated the effect of dosage of demulsifiers on their effectiveness. They noticed that overdosing with a flocculating chemical used for demulsification will result in a deterioration of its performance. Therefore, to achieve a satisfactory dewatering process, an optimization of the chemical dosage and accurate process control are necessary. The choice and dosage of demulsifiers is a black art and the design of demulsifiers remains an ongoing area of research.

2.6 Wettability of Solids

The term ‘wettability’ may be defined as “macroscopic manifestations of molecular interaction between liquids and solids in direct contact at the interface between them” (Berg, 1993). Wettability is closely related to the surface tension or the energies of the surfaces. In a sessile droplet of liquid with direct contact with the surface of a solid, the surface tension forces are at equilibrium (Figure 2.7); that is, the droplet will spread or contract until the surface energies are minimized. Surfaces on which the droplet spreads are wettable by that fluid and surfaces on which the droplet beads are non-wettable.

A solid particle floating on a liquid surface will tend to sink through the surface under gravity or centrifugal forces. However, a non-wetting particle will experience an upward surface tension force. This force arises because the sinking particle exposes more surface

area to the non-wetting phase increasing the interfacial energy of the system. The balance of the interfacial and gravity forces will determine if the particle sinks or floats. Since the interfacial tension force is proportional to the circumference while the gravitational force is proportional to the volume of the particle, smaller particles are more likely to float.

The contact angle θ of the droplet and the solids surface is a measure of the surface's wettability. A contact angle greater than 90° indicates a non-wettable surface, while a surface with a contact angle of less than 90° is considered wettable. In the petroleum industry, a contact angle of less than 60° indicates a wettable surface, an angle greater than 120° indicates a non-wettable surface, and an angle between 60 and 120° indicates an intermediately wettable surface. The relation between the contact angle and the surface tensions around the droplet was defined by Young in 1805 (MacRitchie, 1990), Equation 2.7;

$$\gamma_{LV} \cos\theta = \gamma_{SV} - \gamma_{SL} \qquad \textbf{(2.7)}$$

where γ_{LV} is the surface tension between liquid and vapor, γ_{SV} is the surface tension between solid and vapor, γ_{SL} is the surface tension between solid and liquid, and θ is the contact angle at which the liquid-vapor interface meets the solid-liquid interface (Hiemenz and Rajagopalan 1997).

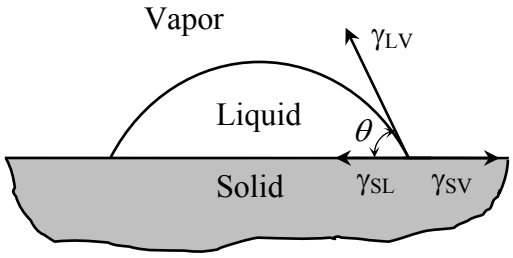

Figure 2.7 Surface tension balance on a sessile droplet on a solid's surface (Adopted from Hiemenz and Rajagopalan, 1997).

Among several techniques for measuring the wettability, there are two commonly used techniques: the Zisman contact angle method and the floatation method (Ozkan and Yekeler, 2003). Zisman *et al*., (1964) developed a technique to measure the wettability by plotting $\cos\theta$ against γ_{LV} (Figure 2.8). This plot gives a line which intercepts the x-axis at $\gamma_C = \gamma_{LV}$ where γ_C is defined as critical surface tension of wetting. At $\gamma_C \geq \gamma_{LV}$, the liquid spreads on the solid's surface and wets it. When $\gamma_C < \gamma_{LV}$, the liquid does not wet the solid (Ozkan and Yekeler, 2003).

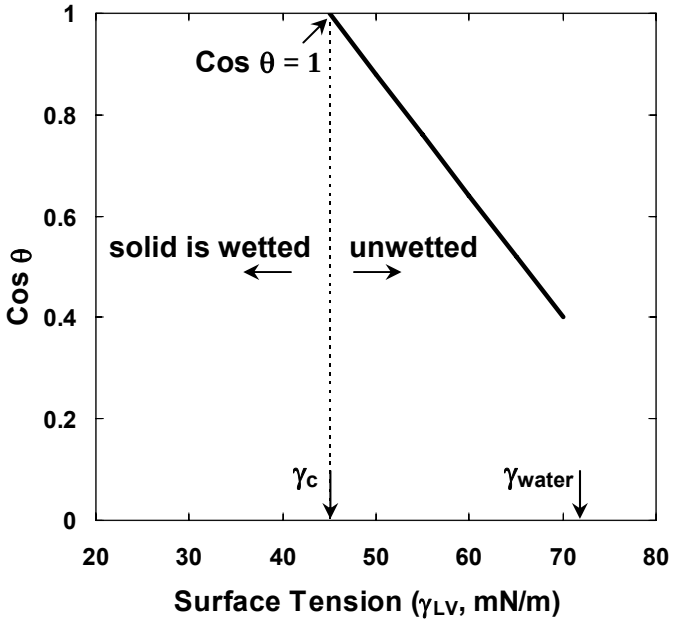

Figure 2.8 The Zisman contact angle method for determining the γ_c value (Adopted from Ozkan and Yekeler, 2003).

In the floatation method, the percentage recovery (%R) is plotted versus the liquid surface tension (γ_{LV}). Percentage recovery is the percentage of solids that remain on the surface. Figure 2.9 shows that γ_C is determined from the extrapolation of the linear part of the curve to the surface tension axis (Ozkan and Yekeler, 2003).

The Zisman method of obtaining γ_C is useful for solids with flat surfaces, while the floatation method is more suitable for hydrophobic powders (Yarar and Kaoma, 1875).

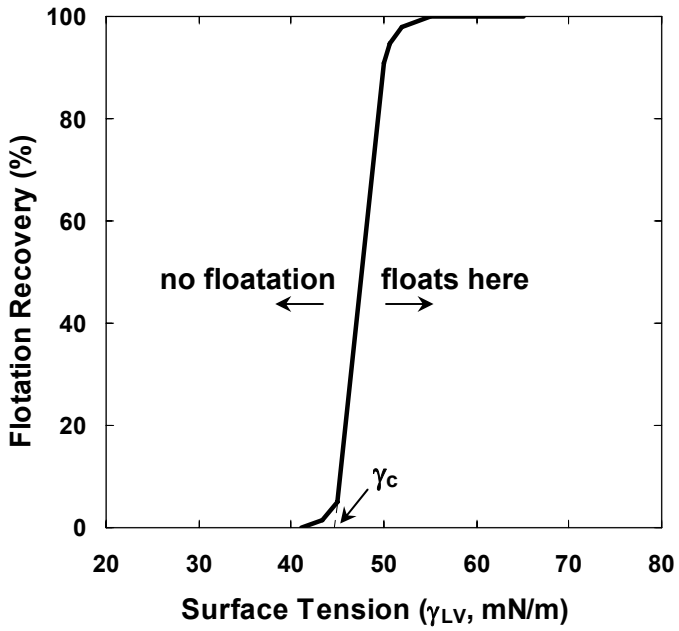

Figure 2.9 Flotation method for determining the γ_c value (Adopted from Ozkan and Yekeler, 2003).

Wettability of Oil Sand Fine Solids:

Chen *et al*. (1999) studied the wettability of oil sand fine solids extracted from bitumen froth using the Zisman contact angle method. They also studied the partitioning of fine solids between aqueous, organic, and their interphases by shaking some powder in a small vessel filled with diluent and water. The diluents were different ratios of n-heptane and toluene. Chen *et al*. (1999) made the following observations:

- The water-wettability of fine solids in bitumen froth increases by increasing paraffinic components of the oil phase. A possible explanation is that the weaker interactions of apolar molecules with solids compared with that of polar molecules.
- Washing the solids with toluene increases their water-wettability significantly, while washing them with heptane does not change it. A reason could be the strong solubilization of toluene which removes the adsorbed organic matter from the surface of the fine solids.
- Drying particles decreases their water-wettability significantly and this change is irreversible. The reasons behind this phenomenon have not been studied;

however, the evaporation of moisture and solvent during drying apparently causes a closely packed assembly of organic molecules to adsorb on the solid.

- The water-wettability of fine solids is closely related to their partitioning among the various phases. Bi-wettable fine solids adsorb at water-oil interfaces and contribute to the stability of dispersed water droplets in the oil phase in froth treatment processes. The dispersed water droplets are responsible for the entrainment of water and fine solids in bitumen produced from froth treatment.

These results indicate that in oil sand froths, bi-wetted or oil-wet fine solids could accumulate at the water-oil interface. Small asphaltene-coated emulsion droplets which are oil-wet are expected to behave in the same manner.

2.7 Summary

The product of the hot water oil sand extraction process is a froth which contains approximately 60 to 65 wt% bitumen, 28 to 34 wt% water, and 6 to7 wt% solids (Hepler, 1994). The froth is diluted with either naphtha or paraffinic solvent and further treated to separate the bitumen. Higher dilution ratios are sometimes required to eliminate most of the water from the product bitumen for poorer quality oil sands, for froths produced at high shear, and for froths produced at non-optimum addition of sodium hydroxide during extraction. Poor froth treatment performance may be related to the formation of a rag layer at the water/oil interface, which typically consists of water droplets and solids suspended in the continuous oil phase. This rag layer can break off and flow to the water outlet resulting in lower oil recovery or flow to the oil outlet reducing the product quality.

There are several possible explanations for rag formation, however likely mechanisms for rag layer formation are:

- Hindered settling
- Slow coalescence of water-in-oil emulsions
- Accumulation of oil-wet fine solids or asphaltene-coated water droplets

In a continuous process, hindered settling may be slow enough that some water droplets may exit the vessel before they reach the water-oil interface. If coalescence is slow, the droplets will accumulate at the interface faster than they can move into the water phase.

Oil-wet fine particles or small water droplets may accumulate at the interface and form a barrier that prevents larger droplets from reaching the interface and coalescing.

Chapter 3

Experimental Methods and Characterization of Materials

In this chapter, the experimental procedures are presented. Froth samples required for the experiments and the procedures to extract froths from oil sand samples are discussed. The main experimental method in this work was the "Stepwise Centrifuge Test". This test was used to assess rag layer formation mechanisms and the effect of operating conditions on rag layer formation. Note, this test does not replicate the high speed, low residence time conditions of the commercial continuous centrifuge process but rather is used to identify mechanisms and assess the effects of other process variables. The procedure is outlined in this chapter but some variations are detailed in later chapters. The determination of rag layer, sediment composition and the capture of micrographs of rag layers are presented. Solids characterization is also discussed including the measurement of size distributions and assessment of floatability.

3.1 Materials

Oil Sand Samples:

Two oil sand samples, designated LQOS3 and AQOS2, were obtained from Syncrude Canada Ltd. The bitumen, water and solids content of the oil sand samples were determined at the Syncrude Research Centre using Dean-Stark extraction and the fines content of the solids was determined by laser light scattering analysis (Bulmer and Starr, 1979). Fines are defined as solids less than 44 μm in diameter. Table 3.1 shows the composition of the two oil sand samples.

Table 3.1 Composition of the oil sand samples

	LQOS3, wt%	AQOS2, wt%
Bitumen	5.5	10.4
Water	1.1	3.4
Solids	93.6	85.8
Fines (<44 μm)*	30.4	27.6

*Weight percent of fines in solids

The general criteria for oil sands quality has been defined by Pow *et al*. (1963) and it is related to bitumen content of the oil sands, Table 3.2. Using this criteria, the LQOS3 is a low quality oil sand and the AQOS2 is an average quality oil sand.

Table 3.2 Oil sands quality criteria

	Bitumen, wt%
Rich	12~14
Average	10~11
Lean	6~9

Upon receipt, the oil sand sample pails were dated and any clay chunks in the samples were broken down to pea-size. Samples were transferred to plastic bags to prevent evaporation of the free water. Then they were mixed and homogenized by hand, and transferred to a polyethylene pail. As recommended by Schramm and Smith (1987), the oil sand samples were stored in the dark in a freezer in order to minimize the effects of aging.

The LQOS3 sample was of unusually poor quality. Figure 3.2 shows that the LQOS3 sample was far more consolidated than the more typical AQOS2 sample shown in Figure 3.1. The LQOS3 sample was ground and sieved in order to obtain the proper grain size for the extraction experiments.

Figure 3.1 An average quality oil sand (AQOS2).

Figure 3.2 A low quality oil sand (LQOS3).

Other Materials:

Athabasca coker-feed bitumen was obtained from Syncrude Canada Ltd. Commercial grade n-heptane (Conoco Phillips), reagent grade toluene (Univar), histology grade 2-propanol (EM Science), reagent grade sodium hydroxide (EM Science), anhydrous methanol (Fisher Scientific), Nitrogen (PRAXAIR Canada Inc.) and Type 4A molecular sieves (Fisher Scientific) were used in this study. Reverse osmosis (RO) water was supplied from the University of Calgary water plant. The Karl Fischer titration reagent was Aqualine^{TM} Complete 5 which was a mixture of iodine, sulfur dioxide and imidazole (Fisher Scientific).

Asphaltenes were required for one experiment and were separated from Athabasca coker feed bitumen using the ASTM D4124 method. n-Pentane was added to bitumen in a ratio of 40 cm^3 per gram of bitumen, the mixture was sonicated for 45 minutes at room temperature and then left for 24 hours. Most of the supernatant was decanted and filtered through Whatman filter paper number 2 (8 micron pore size). The residue in the beaker was diluted again with a 4:1 cm^3/g ratio of n-pentane to the original bitumen. After sonication and 24 hours of equilibration, the mixture was filtered through the same filter paper. The filter cake (asphaltenes) was washed with n-pentane for 5 days, and then dried in a fume hood overnight.

3.2 Bitumen Extraction from Oil Sands

Bitumen was extracted from oil sands using a Denver Cell extraction apparatus obtained from the Saskatchewan Research Council Pipeflow Technology Centre, Figure 3.3. The flotation was based on the Syncrude method as outlined below.

Figure 3.3 The Denver Cell unit.

Sample Preparation

The frozen oil sand was partially thawed and approximately 500 g of the sample was weighed. The sample was allowed to reach room temperature before the extraction. RO water was preheated to the desired temperature, which for most cases was 80 °C, but in some experiments 23 °C and 50 °C temperatures were used instead.

Denver Cell Extraction

Approximately 300 g of RO water and the 500 g oil sand sample were added to the Denver pot and NaOH was added to the water as required. Then the impeller was turned on to 2100 rpm for 5 minutes. After 5 minutes of mixing, 600 g of pre-heated water was added to the Denver pot and the impeller speed was adjusted to 1200 rpm. At the same time, the Denver Cell pot was aerated with 300 cm^3/min of nitrogen injected through the impeller shaft. After another 5 minutes of mixing, the impeller and nitrogen flow were turned off, and all the froth was skimmed from the surface of the Denver pot.

The extraction experiments were conducted at 23°C, 50°C and 80°C for LQOS3, but they were only conducted at 80°C for AQOS2. Figures 3.4 and 3.5 are processibility plots of oil recovery versus the amount of NaOH added for the LQOS3 and AQOS2 samples, respectively. Figures 3.6 and 3.7 are the corresponding froth compositions for the respective oil sand samples. Some oil sands exhibit a maximum bitumen recovery and bitumen content in the froth at an optimum amount of NaOH added during extraction. However, the maximum bitumen recovery for the LQOS3 sample occurred at zero NaOH addition. The AQOS2 extraction was not sensitive to NaOH addition and there was no clear best amount. For the froth experiments presented in this study, the extractions were conducted at 0 and 0.04 wt% NaOH for LQOS3 and at 0 NaOH for AQOS2.

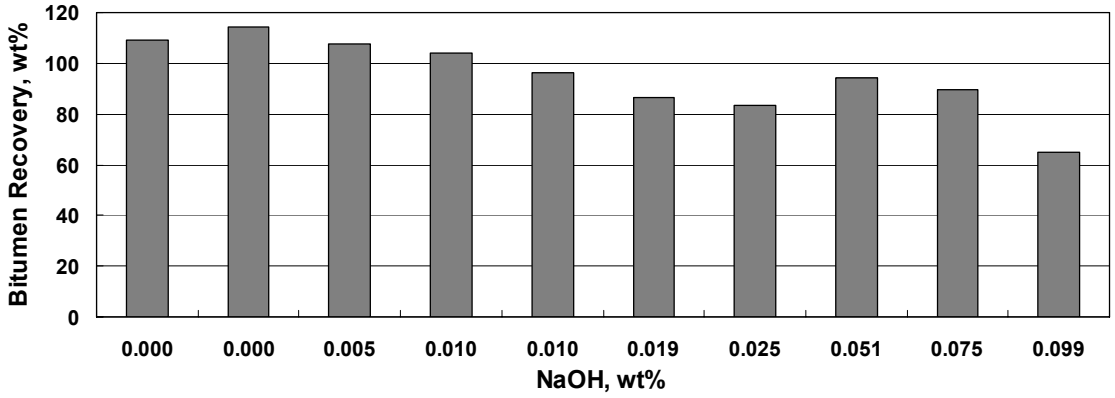

Figure 3.4 Processibility curve for Denver Cell extractions for LQOS3 at 50°C. At 0.0 wt% NaOH, two runs were conducted to confirm the repeatability of the data.

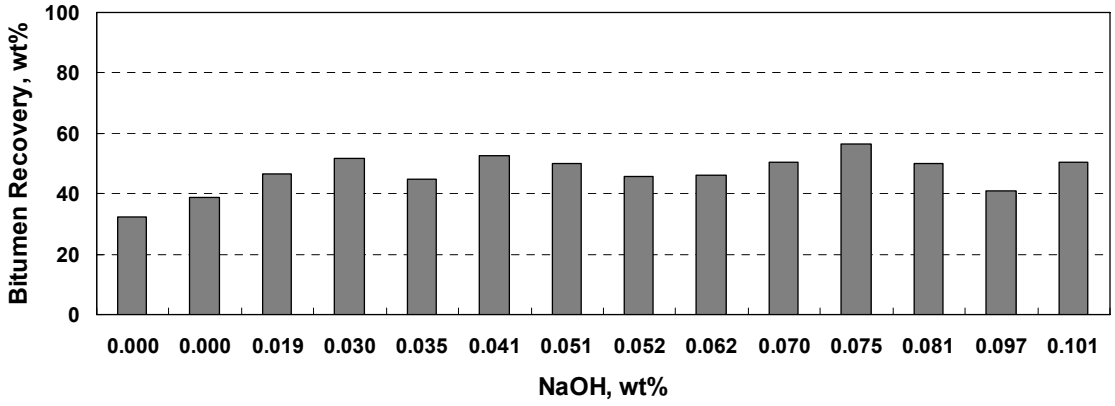

Figure 3.5 Processibility curve for Denver Cell extractions for AQOS2 at 80°C. At 0.0 wt% NaOH, two runs were conducted to confirm the repeatability of the data.

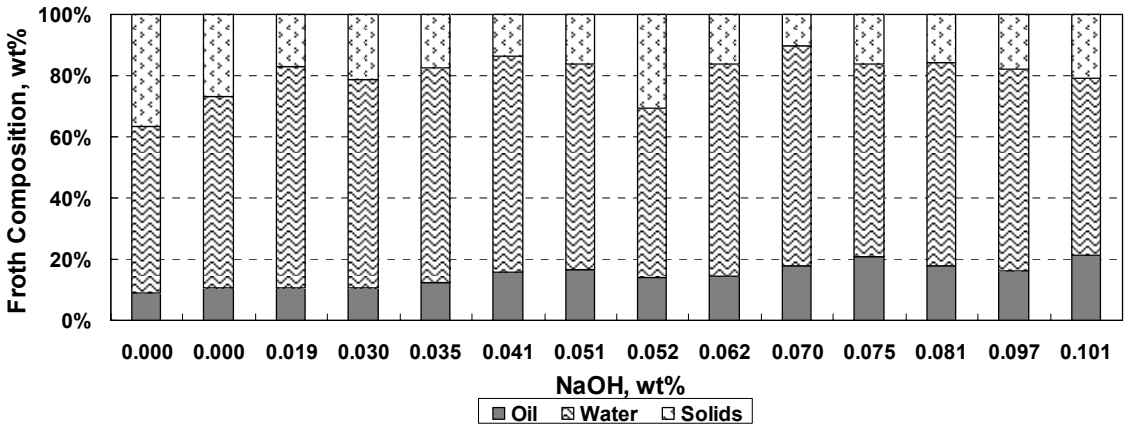

Figure 3.6 Froth compositions for Denver Cell extractions for LQOS3 at 50°C vs. NaOH addition. At 0.0 wt% NaOH, two runs were conducted to confirm the repeatability of the data.

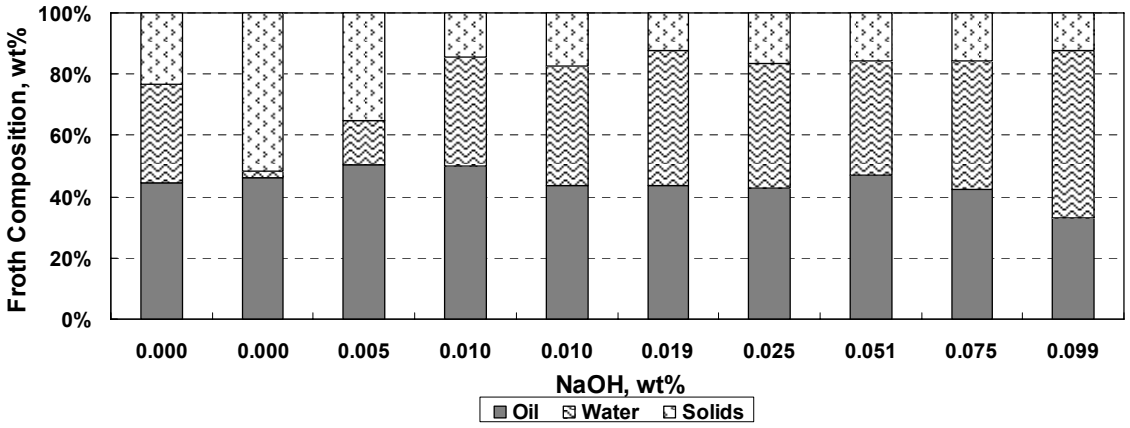

Figure 3.7 Froth compositions for Denver Cell extractions for AQOS2 at 80°C vs. NaOH addition. At 0.0 wt% NaOH, two runs were conducted to confirm the repeatability of the data.

3.3 Determination of Froth Composition

The Syncrude method (Bulmer, J.T., and Starr, J., 1979) was used to determine the bitumen, water and solids content of the froth. A subsample of froth obtained from the bitumen extraction experiment was used for this assay.

Solvent Preparation

A mixture of 26 vol% 2-propanol and 74 vol% toluene was prepared in a 4 liter bottle. Type 4A molecular sieves were added to the bottle 24 hours before the experiment to dry the solvent mixture. Small volumes of 2-propanol or toluene were added so that the mixture density was between 0.8435 to 0.8445 kg/L, as measured with an Anton Paar DMA46 density meter.

Sample Preparation

In a 1 liter Nalgene bottle, approximately 500 ml of the solvent mix was added to 7 to 10 g of froth, and then mixed on a mechanical roller for one hour. After mixing, the mixture was allowed to settle for 1 minute to remove coarse solids. Approximately 25 ml of the sample was transferred to a small Nalgene bottle to be used for water determination. To remove the fine solids, another 10 to 15 ml of the sample was drawn in a glass Luer-lok syringe and was filtered through a nylon 0.45 μm Millipore Millex filter. This sample was kept in capped test tubes to avoid solvent evaporation, and was used for the bitumen determination.

Water Determination

The water content was determined by using a model 787 Karl Fischer Titrator (787 KF Titrino Metrohm). The reagent was Aqualine^{TM} complete 5, which contains iodine, sulfur dioxide and imidazole. The electrolyte solution used for titrator was a mixture of 26 vol% 2-propanol and 74 vol% toluene. Luer-lok tip syringes with a 20 gauge 1.5 inch needle were used to transfer some 1 cm^3 of the sample to the Karl Fischer. Water percent in the sample was determined by comparing the milliliter of titrator used for each sample with a calibration curve. The calibration curve was prepared by measuring the response of the

apparatus to water standard samples, which were made with a known mass of water in a mixture of 26 vol% 2-propanol and 74 vol% toluene.

Bitumen Determination

The previously prepared 10 to 15 ml filtered samples were used for bitumen determination. A glass fiber filter paper was dried at 70°C for at least one hour and then weighed to 4 decimal places. 5 ml of the sample was dispensed from a 5 cm^3 glass pipette onto the filter paper. After drying the filter paper in a fume hood, the filter was reweighed and the mass of bitumen determined. The glass pipette was calibrated beforehand at room temperature to reduce measurement errors.

Solids Determination

Solids content was determined by mass difference of water and oil content of the froth sample. Table 3.3 shows the froth compositions for the two oil sands samples.

Table 3.3 Composition of LQOS3 and AQOS2 froths. Data is the average of all assays for each oil sand's froth.

	LQOS3, wt%	AQOS2, wt%
Bitumen	9.7	44.6
Water	59.8	29.5
Solids	30.5	25.9

3.4 Determination of the Onset of Asphaltene Precipitation

When choosing the ratios of solvent to froth for the extractions, it was necessary to determine the onset of asphaltene precipitation. In the context of this work, the onset of asphaltene precipitation is the composition at which asphaltenes begin to precipitate from an oil diluted with a solvent. Athabasca coker feed bitumen was used in this experiment.

In this study, a solution of X vol% heptane and Y vol% toluene is denoted as heptol X/Y. The onset of asphaltene precipitation was determined for three different heptols (heptol 80/20, heptol 70/30, and heptol 50/50).

The desired volumes of toluene and heptane were measured in a graduated cylinder and the composition was verified with the Anton Paar DMA46 density meter. The densities of the 80/20, 70/30 and 50/50 heptols were 0.722, 0.740, and 0.777 g/cm³, respectively. Centrifuge tubes were weighed and then filled with the desired solvent to bitumen mass ratios. The tubes were agitated on a shaker table for 20 minutes, sonicated for 40 minutes, and then left to settle for 24 hours.

After 24 hours, the tubes were centrifuged at 3700 rpm for 5 minutes and the supernatants decanted. The residue in each tube was washed three times with the same solvent used in the initial dilution. The residue was dried overnight in an oven at 60°C under vacuum and its mass was then determined. The asphaltene yield was calculated, Equation 3.1;

$$\text{Yield} = \frac{m_{AS} - m_S}{m_B} \qquad \textbf{(3.1)}$$

where m_{AS} is the mass of residue (asphaltenes + solids), m_S is the mass of non-asphaltene solids (the mass fraction of solids times the mass of bitumen), and m_B is the mass of bitumen.

The mass fraction of solids in the bitumen was determined as follows. Approximately 3 grams of bitumen was transferred to a glass vial and diluted with at least 25 cm³ of toluene. The solution was agitated for 20 minutes in a shaker table, sonicated for 40 minutes, and then centrifuged at 4000 rpm for 5 minutes. The supernatant was decanted

and the residue washed as described above. The residue was dried in a vacuum oven overnight in 80°C and its mass was then determined. The solids content is mass of residue divided by the mass of bitumen. The solid content of bitumen was determined to be 0.28 wt%.

Figure 3.8 shows fractional asphaltene yields for different solvents at 23°C on a solids-free basis. The heptol 70/30 and heptol 80/20 data were collected in this study and the n-heptane data were taken from literature (Akbarzadeh *et al.*, 2005). The onsets were determined by extrapolating the yields to zero. The precipitation onsets in heptol 80/20 and 70/30 occur at a solvent mass fractions of approximately 0.76 and 0.9, respectively. No asphaltene precipitation was observed in heptol 50/50.

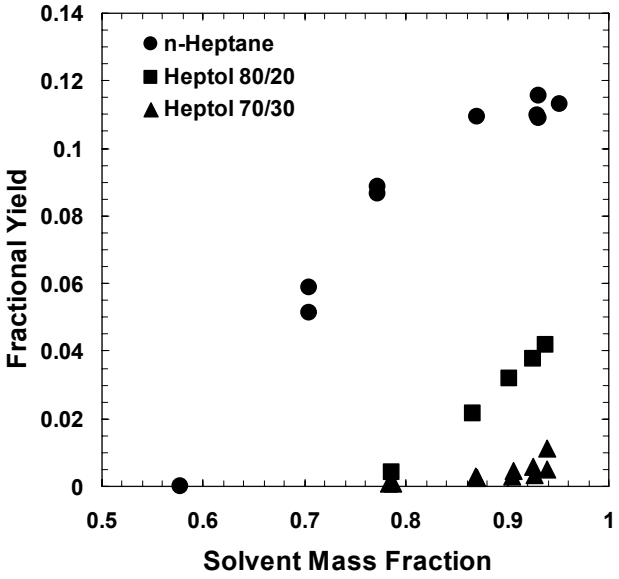

Figure 3.8 Asphaltene precipitation yields at 23°C for n-heptane, heptol 70/30 and heptol 80/20. Data for n-Heptane was taken from Akbarzadeh *et al*., 2005.

3.5 Stepwise Centrifuge Tests

Romanova et al., 2006 assessed the effectiveness of a froth treatment by centrifuging a test tube containing diluted froth for 5 minutes at 4000 rpm. The diluted froth usually separated into an oil layer, a rag layer, a water layer, and a sediment layer, as shown in Figure 3.9.

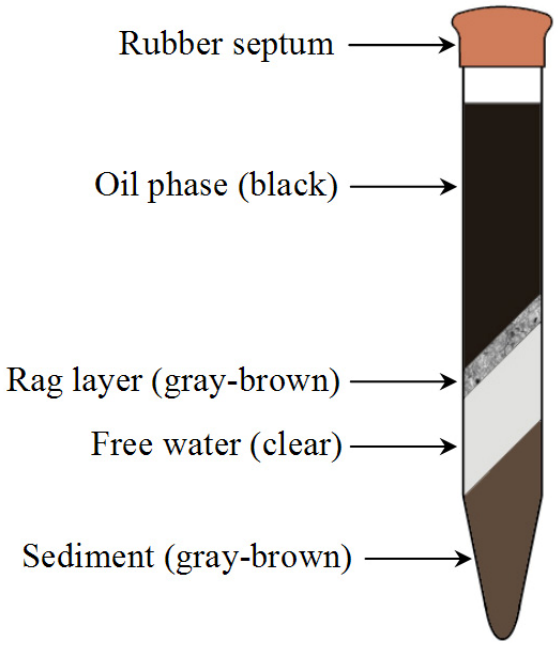

Figure 3.9 Different layers formed in a test tube after 5 minutes centrifuge at 4000 rpm.

The rag layer volumes were usually small, hence it was not possible to assess what factors might have affected rag layer formation. In this study, the method was modified to include a series of centrifugation steps of increasing rotational speed, with the layer volumes being measured after each step. In this way, differences in rag layer formation at different conditions were more easily discerned. The gradual change in rag layer thickness as centrifuge speed increased is shown in Figure 3.10. The procedure used in this study is described in more detail below.

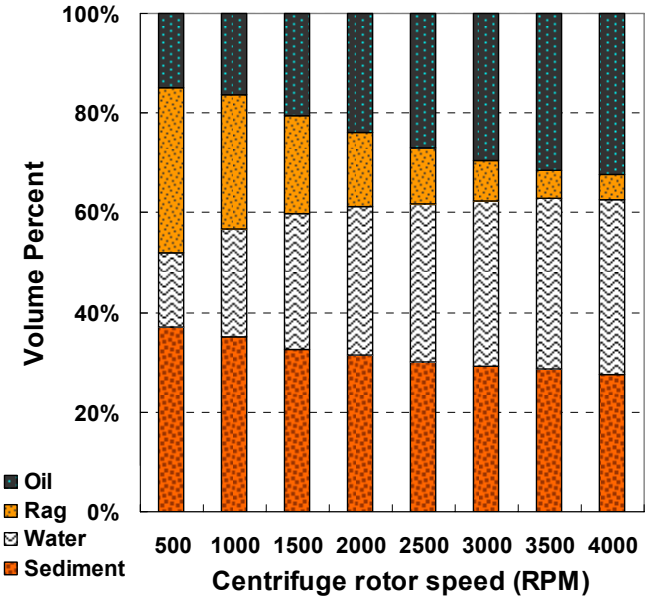

Figure 3.10 Different layers formed in the test tube after each centrifuge step

Solvent Preparation

The diluents in this experiment were toluene, n-heptane and heptol 80/20. Heptol was prepared by mixing the desired volume of n-heptane and toluene. To verify the accuracy of the heptol 80/20 preparation, its density was confirmed to be 0.722 ±0.0003 kg/m³, as measured by an Anton Paar DMA46 density meter.

Sample Preparation

The froth from a Denver Cell bitumen extraction was diluted with one of the previously described solvents at the dilution ratios given in Table 3.4. For heptane and heptol 80/20, the lower dilution ratio was below the onset of asphaltene precipitation and the upper ratio was above the onset of precipitation.

Table 3.4 Dilution ratio and onset of asphaltene precipitation for the three solvents used in stepwise centrifuge tests

Solvent	Dilution Ratio (g solvent / g bitumen)	Onset of Precipitation (g solvent / g bitumen)
Toluene	4.11 and 8.52	N/A
Heptol 80/20	0.70 and 5.14	3.0 ±0.3
Heptane	0.66 and 2.66	1.5 ±0.3

Step-Wise Centrifugation

The experiment was conducted at either 23°C or 60°C. A froth bottle that had been stored in a refrigerator was preheated for 20 minutes in a 60°C water bath to reduce the viscosity of the sample. The froth was mixed using a spatula and a sample was transferred to a test tube. The diluent was added at 23°C to the test tube to obtain the desired solvent to bitumen ratio. The test tube contents were mixed using a shaker table for 5 minutes. If the experiment was conducted in 60°C, the test tube was preheated for 15 minutes in a water bath. For the experiments at 23°C no preheating was required.

The test tube was centrifuged in 500 rpm for 5 minutes. After centrifuging, the volumes of the oil, rag, water, and sediment layers were measured. For the 60°C experiments, the test tube was then heated in a water bath for 5 minutes. For the 23°C experiments, the test tube was left standing at ambient conditions for approximately 1 minute. Note, preliminary experiments indicated that, at 23°C, the rag layer volume changes only occurred while centrifuging and little or no change occurred with gravity settling. The test tube was then centrifuged for another 5 minutes at 1000 rpm, and the layer volumes again measured.

The centrifugation and heating steps were performed a total of 8 times. The centrifuge speed was increased 500 rpm each time to a final speed of 4000 rpm. With the centrifuge used in this study, 4000 rpm is equivalent to an acceleration of 1640 times gravity.

Experimental Variations

A number of variations were performed in the step-wise centrifugation tests to assess possible mechanisms for rag layer stability. These variations are presented in the results and discussion Chapter 5. Two cases required preparation of other materials: 1) the addition of an emulsion to the froth; 2) the addition of fine solids to the froth. The preparation of the emulsion and the extraction of the fine solids are described below.

Emulsion Preparation: Following the same procedures described in step-wise centrifugation, a froth sample was diluted with toluene in a test tube but centrifuged only at 4000 rpm for 5 minutes. The oil phase was decanted with a plastic pipette and was transferred to a small glass bottle. About 5 vol% RO water was added slowly to the glass bottle and was homogenized using a *CAT-520D* homogenizer with a 17 mm flat rotor generator at 18000 rpm for five minutes.

Fine solids extraction: Fine solids were extracted from rag layer material by diluting it with toluene and centrifuging out the undissolved solids. A froth sample was diluted with toluene and the test tube was centrifuged at 1500 rpm for 5 minutes. Oil was decanted using a plastic pipette and the rag layer was removed with a small spatula.

The rag material was placed in a test tube, diluted with toluene, and sonicated until it was completely dispersed. The test tube was then centrifuged at 6000 rpm for 5 minutes and the diluted bitumen and water was decanted with a plastic pipette. The sonication and centrifuge steps were repeated until the supernatant was clear. The residue of fine solids was kept in toluene in order to maintain their wettability.

3.6 Material Balance Check

The step-wise centrifuge tests involve measuring the volume of four layers: oil, rag, water, and sediment. Each layer may contain three components: oil, water, and solids. The sum of the components must equal the overall composition of the froth. Hence, a material balance can be performed on the measured layer volumes and compared with the

original froth composition. To perform the material balance, the layer compositions are required.

The hydrocarbons were assumed to be well mixed so that the solvent-to-bitumen ratio was uniform throughout the system. The oil layer was assumed to contain only diluted bitumen. The water layer was assumed to contain only water. The rag layer and sediment compositions are discussed below.

Rag Layer Composition

The procedure described for solids extraction was used to obtain the rag layer from the bitumen froth. Three rag layers were examined: 1) from LQOS3 froth diluted with n-heptane to a ratio above the asphaltene precipitation point; 2) from AQOS2 froth diluted with n-heptane to a ratio above the asphaltene precipitation point; 3) from LQOS3 froth diluted with toluene. The LQOS3 samples were collected after the 1500 rpm centrifuge step and the AQOS2 sample was collected after 1000 rpm centrifuge step. The reason was that rag volumes in the 1500 rpm for AQOS2 froth were inadequate for the experiment. The rag layer material is expected to contain oil, water, solids, and some precipitated asphaltenes.

In all the tests, the rag layer material was transferred to a glass test tube of known mass and centrifuged at 6000 rpm for 5 minutes resulting in an oil, water, and sediment layers. The oil layer was decanted with a small plastic pipette. The mass of the oil (solvent + bitumen) was determined from the change in mass of the test tube.

In all cases, the oil was spread drop wise on Whatman glass microfibre 934-AH filter (1.5 micron pore size). The filter paper had been dried in an oven for at least an hour at 70°C and weighed. After adding the oil, the filter paper was again dried in a fume hood, weighed and the mass of bitumen determined from the weight difference. For the heptane diluted rags the bitumen in the oil phase was assumed to be mostly maltenes because most of the asphaltenes had precipitated and had separated into the sediment layer.

In all the tests, water also was decanted with a small plastic pipette and its mass determined by weight difference. Since the sediment settled below the water layer, it was assumed to consist of solids in a water continuous phase. The mass of the water-filled sediment was determined. The sediment was then dried overnight at 80°C at atmospheric conditions and the dry weight determined. The change of mass was assumed to be water and was added to the previously determined mass of water.

For the heptane diluted rag layers, the dried sediment was dispersed in n-heptane by sonication and centrifuged at 4000 rpm for 5 minutes. The sonication and centrifuge steps were performed until the supernatant was clear. Then the sediment was dried overnight under vacuum at 60°C and weighed. Since only maltenes are soluble in heptane, the change in mass was considered to be maltenes. The same procedure was used for washing the dried sediment with toluene in this case, the change in mass was assumed to be asphaltenes.

For the toluene diluted rag, there were no precipitated asphaltenes because they are soluble in toluene. Therefore, the above procedure was used except that the sediment was washed only with toluene, and the change in mass was assumed to be bitumen.

Rag layer compositions were determined for two LQOS3 and one AQOS2 froth samples. The froth samples were diluted with toluene and n-heptane for LQOS3 and the AQOS2 sample was diluted with n-heptane only. The dilution ratios in the froth treatment were 2.66 g/g heptane-to-bitumen, and 4.11 g/g toluene-to-bitumen. Note, some asphaltenes precipitated in the heptane diluted froth. The compositions are provided in Table 3.5. Volumetric compositions are required later and are shown in Table 3.6. Note, rag layer volumes were different in the froth from different oil sands and they obtained from different rpms to collect the proper volume for the tests. Densities of 684, 867, 1000, and 1800 kg/m^3 were used for the heptane, toluene, water, and solids, respectively. The density of the rag layer solids was measured by Ms. Elaine Stasiuk using the Archimedes principle. The asphaltenes density used was 1192 kg/m^3 (Akbarzadeh et al., 2005). The

bitumen density was calculated 1006 kg/m³ using Equation 3.2 (Badamchizadeh *et al*., 2006):

$$\rho_{Bitumen} = (1020.0 - 0.6317T)e^{((0.02521T+6.8072)P\times10^{-7})} \quad \textbf{(3.2)}$$

where $\rho_{Bitumen}$ is the bitumen density in kg/m³, T is the temperature in °C and P is the pressure in kPa.

Table 3.5 Mass composition of rag layers from LQOS3 and AQOS2 froths diluted with n-heptane or toluene at 23°C. LQOS3 samples were centrifuged at 1500 rpm and AQOS2 sample was centrifuged at 1000 rpm.

Component	Heptane Diluted LQOS3 wt%	Toluene Diluted LQOS3 wt%	Heptane Diluted AQOS2 wt%
Solvent	37.3	42.7	22.3
Bitumen	-	12.4	-
Maltenes	12.3	-	11.9
Asphaltenes	2.9	-	9.6
Water	32.1	38.3	45.9
Solids	15.4	6.7	10.2

Table 3.6 Volumetric composition of rag layers from LQOS3 and AQOS2 froths diluted with n-heptane or toluene at 23°C. LQOS3 samples were centrifuged at 1500 rpm and AQOS2 sample was centrifuged at 1000 rpm.

Component	Heptane Diluted LQOS3 vol%	Toluene Diluted LQOS3 vol%	Heptane Diluted AQOS2 vol%
Solvent	49.4	47.5	31.2
Bitumen	-	11.9	-
Maltenes	11.5	-	11.8
Asphaltenes	2.2	-	7.7
Water	29.1	37.0	43.9
Solids	7.8	3.6	5.4

Sediment Composition

The porosity and composition of a sediment formed from the heptane and toluene diluted LQOS3 froths were determined as deposited. The sample was taken from the same experiment used for the rag layer composition measurement. It was assumed that the pore space was filled with only water since the sediment layer was below the water layer; that is, in a water continuous phase. The dilution ratio of heptane-to-bitumen was 2.66 g/g, with some asphaltenes precipitating. The dilution ratio of toluene-to-bitumen was 4.11 g/g. In the case of heptane, some of the precipitated asphaltenes did end up in the sediment. Some maltenes were found in the sediment and were assumed to have been adsorbed on or trapped within the solids. The composition was determined as follows:

For n-heptane diluted froth, all the material above the sediment layer in the test tube was decanted with a plastic pipette and the tube surface was cleaned with Kimwipes lint-free wipers. The weight and volume of the sediment was measured. The pore space was liquid filled at the time of the measurement. The tube was dried overnight in an oven at 80°C under atmospheric conditions and the mass remeasured. The mass of evaporated water

was simply the change in mass. The porosity of the sediment was determined to be 44.1 vol% by dividing the volume of evaporated water to the total volume of sediment.

The dry sediment was then washed with n-heptane and the tube was dried overnight under vacuum at 60°C, followed by a mass measurement. Since only maltenes are soluble in heptane, the mass of maltenes was equal to the change in the mass of the test tube. The dry sediment was then washed with toluene; the test tube dried again, the mass measured, and the mass of the remaining solids and asphaltenes calculated.

For toluene diluted froth, the porosity of the sediment was not measured because the test tube used in this experiment was not graduated. The same procedure was implemented to determine the sediment components but the dry sediment was washed only with toluene. The mass measured after drying the test tube was used to calculate the mass of the remaining solids and bitumen. Table 3.7 presents the composition of the sediment layer for these two cases.

Table 3.7 Composition of sediment layer from LQOS3 froth diluted with n-heptane and toluene at 23°C.

Component	Heptane Diluted LQOS3 wt%	Toluene Diluted LQOS3 wt%
Bitumen	-	6.2
Maltenes	3.2	-
Asphaltenes	2.7	-
Water	28.9	44.7
Solids	65.2	49.1

The overall froth composition was calculated from the layer volumes and compositions. The calculated composition is compared with the measured froth composition shown in Table 3.8. The material balances for froth diluted with n-heptane and toluene close to within 2.8% and 5.4%, respectively. Considering the number of mass and volume measurements used to calculate the composition as well as the variability of the froth samples, the overall agreement with the measured data is very good.

Table 3.8 Comparison of measured and calculated froth compositions.

	Heptane diluted froth		Toluene diluted froth	
	Assay, wt%	Calculations, wt%	Assay, wt%	Calculations, wt%
Bitumen	15. 7	12.3	10.1	13.4
Solids	26.4	30.7	17.2	28.8
Water	57.9	59.8	72.7	63.2
Total	100.0	102.8	100.0	105.4

3.7 Micrographs of the Rag Layer

A froth sample from LQOS3 was diluted with n-heptane and centrifuged at 1500 rpm for 5 minutes. Small samples of the rag layer from four different layers from the top to the bottom of the rag layer were transferred using a small spatula to concave glass slides and then covered with glass slip covers. The micrographs were taken with a Carl Zeiss Axiovert S100 inverted microscope equipped with a video camera and an Image Pro image analysis software.

3.8 Size distribution of Rag Layer and Sediment Solids

Solid particles were obtained both from rag layer and sediment layers as described in section 3.5. The particle size and size distribution of solids were obtained with a Malvern Instrument Model 2000 Mastersizer particle size analyzer. The analyzer's detection range was from 0.020 to 2000 μm. Samples were prepared by adding approximately 0.2 grams

of solids to about 20 ml of RO water. Both sonication and heating (80°C) were used to disperse solids in water. The mixture was then send to the 2000 Mastersizer particle analyzer.

3.9 Floatability of Rag Layer and Sediment Solids

Rag layer and sediment solids samples were recovered from the step-wise experiments as described in section 3.5. The samples were stored in toluene in an attempt to maintain their wettability; as drying does change the wettability of the solids (Chen, Finch and Czarnecki, 1999).

Floatability of Rag Layer Solids

The floatability of the rag layer solids was qualitatively assessed using a mixture of water and methanol. A layer of particles was spread on the surface of a mixture of water and methanol, and the methanol content was step-wise increased and the percentage of floating particles was measured at each step. Larger and more water-wet particles tend to sink at low methanol mole fractions while smaller and more oil-wet particles tend to float in an increase in mole fractions of methanol.

The apparatus shown in Figure 3.11 was developed for this experiment. A glass dish containing a solution of methanol and RO water was placed on the stage of a Carl Zeiss Axiovet S100 microscope. A small cylinder was placed in the dish so that it enclosed a circular area at the methanol/water interface. A floating polystyrene piston was placed within the cylinder. A Teflon sheet of 0.82 mm ID hole at its center was attached to the bottom of the piston. To perform an experiment, a layer of solids was placed within this hole. The Teflon sheet prevented the solids from spreading beyond the hole or sticking to the walls. The piston allowed the chamber to rise as methanol was added to the system.

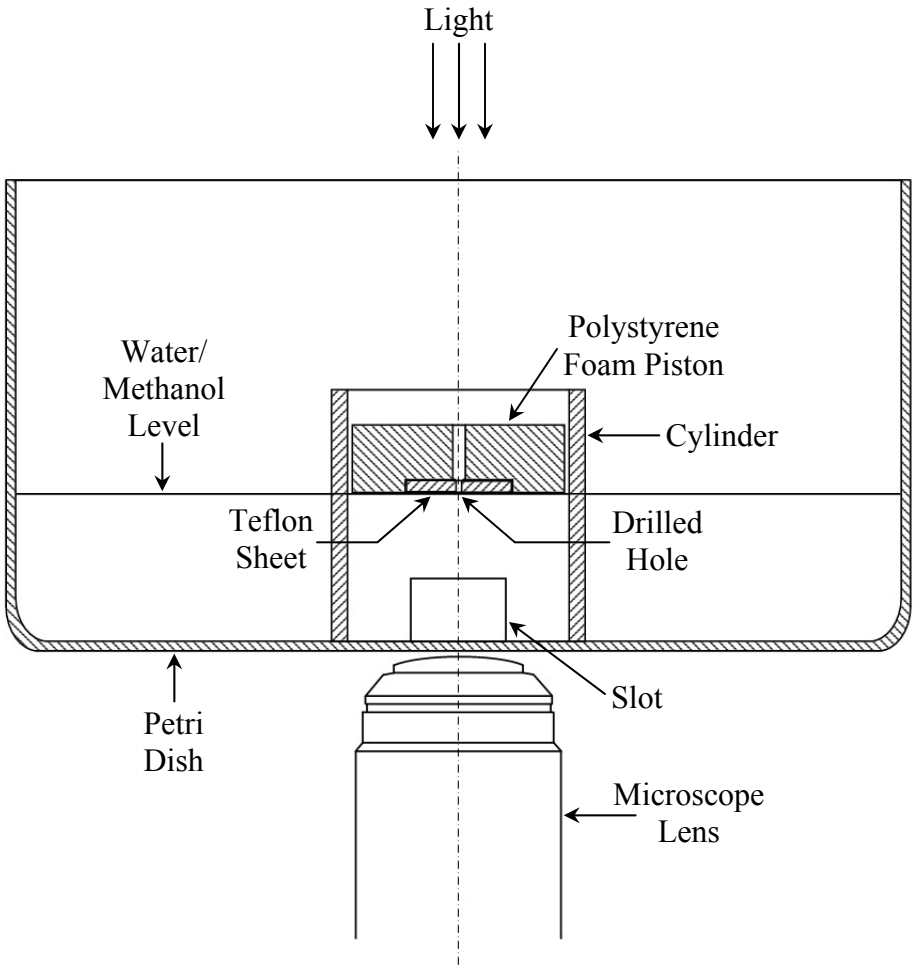

Figure 3.11 Schematic of apparatus for floatability tests.

The size of the hole was chosen so that the microscope could focus on the entire area of the hole. Images were captured with a video camera and analyzed using the Image Pro software. The area covered with fines was dark in the images. When the particles sank, some light areas appeared. The amount of floating particles was determined from the ratio of the dark area divided by the total area of the hole.

For this technique, the layer of particles on the methanol/water surface was assumed to be a monolayer. To obtain a monolayer, the solids were dispersed in toluene by sonication.

Droplets of fines and toluene were transferred to the surface of RO water in the hole in the Teflon sheet. Upon evaporation of toluene a thin layer of fines remained on the water surface. Enough solids were added to cover just the surface of the hole.

Methanol then was added to water using a Luer-lok tip syringe with a 20 gauge 1.5 inch needle to obtain the desired volume fraction and the mixture was mixed by a small magnetic stir bar for one minute. During mixing, the glass dish was covered with a watch glass to reduce the evaporation of methanol. Each time methanol was added the height of the liquid interface was increased. However, the microscope lens could only focus to less than two centimeters from the lens surface. Therefore, for each new volume fraction some of the solution was withdrawn from the Petri dish using the syringe.

Floatability of Coarse Solids

Due to larger size of coarse solids in the sediment (5 to 6 micron mean particle diameter), the microscope measurement was not used and the weight percent of floating solids was determined by weight difference. Some droplets of dispersed solids in toluene were transferred to the pure RO water surface; once transferring, almost all of the solids immediately sank. The solids from the water surface were transferred to a small beaker. Both the beaker and the Petri dish were dried for 48 hours under vacuum at 50 and 80°C and the mass determined. Note, over 95 wt% of the solids sank in the water.

Chapter 4

Hindered Settling Model

Froth treatment processes employ either gravity settling or centrifugation. Since froth consists of water droplets and solid particles, these processes involve hindered settling. A numerical model was developed based on well established hindered settling model to help assess the role of hindered settling on rag layer formation.

4.1 Development of the Model

The velocity of a single particle settling through a dispersion of particles is given by Equation 4.1 (Masliyah, 1979):

$$v_s - v_f = \frac{a d_s^2 (\rho_s - \rho_f)}{18 \mu_f} \alpha_f F(\alpha_f) \qquad \textbf{(4.1)}$$

where v_s is the velocity of the particles, v_f is the fluid velocity and d_s is the particle diameter. ρ_s and ρ_f are the particle and fluid densities, respectively and α_f is the volume fraction of fluid or the suspension voidage. The term $F(\alpha_f)$ is a function that accounts for particle concentration, Equation 4.2:

$$F(\alpha_f) = \alpha^n \qquad \textbf{(4.2)}$$

The exponent *n* is an empirically determined constant and, in this model, it is calculated using equations 4.3 to 4.7 (Richardson and Zaki, 1997):

For Re < 0.2

$$n = 4.65 + 19.5 d / D$$

(4.3)

for $0.2 < \mathrm{Re} < 1$

$$n = (4.35 + 17.5d / D)\,\mathrm{Re}^{-0.03} \quad \textbf{(4.4)}$$

for $1 < \mathrm{Re} < 200$

$$n = (4.45 + 18d / D)\,\mathrm{Re}^{-0.1} \quad \textbf{(4.5)}$$

for $200 < \mathrm{Re} < 500$

$$n = 4.45\,\mathrm{Re}^{-0.1} \quad \textbf{(4.6)}$$

and for $\mathrm{Re} \geq 500$

$$n = 2.39 \quad \textbf{(4.7)}$$

where d is the diameter of a spherical particle and D is the diameter of the settling vessel. Note, at Reynolds numbers greater than about 500, n is independent of d/D and the Reynolds number. Based on the small diameter of the particles found using the stepwise centrifuge tests, the ratio of d/D was considered negligible.

Equation 4.1 provides the settling rate of an individual particle and shows that the settling rate of an individual particle depends on the local concentration of other particles. In a vessel, the settling of the suspension is simply the collective settling rates of all of the particles. In most cases, there are two regions of interest (Shih, Gidaspow and Wasan, 1987) as shown in Figure 4.1: 1) an upper interface between the uppermost particles and the particle-free fluid above; 2) a lower interface between settling particles and a rising sediment.

For an initially homogeneous suspension of monodisperse particles, all of the particles can be assumed to settle at the same rate. In this case, Equation 4.1 can be used to determine the movement of the upper interface. When a polydisperse dispersion like a froth is settling in a vessel, the local concentration changes over time as particles of difference size and density settle at different rates. Hence, an iterative procedure is required.

A numerical model developed by Valinasab and Yarranton (2006) was adapted for this study. In this model, a cylindrical settler is divided into layers of equal height, Figure 4.1. At time zero, the particles in the model are uniformly distributed throughout the vessel. At each time step, the concentration of the particles in each layer is determined and the settling rate of each particle is calculated. The distance each particle moves is calculated and its location updated. The concentration of particles in each layer is updated and the next iteration begun. When the particle concentration in the lowest non-sediment layer reaches the concentration of a sediment, that layer is considered to be a sediment layer and no further settling is occured into that layer. The height of the upper interface and the top of the sediment are determined at each time step.

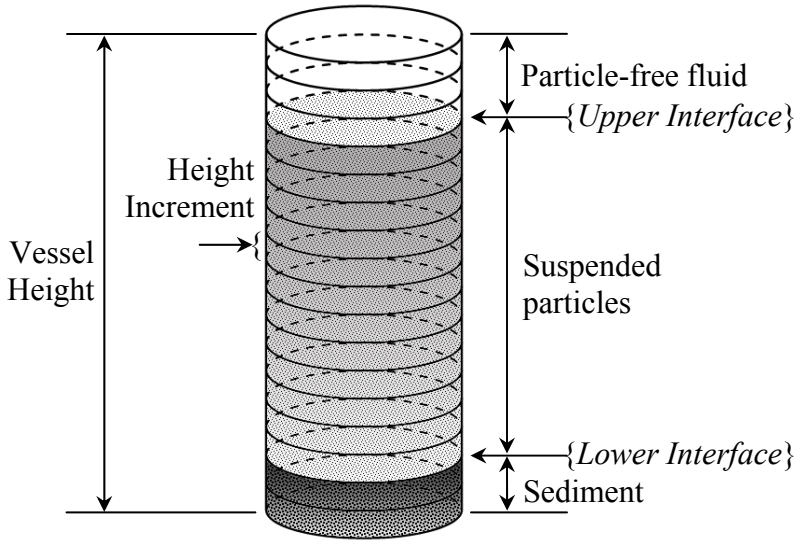

Figure 4.1 Geometry of the settling model (Adopted from Valinasab, 2006)

It is not practical to track every particle in a concentrated dispersion. Instead, the locations of a limited number of particles are calculated in the model, typically about 10000 particles. The actual particle volume fractions are scaled up from the model particles and these volume fractions are used to determine the fluid volume fractions for the settling equation, equation 4.1.

Modifications made to the literature hindered settling are discussed in the following:

1. The original model used a fixed acceleration in the settling rate calculation. In the modified version, an initial centrifuge rotor speed of 500 rpm was used and the acceleration was determined from Equation 4.8:

$$a = r\omega^2 \tag{4.8}$$

where a is the particle acceleration, r is radius of path of particle, and ω is the angular velocity. In this study, the radius was set to 6.75 cm. After each centrifuge step time (5 minutes), 500 rpm was added to the previous step centrifuge rpm. At the end of each centrifuge step time, the volume fraction of each particle type was calculated and was then used to obtain the volumes of oil phase, rag layer, water and sediment. The program terminated when the settling time was equal to the total centrifuge time of 40 minutes.

2. To calculate the exponent of n in Equations 4.3 to 4.7 the Reynolds number of a single settling particle at its terminal velocity in an infinite medium is required (Richardson and Zaki, 1997). The following method was used to determine n (McCabe, Smith and Harriott, 1985):
    a. Input a low Reynolds number (Re = 0.1).
    b. Calculate the drag coefficient from Equations 4.9 to 4.15 by fitting to drag coefficient plot of Figure 4.2 for spherical particles. Equations 4.9 to 4.15 can only be used for the following Reynolds:

for $0.05875 \leq \mathrm{Re} \leq 7.015$

$$C_D = 31.92883\,\mathrm{Re}^{-0.93346} \tag{4.9}$$

for $7.015 < \mathrm{Re} \leq 512.9$

$$C_D = 15.01402\,\mathrm{Re}^{-0.54452} \tag{4.10}$$

for $512.9 < \mathrm{Re} \leq 4764$

$$C_D = 1.50593\,\mathrm{Re}^{-0.16210} \quad \textbf{(4.11)}$$

for $4764 < \mathrm{Re} \leq 34670$

$$C_D = 0.15572\,\mathrm{Re}^{0.10648} \quad \textbf{(4.12)}$$

for $34670 < \mathrm{Re} \leq 264800$

$$C_D = -7.35980\times10^{-18}\,\mathrm{Re}^3 + 1.62260\times10^{-12}\,\mathrm{Re}^2 - 3.46881\times10^{-7}\,\mathrm{Re} + 0.48848 \quad \textbf{(4.13)}$$

for $264800 < \mathrm{Re} \leq 338800$

$$C_D = 1.71921\times10^{28}\,\mathrm{Re}^{-5.28541} \quad \textbf{(4.14)}$$

for $338800 < \mathrm{Re} \leq 5012000$

$$C_D = 0.03920 \quad \ln(\mathrm{Re}) - 0.40175 \quad \textbf{(4.15)}$$

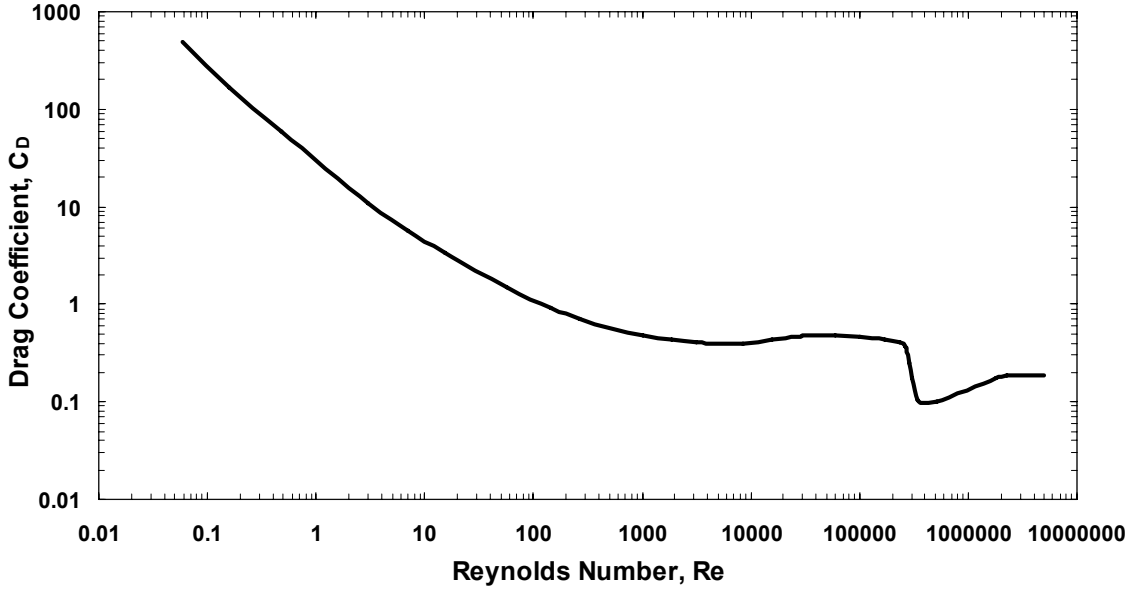

Figure 4.2 Drag coefficient for spheres (Data adopted from Donley, 1991).

c. Calculate terminal velocity of a single particle using Equation 4.16;

$$v_t = \sqrt{\frac{4a(\rho_p - \rho)d}{3C_D\rho}} \quad \textbf{(4.16)}$$

where v_t is the terminal velocity of a single particle in an infinite medium, ρ_p is density of the particle, ρ is density of the medium and C_D is the drag coefficient.

d. Calculate the Reynolds number with v_t.
e. Use the calculated Reynolds number in step "b" and recalculate the "Re" until convergence is achieved ($\varepsilon \leq 0.01$).

The program used the Reynolds number calculated in the previous step and then n was calculated from Equations 4.3 to 4.7.

3. Four types of particles were defined: free water, emulsified water, coarse solids, and fine solids. Coarse solids were permitted to settle through any layer except the sediment layer. Free water was permitted to settle through any layer except for a sediment layer as the void space was assumed to be full of water. Emulsified water and fine solids were not permitted to settle through a water-oil interface.

4. The free water droplets were allowed to settle unhindered and the velocity was calculated using Stokes Law (McCabe, Smith and Harriott, 1985). This step was required to avoid very high particle concentrations which slowed the settling rate to almost zero. It is likely that the free water coalesces rapidly and forms continuous flow channels rather than undergoing hindered settling. These channels could be observed in some of the experiments. The very rapid formation of the free layer (formation began in just a few seconds) in all experiments suggests that this channel flow occurred in all cases.

5. Only free water particles were permitted to settle into a sediment layer, displacing the oil medium. Once the volume fraction of fluid and solid particles equaled unity in a sediment layer, no further settling was permitted into that layer.

6. If the volume fraction of free water in a layer was more than a defined maximum (0.5 was used in this study), then that layer was considered to be a free water layer. Fine solids and emulsified water were not permitted to settle into the uppermost free water layer. The uppermost free water layer was determined by finding the free water layer adjacent to a non-free water layer above it. Note, particles already in the free water layer were still free to settle through that layer.

7. In some cases, a layer from the bottom of the vessel may be full of free water, while coarse solids continue to settle into that layer. In this case, a counterflow of water was calculated equal in volume of the solids that settled into that layer. This water volume was added to the layer above. This process continued until no more solids were settling or the layer became a sediment layer.

8. To simplify the program, the medium density and viscosity were assumed to equal the oil phase properties for all the layers. This assumption results in too high a viscosity and too low a density in the water layer. Hence, the settling rate of particles through the water layer will be underpredicted. The only output affected is the rate of sediment formation. The sediment forms so rapidly that this error is trivial. As well, the settling rate in the free water layer was not of interest in this study.

A schematic of the logic flow of the developed settling program is provided in Figures 4.3 and 4.4.

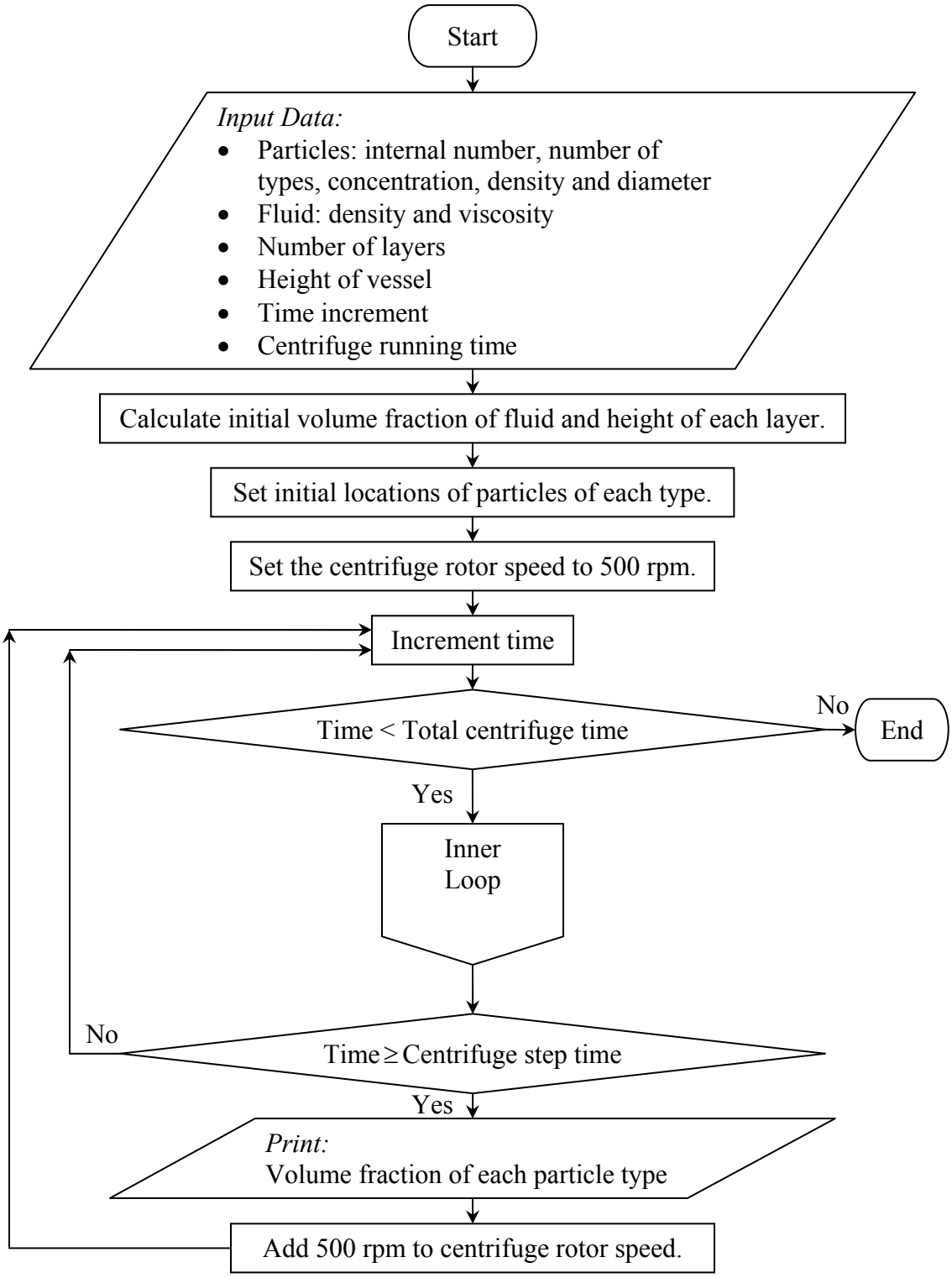

Figure 4.3 Flow diagram of the numerical model

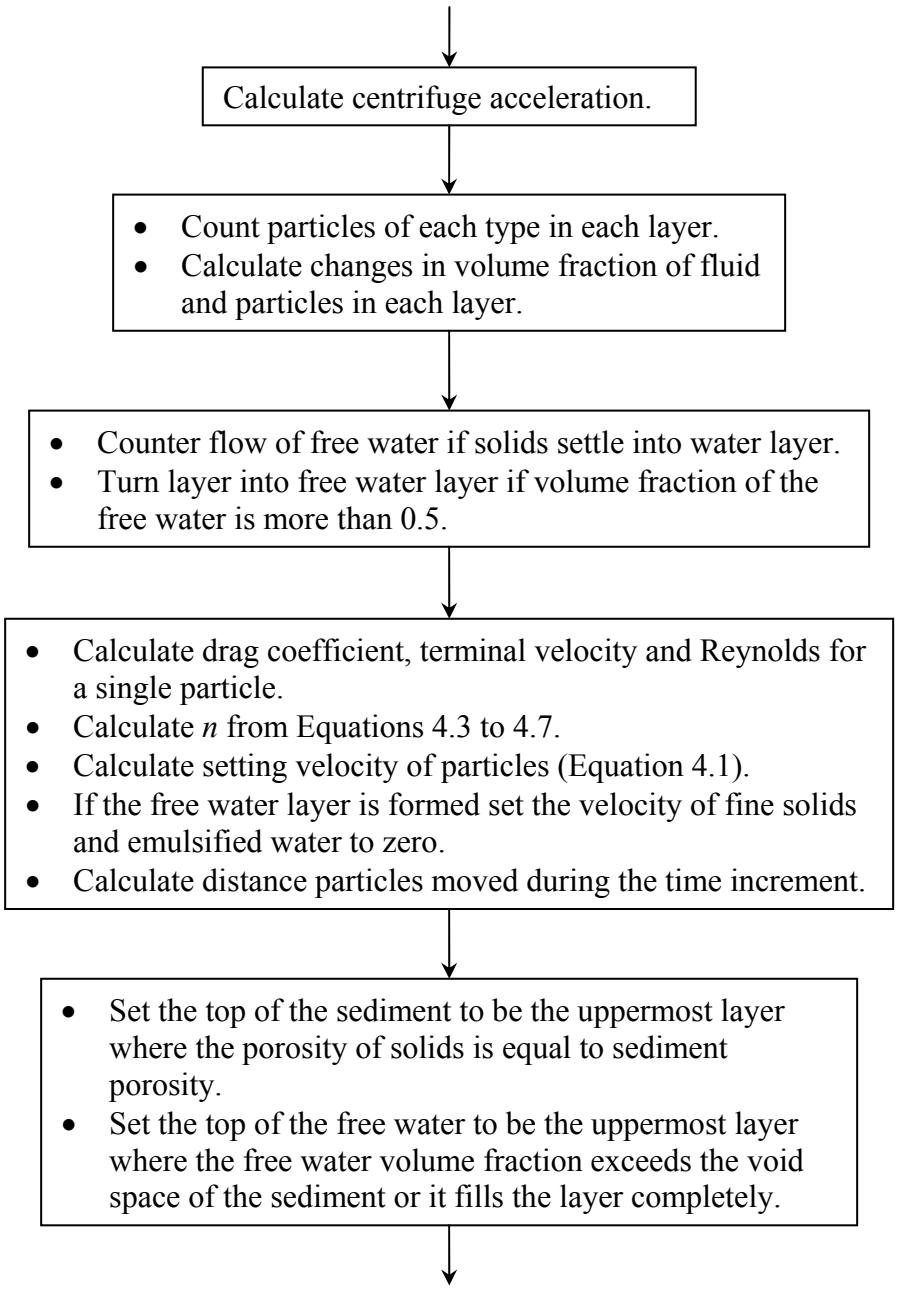

Figure 4.4 Flow diagram of the model's inner loop

4.2 Model Validation

Before using the model to simulate stepwise centrifuge tests, it was tested on two sets of data obtained from literature for settling of bitumen froth diluted with a paraffinic solvent (Long, *et al*., 2004). Long, *et al*. (2004) studied the structure of water-droplet/dispersed-solids/precipitated-asphaltenes (WD/DS/PA) aggregates in diluted bitumen froth as well as the effect of mixing temperature on the settling rate of these aggregates. They used the Richardson-Zaki approximation to model the hindered settling rate, Equation 4.18, (Richardson and Zaki, 1997);

$$u = u_0 \alpha^n \qquad \textbf{(4.18)}$$

where u is the hindered settling rate and u_0 is the free settling rate of the aggregates. They developed an experimental method to determine values of α and n using their data, Table 4.1. Table 4.1 also shows the reported composition and properties of the suspension and the structural parameters of the WD/DS/PA aggregates; however the sediment porosity was not reported. Values of 47.5% and 50% were found to fit the final height of the sediment at 30 and 70°C, respectively.

Table 4.1 Structural parameters of the WD/DS/PA aggregates and properties of the suspension from Long *et al*. (2004).

	Mixing temperature, °C	
	30	70
Solvent-to-bitumen ratio (C7/ bitumen), wt/wt	3	3
Settling temperature, °C	30	30
Average diameter of the aggregates, μm	56	90
Volume fraction of aggregates in suspension, 1-α	0.123	0.127
Average effective density of aggregates, g/ml	0.884	0.868
Density of the medium (oil phase), g/ml	0.7403	0.7403
Viscosity of the medium (oil phase), mPa.s	0.817	0.817
Richardson-Zaki coefficient, n	11.43	7.02

Figure 4.5 shows Long *et al*.'s (2004) experimental data for the two cases of Table 4.1 and the predictions from the numerical hindered settling model. The model correctly matches the movement of the upper interface including the point at which it joins the sediment. Note, the compaction of the sediment is not included in the model. Moreover, the values of *n* in Long *et al*.'s (2004) paper have been obtained experimentally and are slightly greater than the values than can be obtained from Equations 4.3 to 4.7. This might be a possible source of error in the model assumptions that resulted in a small deviation from Long *et al*.'s (2004) data. While the values obtained from Richardson-Zaki, Equations 4.3 to 4.7, for the coefficient *n* are consistent for our data, obtaining experimental higher values for *n* is not unusual (Burger *et al*., 1999).

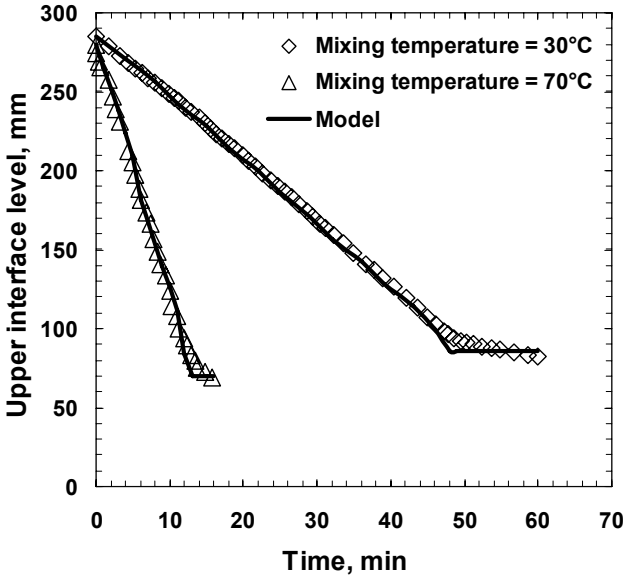

Figure 4.5 Height of the upper interface from settling data of C7-diluted bitumen froth (Long, *et al*., 2004) compared with the model results

Chapter 5

Rag Layer Composition

Rag layers formed from heavy oils and bitumens are expected to be similar to rag layers in conventional oils. Typically, these rag layers are oil continuous with dispersed water-in-oil emulsions, solids, and oil-in-water-in-oil multiple emulsions. In this chapter, visual observations of the rag layer from oil sands froth are reported. The distribution of the water and solids is reported, and the floatability of the solids is determined. The rag layer composition is determined reported as the oil, water, and solids content.

5.1 Rag Layer Components

Visual Observations

Figures 5.1 and 5.2 are micrographs of material from the top and the bottom of the rag layer prepared from LQOS3 froth diluted with n-heptane at a ratio of 0.66 g diluent per 1 g bitumen and centrifuged at 2000 rpm. The gray color in these images is the diluted bitumen continuous phase. The transparent spheres are water droplets and the black particles are small water droplets, silica, and clays. Note, at the S/B ratio of 0.66 g/g no asphaltenes precipitate. The large translucent patches in Figure 5.2 are likely free water that has settled to the bottom of the microscope slide. No evidence of complex emulsions was detected from these measurements under normal light.

These observations are comparable to the observations of Chen *et al*. (1999). They diluted a bitumen froth sample with heptane at a 2:1 heptane-to-froth weight ratio. In the rag layer that formed after two hours settling, they reported the presence of fine solids, water, asphaltenes, and diluted bitumen. They also noted the presence of fine solids less than 1 μm in diameter.

Emulsified water and solid particles were observed in all rag layers. The bottom layer contained larger water droplets and some free water. While it is not obvious from just two pairs of images, the bottom layer also contained more solid particles. In general, the particles were smaller in the upper layers of rag. These observations are expected within a settling process.

The micrographs also show that, after preparation on the microscope slide, fine particles and emulsified water droplets were scattered randomly in the oil phase. Any significant aggregation that may have occurred during settling was disrupted when the samples were collected. This observation suggests that the rag layer is a loose structure of layed materials at the interface rather than a consolidated matrix of fine solids and emulsion.

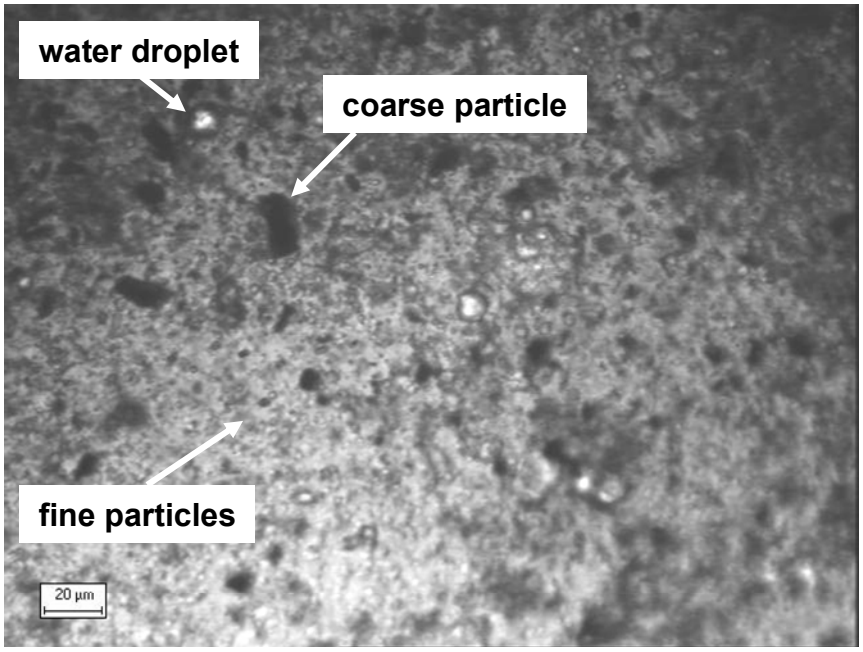

Figure 5.1 Micrograph of a sample from the top layer of the rag layer.

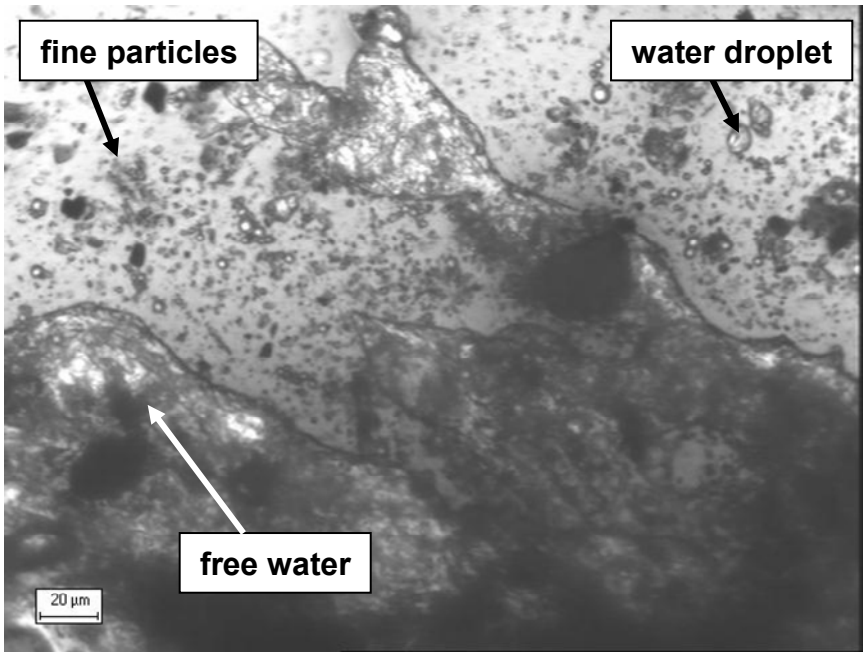

Figure 5.2 Micrograph of a sample from the bottom layer of the rag.

Emulsified water

A size distribution of emulsified water in the rag matrix was obtained from several micrographs of rag layers using the Image Pro image analysis software of Carl Zeiss Axiovert S100 microscope. Figure 5.3 shows number and volume frequency of emulsified water in the rag layer formed in LQOS3 froth diluted with n-heptane. The average drop mean diameter is 6.2 microns. This distribution includes samples from several locations within the rag layer and is intended to indicate the average distribution of the whole rag layer. As noted in Figures 5.1 to 5.2, the drop size increases from the top to the bottom of the rag layer.

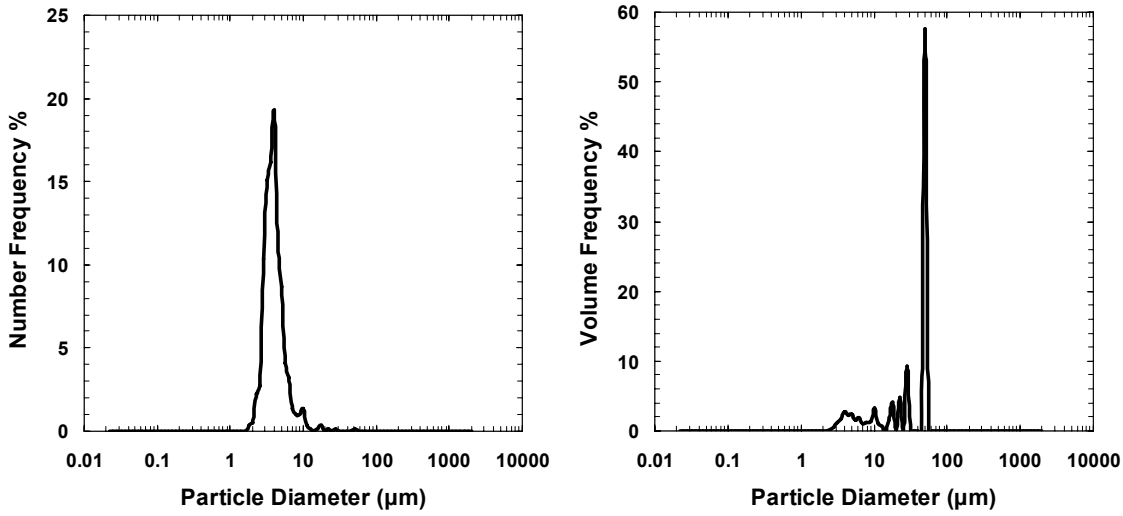

Figure 5.3 Number and volume frequency of emulsified water droplets in rag layer formed in LQOS3 froth diluted with n-heptane.

Rag Layer and Sediment Solids

Figure 5.4 shows number and volume frequency of the solids extracted from rag layers in LQOS3 and AQOS2 froths diluted with n-heptane. The number mean diameter of the particles from the LQOS3 rag is 0.14 μm, much smaller than the mean diameter of 3.98 μm for the particles from the AQOS2 rag. The volume frequency distribution indicates that the main difference between the LQOS3 and AQOS2 particles is a significant amount of 0.05 to 0.5 μm diameter particles in the LQOS3 sample. The very fine particles in the LQOS3 are of interest because fine particles have been implicated in stabilizing water-in-oil emulsions (Sztukowski and Yarranton, 2004), which would then contribute to rag layer growth. Indeed, larger rag layers are observed with the LQOS3 froth.

Figure 5.5 shows the size distribution of the solids extracted from sediment layers in LQOS3 and AQOS2 froths diluted with n-heptane. The size distributions for the two samples are similar although the AQOS2 sample contains a broader range of larger particles. The mean particle diameter for the sediment layers from LQOS3 and AQOS2 froths are 4.94 and 5.79 microns respectively.

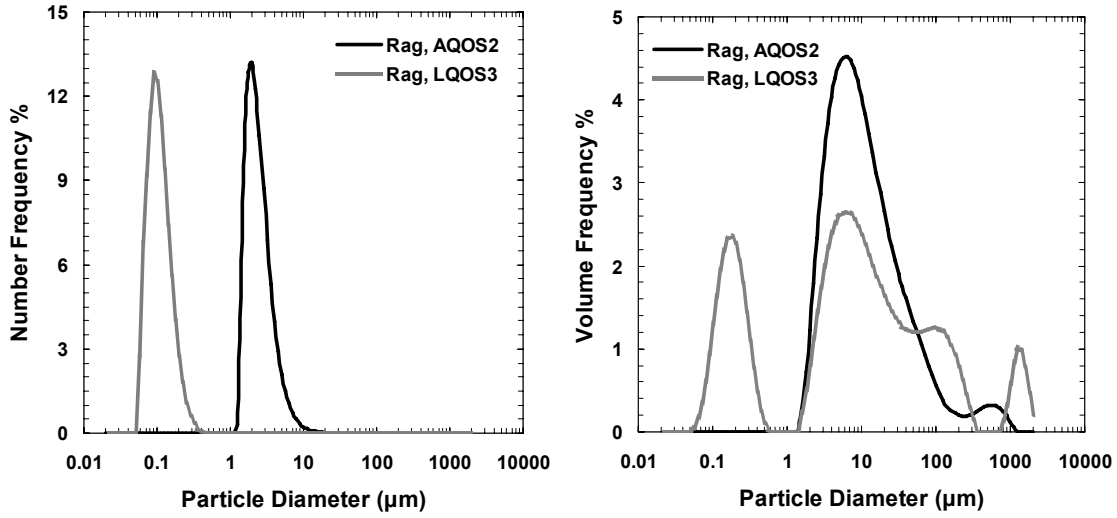

Figure 5.4 Number and volume frequency of solids in rag layer extracted from LQOS3 and AQOS2 froths diluted with n-heptane.

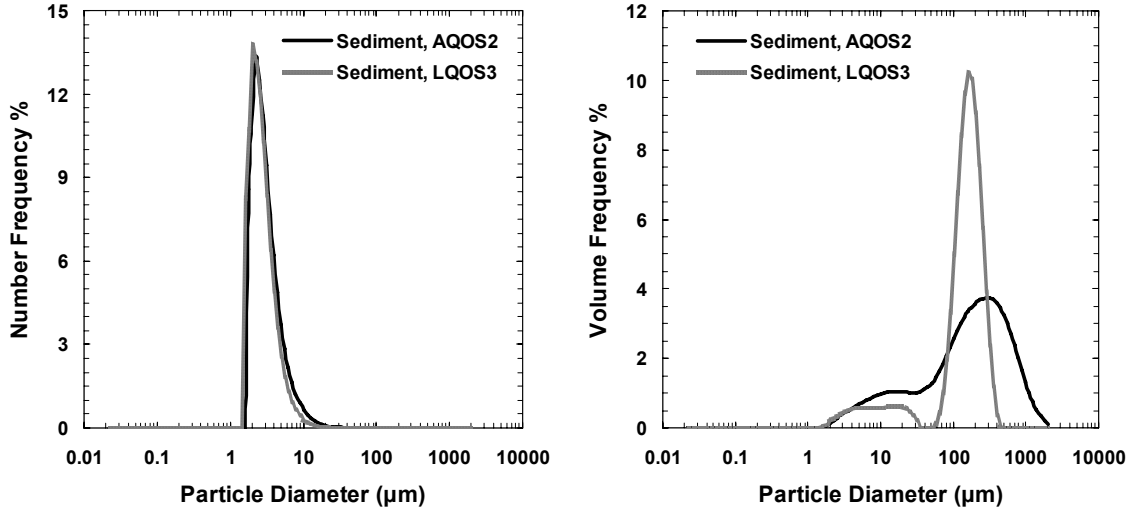

Figure 5.5 Number and volume frequency of solids in sediment layer extracted from LQOS3 and AQOS2 froths diluted with n-heptane.

Composition of Solids

The composition of the solids in the rag layer was not determined in this study. However, Sztukowski and Yarranton (2004) studied the composition of fine solids from Athabasca bitumen using X-ray diffraction, scanning electron microscopy, and transmission electron microscopy. Based on their studies, the fine solids in oil sands are plate-like clay particles mainly composed of kaolin minerals. They also observed smaller quantities of non-clay minerals such as pyrite, quartz, and titanium oxide.

Kotlyar, Kodama, Sparks and Grattan-Bellew, (1987) studied bitumen-free solids from different grades of Athabasca oil sands. They found the solids are enriched with metals (Cr, Ni, V, Zr, Al, Fe, Mn), and sulfur, both in fine and coarse solids. They also analyzed the mineralogical compositions of coarse and fine solids samples by X-ray diffraction. They reported the presence of mica, kaolinite, quartz and feldspar in these solids. Based on their studies, the majority of solids are comprised of non-crystalline inorganic components.

Yan, Gray, and Masliyah (2001) found that kaolin clays can adsorb asphaltenes to form intermediate to oil-wet particles. It is likely that the fine solids from an oil sands froth are intermediate to oil-wet particles.

Floatability of solids

The floatability of the rag layer and sediment solids was measured in solutions of water and methanol using the method described in Chapter 3. Figure 5.6 shows the floatability of the rag layer solids. The solids float on water and do not sink until the liquid phase composition reaches 70 vol% methanol. The flotation of the solids depends both on their size and their wettability; that is smaller; more oil-wet solids will sink at higher methanol content. While the effects of size and wettability cannot be separated in this test, the results are consistent with intermediate to oil-wet particles.

In contrast, over 95% of the coarse solids from the sediment layer settled immediately in water. These relatively large particles are probably water-wet silicates. The large contrast

between the floatability of the rag layer and sediment solids is consistent with the observed settling behavior. The sediment tends to form very rapidly as the coarse water-wet solids settle almost unimpeded. The fine, possibly oil-wet, solids are unable to pass through the free-water layer and collect at the oil-water interface as part of the rag layer.

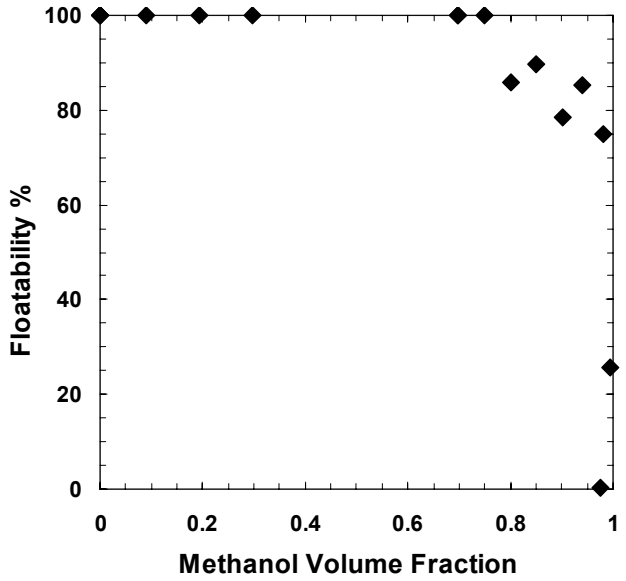

Figure 5.6 Wettability of fine solids measured by their floatability

5.2 Rag Layer Composition

Two methods were used to investigate the composition of rag layer: 1. analysis of samples; 2. material balance calculations from step-wise centrifuge tests. The sample analysis was presented in Chapter 3 and will be used to check the material balance calculations.

Figure 5.7 shows how the volumes of the sediment, free water, rag, and oil layers change during a stepwise centrifuge test. During each centrifuge step, the rag layer shrinks, liberating oil, water, and possibly some solids. At the end of the final centrifuge step, the volume of the rag layer was less than 5% of its initial volume at 500 rpm. Since the final

volume is so small, the initial oil and water content of the rag layers could be determined with reasonable accuracy based on the volumes of liberated oil and water. The calculated solid content depends on the assumed composition of the final rag layer, which was adjusted to best match the experimental data.

The following assumptions were made for the material balance calculations:

- No measurable solids settled from the rag layer after the 500 rpm step. This assumption was based on the observations from the experiments which showed little evidence of increasing the sediment volume at higher rpms. Some settling of solids almost certainly occurred but could not be assessed because the sediment was compacting simultaneously.
- There is no water in the rag layer after centrifuging at 4000 rpm. Visual inspection of micrographs of rags remaining after 4000 rpm found solid particles but no evidence of emulsified water. As well, in many cases, assuming final water contents greater than 10 vol% led to physically impossible initial compositions.
- The solids content of the rag layer after 4000 rpm was 70 vol%. A solid volume fraction of 65% was measured for a sediment layer that had been centrifuged at 4000 rpm. Assumed values of 60 and 70 vol% both provided reasonable agreement with the measured composition for the rag that formed in heptane diluted LQOS3 froth, Table 5.1. Lower solids contents are not consistent with expected particle packing and higher solids contents deviated further from the measured solid content. Note, the compositions determined for toluene diluted LQOS3 froth, Table 5.2, appear to under-predict the water content in all cases. However, even if large water volume fractions are assumed in the 4000 rpm rag layer, the measured water content cannot be matched. The likely reason for the discrepancy was that the froth sample that was used for the composition measurement was not the same sample used in the step wise tests. Unfortunately, there are no more samples with which to repeat the measurements.

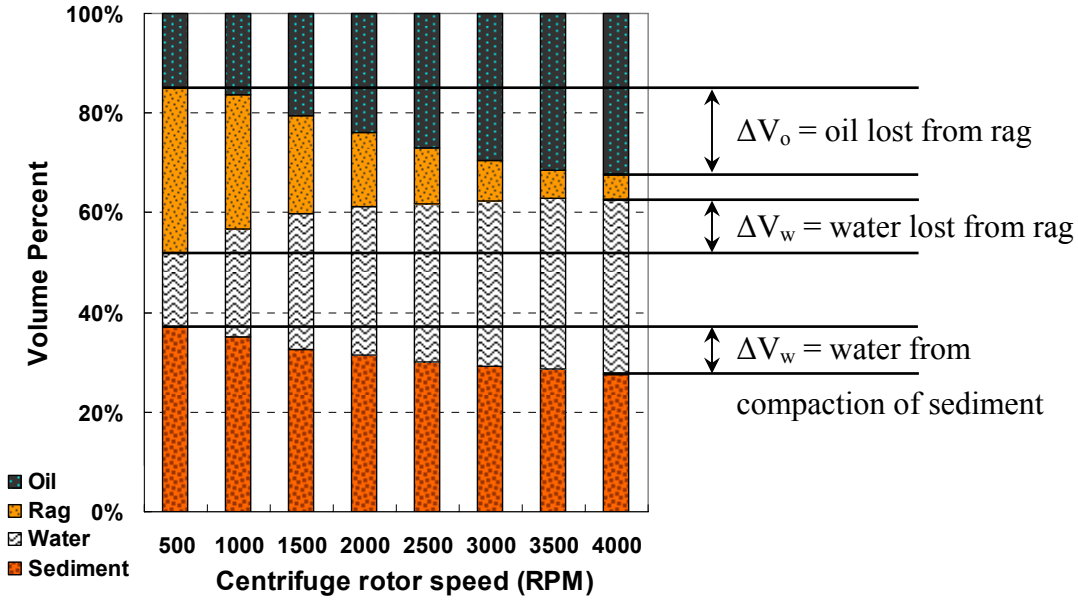

Figure 5.7 Volume differences of rag layer at 4000 and 500 rpm

Table 5.1 Rag components of LQOS3 froth diluted with n-heptane at 1500 rpm.

	Experiment, vol%	Material balance calculations, Solids vol%		
		70%	60%	50%
Oil	60.7	64.7	65.5	66.2
Water	29.2	24.1	24.1	24.1
Solids	10.0	11.2	10.4	9.7

Table 5.2 Rag components of LQOS3 froth diluted with toluene at 1500 rpm.

	Experiment, vol%	Material balance calculations, Solids vol%		
		70%	60%	50%
Oil	59.3	61.1	64.4	67.6
Water	37.1	18.7	17.4	16.5
Solids	3.6	20.2	18.3	15.8

Material balance calculations were performed to determine the composition of the rag layer at 500 rpm based on the data of Appendix A. The data was first screened to remove data with low initial rag volumes or high scatter in the layer volume measurements. Approximately 50% of the data were used in the material balance calculations. The calculated volumetric compositions for LQOS3 and AQOS2 diluted froths after the 500 rpm centrifuge step are given in Tables 5.3 and 5.4, respectively.

The solids contents in the rag layers are nearly equal, although slightly lower in toluene diluted froths. However, this apparent equality may be an artifact caused by the assumption that solids content in the final rag layer was 70 vol% in all cases. The rag layers in heptane and heptol 80/20 diluted froths have significantly higher water content than those from toluene diluted froths. As will be discussed in Chapter 7, the heptane and heptol 80/20 rag layers are thinner than the toluene rag layers. These results suggest that the rag layers in heptane and heptol 80/20 are more compact resulting in lower oil content, higher water content, and possibly higher solids content. Water droplets and solids are known to flocculate more readily in heptane rather than toluene. Hence, more compact rag layers are expected as the heptane content increases.

Table 5.3 Volumetric composition of rag layer in diluted LQOS3 froths calculated after 500 rpm centrifuge step.

	Heptane, vol%	Heptol 80/20, vol%	Toluene, vol%
Oil	36 ±21	44 ±6	57 ±11
Water	43 ±11	40 ±8	25 ±13
Solids	21 ±12	16 ±3	18 ±11

Table 5.4 Volumetric composition of rag layer in diluted AQOS2 froths calculated after 500 rpm centrifuge step.

	Heptane, vol%	Heptol 80/20, vol%	Toluene, vol%
Oil	18 ±10	35 ±18	58 ±19
Water	59 ±3	42 ±15	26 ±19
Solids	23 ±8	23 ±5	16 ±1

Chapter 6

Mechanisms of Rag Formation

There are several mechanisms that can lead to formation of the rag layer. In this study, three possible mechanisms are considered: a mechanical barrier, hindered settling, and slow coalescence. If the froth contains oil-wet materials, they may accumulate at the interface and form a barrier that prevents water and solid particles from passing through. Hindered settling decreases the rate at which emulsion droplets and solid particles settle. If the settling rate is too slow, rag layers will form in a continuous process. Finally, the emulsified water in froths is stabilized by a coating of asphaltenes (Khadim, Sarbar, 1999) and hence the surface is oil-wet. These droplets may not settle through the interface until they coalesce to large sizes or in effect coalesce with the free water layer. If the coalescence rate is slow, a rag layer may accumulate.

6.1 Mechanical Barrier

As was shown in Section 5.1, diluted froth contains intermediate to oil-wet fine solids and, in some cases, precipitated asphaltene particles. If these oil wet solids accumulate at the water-oil interface, they may prevent small water and water-wet solids from passing through. More and more material would then accumulate creating a rag layer. A series of experiments were performed to test the mechanical barrier concept.

6.1.1 Proof of Concept

To test if accumulated solids could create a barrier at the interface, approximately 10 g/L of precipitated asphaltenes were dispersed in n-heptane and placed on top of a layer of RO water. Asphaltenes are oil-wet particles and do not readily settle into water. Hence, they accumulated at the water-oil interface. Water droplets were then pipetted into to the oil phase and allowed to settle to interface. The droplets were in the order of 1 mm in diameter. The experiment was performed with asphaltenes with co-precipitated solids

(0.34% wt% fine solids) and with asphaltenes from which the solids had been removed. The results were the same in both cases.

Figure 6.1 shows a series of observations of the experiment over time. Figure 6.1a shows the asphaltene particles settling to the interface. Figures 6.1b and 6.1c show the test tube after water has been added. Note, the water-oil interface does not rise even though a substantial amount of water has been added. The amount can be gauged by the rise in the air-oil interface. Clearly, the droplets did not pass through the layer of asphaltene particles. Figure 6.1d is a close up near the water-oil interface and shows that over time the droplets have coalesced. Even after coalescence, the water only rarely passed through the interface under gravity force. However, by applying a low centrifuge force (500 rpm for 5 min), the droplets readily passed through the interface.

A second experiment was conducted using the same procedure but with heptol 50/50 as the solvent. In this case, the asphaltenes were dissolved in the solvent and no interfacial barrier was anticipated. Figure 6.2 shows that the water droplets in this experiment immediately passed through the interface and joined the free water layer.

These experiments demonstrate that relatively large water droplets will join the water phase unless a mechanical barrier is present. The results confirm that oil-wet solids can form a mechanical barrier but the barrier may only be effective at normal gravity or very low centrifuge forces. Note, only relatively large droplets of water were examined. Small droplets of emulsified water are known to accumulate at the interface (Long *et al*., 2002) and may act as a barrier as well.

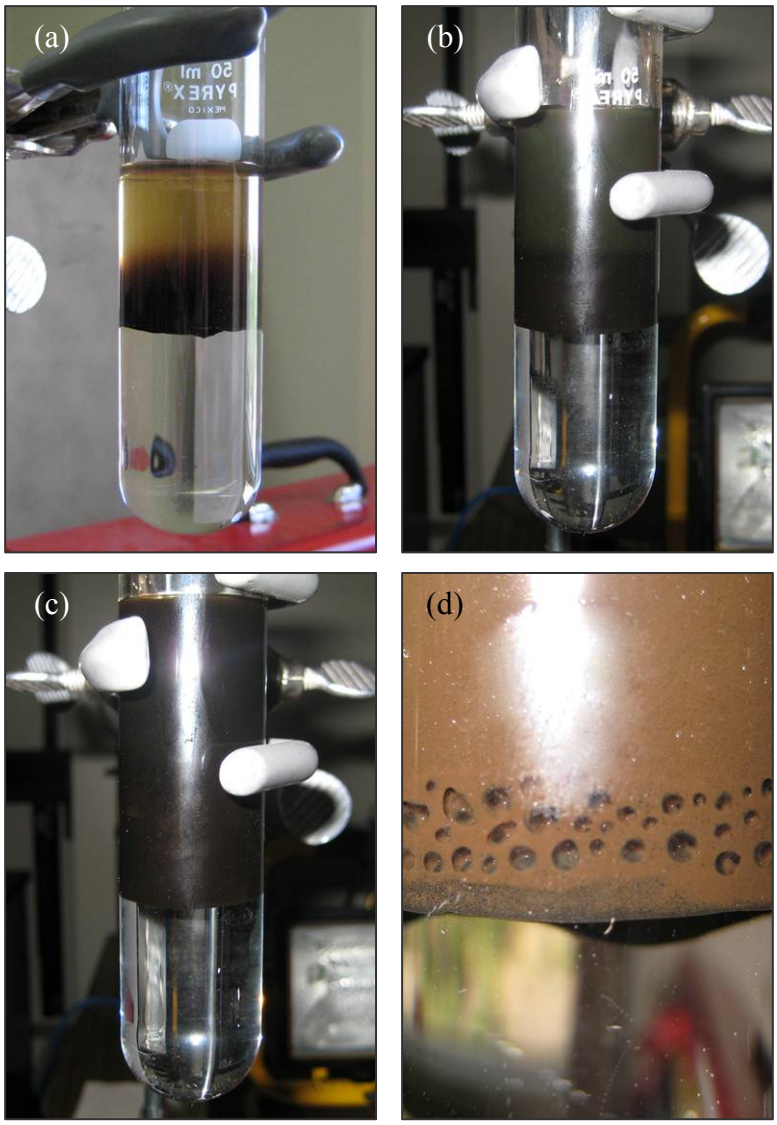

Figure 6.1 The mechanical barrier set up: asphaltenes settled at the interface, no water added (a); water added (b); more water added (c); coalescing droplets (d)

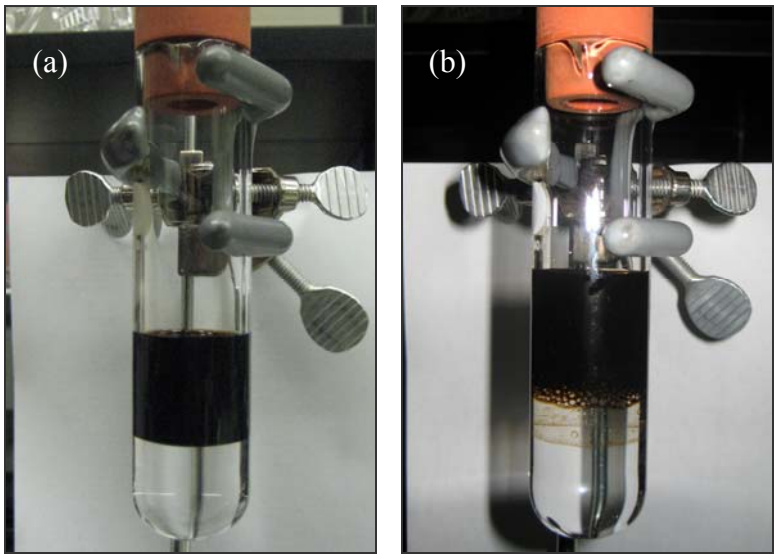

Figure 6.2 The mechanical barrier doesn't form in heptol 50/50: before adding water droplets (a), after adding water (b)

6.1.2 Evidence of Mechanical Barrier in a Diluted Froth

The ability of a diluted froth to form a mechanical barrier was not directly tested. However, some indirect evidence arose from a non-related experiment. In this experiment, diluted froth was added to the water-oil interface similar to the previous section. Using the procedure of the stepwise centrifuge tests, a sample of AQOS2 froth was diluted with n-heptane to above the onset of asphaltene precipitation and transferred to the surface of free water (Figure 6.3a). The diluted froth was not mixed with the water. The test tube was centrifuged following the procedure of the stepwise centrifuge tests.

Figure 6.3b shows that at 500 rpm a rag layer forms at water-oil interface while the coarse solids settle to the bottom of the test tube. Figures 6.3c and 6.3d show the test tube at 1500 and 2500 rpm, respectively. At 2500 rpm, the disc-like rag layer sinks part way into the water layer. Although it is submerged, it retains its shape and structural integrity. It is likely that such a rigid composite would act as a barrier at the interface.

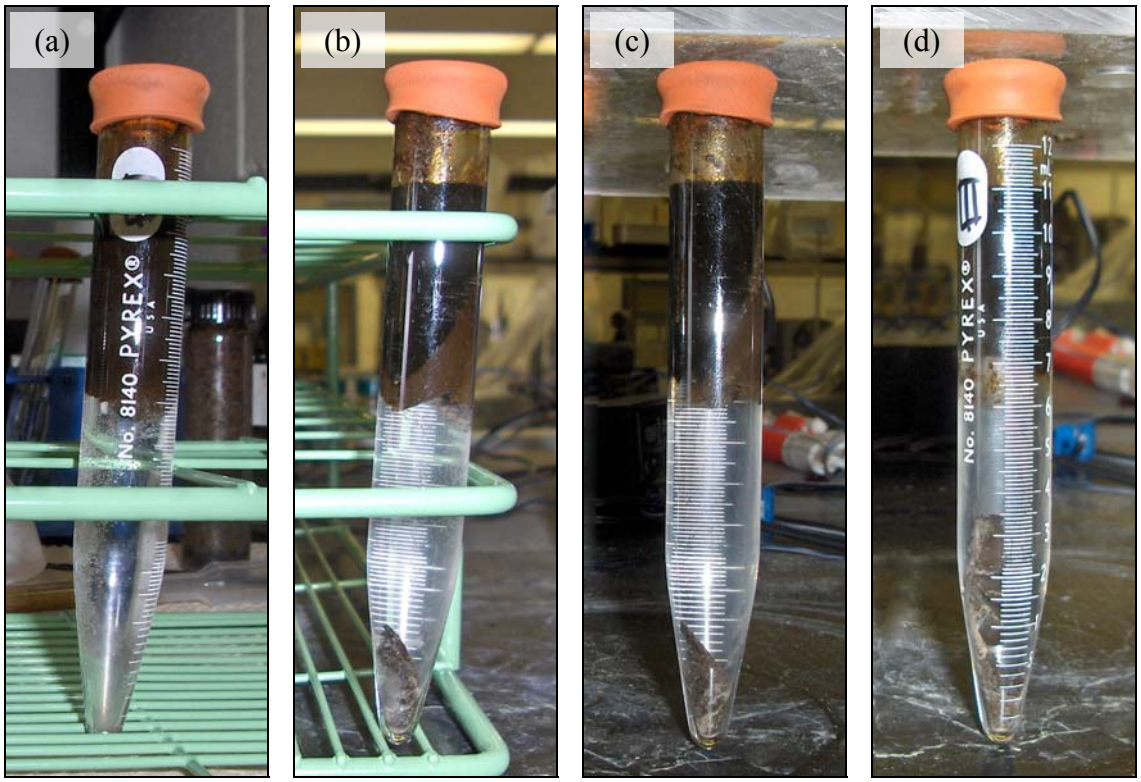

Figure 6.3 Adding diluted froth to the water surface: prior to centrifuge (a); after 500 rpm (b); after 1500 rpm (c); after 2500 rpm (d)

6.1.3 Contribution of Fine Solids to Mechanical Barrier

Two experiments were conducted to investigate the effect of quantity of fine solids on rag formation. In both experiments fine solids in the rag layer were extracted and stored in toluene in order to avoid a change in their wettability. However, the quantity of fine solids and the method for extracting the fines were different in both experiments.

In the first experiment, fines were extracted from rag layer by the following method. A sample of LQOS3 froth was diluted with toluene to 2.06 g/g solvent-to-bitumen ratio. The test tube was centrifuged to 4000 rpm for 5 minutes and the rag layer was decanted. The rag layer was filtered using a glass microfiber filter 934-AH, 0.3 μm pore size, in a vacuum filter. The filtered rag which contained fine solids was kept in a capped glass to prevent drying. To perform the experiment, filtered rag layer material from two test tubes were added to diluted froth in another test tube. The amount of solids added to the sample

by this method was approximately double the mass of fine solids in the undiluted froth. The amount of fines in the undiluted froth was increased from approximately 3 to 9 wt%. Then a stepwise centrifuge test was conducted and the rag that formed was compared with a similar case in which no fines were added to the test tube. No major differences in the volumes of the rag layers were observed between the two cases.

The second experiment was conducted by adding fine solids extracted from a sample of LQOS3 froth using the method described in Chapter 3. The fine solids were kept in toluene to preserve their wettability. The solids content in the mixture of toluene and solids was determined as follows. The sample was centrifuged to 6000 rpm for 5 minutes, and the toluene was decanted from the test tube. While the whole sample was kept in a capped test tube in refrigerator, a small portion of it was dried overnight in a vacuum oven at 60 °C. The solids content was determined by weight difference to be 52 wt%. Once the composition was known, a mass of wet solids was added to the froth with additional toluene so that the fine solids content in the undiluted froth increased from 3 to 22.7 wt% and the final dilution ratio was 8.28 g/g solvent per bitumen. Finally, a stepwise centrifuge test was conducted and the rag layer volumes were compared to a sample to which no fines had been added. Surprisingly, when fines were added, no rag layer formed at all.

It appears that the addition of small amounts of fine solids has little effect but large amounts prevent rag layer formation. A possible explanation is that adding large amounts of solids might accelerate coalescence. This effect has been observed in oil field emulsions (Sztukowski and Yarranton, 2005 b).

Overall, it appears that precipitated asphaltenes can act as a barrier at the interface. It also appears that the combination of asphaltenes, fine solids, and emulsified water can form a rigid material that could also act as a barrier. The role of the fine solids is less clear and it is possible in some cases that they may even prevent rag layer formation.

6.1.4 Effectiveness of Mechanical Barrier in Diluted Froths

While it is clear that mechanical barriers can form at the interface, it is not clear how effective this barrier is in diluted froths. If the mechanical barrier is an important mechanism in rag layer accumulation, disturbing the interface with a small wire is expected to disrupt that barrier and allow some water through. In the following experiment, two samples of LQOS3 froth were diluted with n-heptane to a solvent ratio above the onset of asphaltene precipitation and a stepwise centrifuge test was conducted. The only difference between the two samples was that in one of them denoted "mixed", the rag layer was stirred with a small wire after each centrifuge step. Figure 6.4 shows that mixing had no effect on the rag volume compared with the undisturbed rag layer. This experiment suggests that the mechanical barrier dose not play a major role in rag formation.

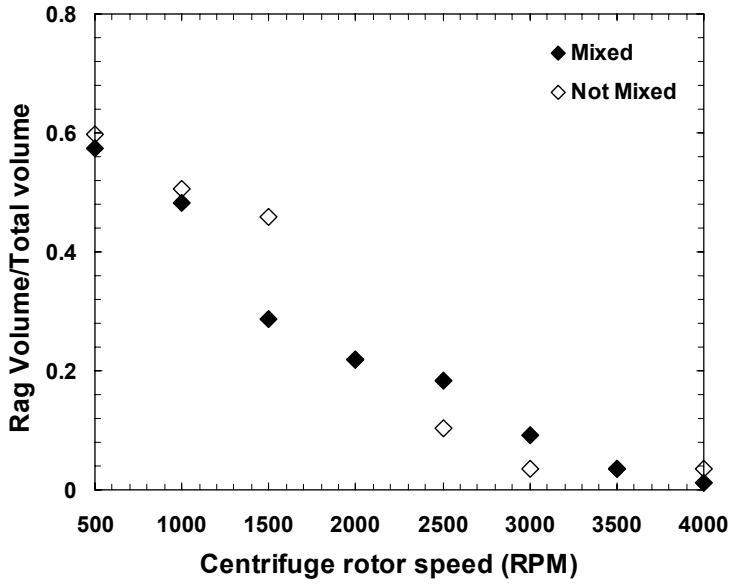

Figure 6.4 Stirring the rag layer after each centrifuge step in stepwise centrifuge test

6.2 Hindered Settling and Slow Coalescence

Let us define “free water” in a froth as relatively large droplets that coalesce easily and “emulsified water” as relatively small droplets that are slow to coalesce. If there is no emulsified water in the froth and no mechanical barrier, then hindered settling is the only mechanism that is likely to contribute to rag layer formation. In this case, the settling behavior of a redispersed diluted froth is expected to be the same as the original diluted froth. Since the mechanical barrier does not appear to be a significant factor, any differences in the settling behavior can be attributed to emulsified water.

6.2.1 Test of Concept

To determine if hindered settling was the only mechanism for rag formation, a stepwise centrifuge test of a redispersed froth was compared with the same test on a standard sample. The tests were performed on two samples of an LQOS3 froth diluted with 8.5 g/g toluene/bitumen. A step wise centrifuge test was performed on the first sample as a control or “base case”. The second sample was centrifuged after dilution for 5 minutes at 6000 rpm to eliminate potential residual emulsified water. Then, a step wise centrifuge test was performed.

Figure 6.5 shows the results of these two experiments. In this figure, columns with‘BC’ are the base case and columns with ‘R’ are the redispersed froth. At low centrifuge speeds, the volumes of rag layer in both test tubes are the same. However, at intermediate speeds, the volumes of the redispersed rag layers are considerably smaller than the base case. At higher speeds, there is no clear difference between the two cases. The results do indicate that there is emulsified water in the original diluted froth. The emulsified water appears to coalesce and pass through to the water layer at intermediate speeds. Virtually all the emulsified water is likely removed by 3500 rpm and therefore the final rag layer volumes are similar. This experiment shows that although hindered settling seems to be the dominant effect at low centrifuge speeds, slow coalescence is also a mechanism in rag layer formation.

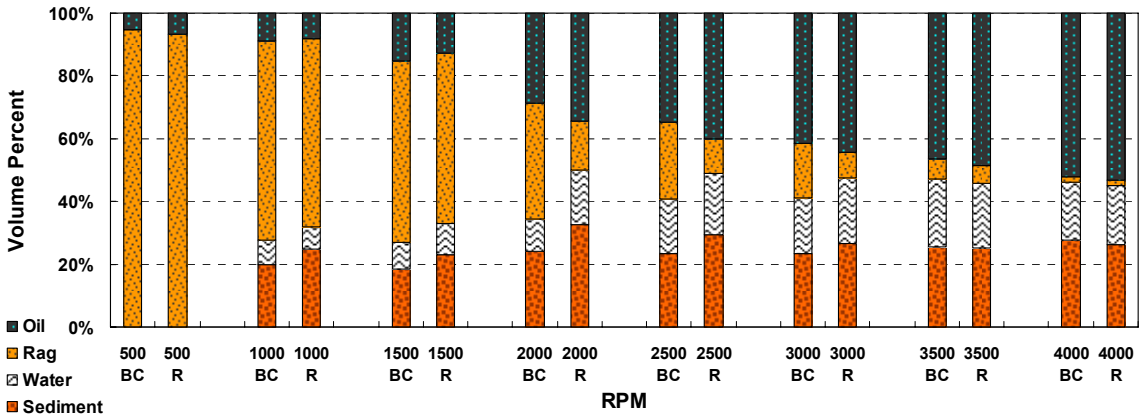

Figure 6.5 Centrifuging a froth sample at 6000 rpm for 5 minutes after its dilution following by its redispersion (columns with 'R'). A stepwise centrifuge test was conducted on this sample along with the base case (columns with 'BC') for comparison.

6.2.2 Confirmation

If reducing the emulsified water from froth by coalescence can change the rag volume, adding it to the system should change the volume as well. In another experiment two LQOS3 froth samples were diluted to 8.52 g/g toluene-to-bitumen ratio. As with the previous experiment, the first sample underwent a step wise centrifuge test and was the 'base case'. The second sample was first centrifuged to 4000 rpm and its oil layer was transferred to a small glass bottle. About 5 volume percent of water was emulsified into the oil using the method described in Chapter 3. The oil and emulsified water were then returned to the same froth sample which was first centrifuged at 4000 rpm. The test tube was redispersed, and the stepwise centrifuge test was conducted.

Figure 6.6 shows the results of this experiment. Columns with 'BC' are again the base case and columns with 'E' are the case with added emulsified water. Figure 6.6 shows that, at low centrifuge speeds, the rag layer volumes in both cases are almost the same. However, at intermediate speeds, the volume of the rag layer when emulsified water was added is significantly larger than the base case. The final rag volumes are similar. This experiment confirms that hindered settling is the dominant mechanism at low speeds but emulsion coalescence is also an important factor. For these diluted froths, coalescence appears to be accelerated at intermediate centrifuge speeds.

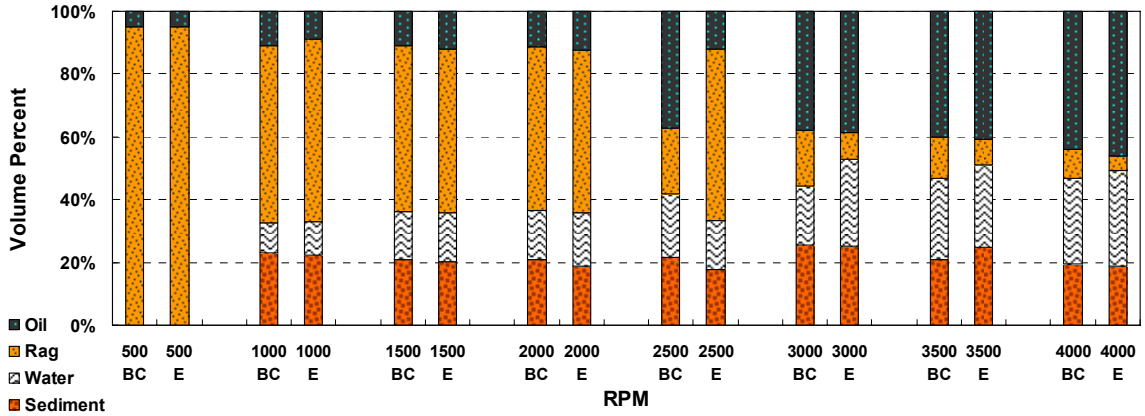

Figure 6.6 5 vol% water was added to the oil layer of a froth sample and homogenized to produce emulsions (columns with 'E'). A stepwise centrifuge test was conducted on this sample along with the base case (columns with 'BC') for comparison.

Note, the differences observed with emulsion coalescence are beyond the scatter of the data. To illustrate, the two base cases are presented in Figure 6.7. The average difference between rag layer volumes is 5.7%. The difference between the emulsified water cases and base cases are approximately 32% at intermediate centrifuge speeds.

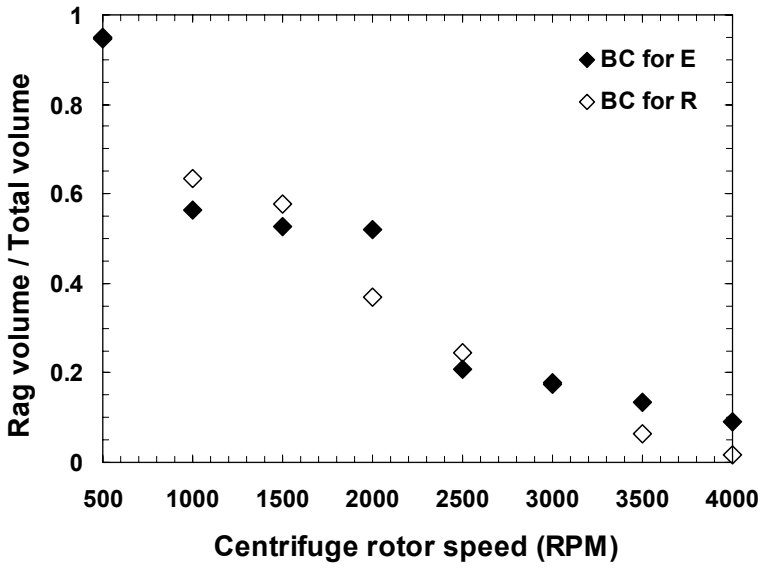

Figure 6.7 Comparing rag layers of the two base cases of Figures 6.5 and 6.6.

6.2.3 Stability of the Emulsions

The emulsions in the diluted froth tests appeared to destabilize at intermediate centrifuge speeds. To confirm this observation, the following experiment was conducted. Using the same method and sample specifications as in previous experiment, an emulsion was made in the oil phase decanted from a diluted froth and a stepwise centrifuge test was conducted. As expected, the emulsified water began to break out at 1500 rpm; however, it did not completely break out until 6000 rpm. This result suggests that the other rag components in the original experiment, such as the solids, may weaken the emulsion.

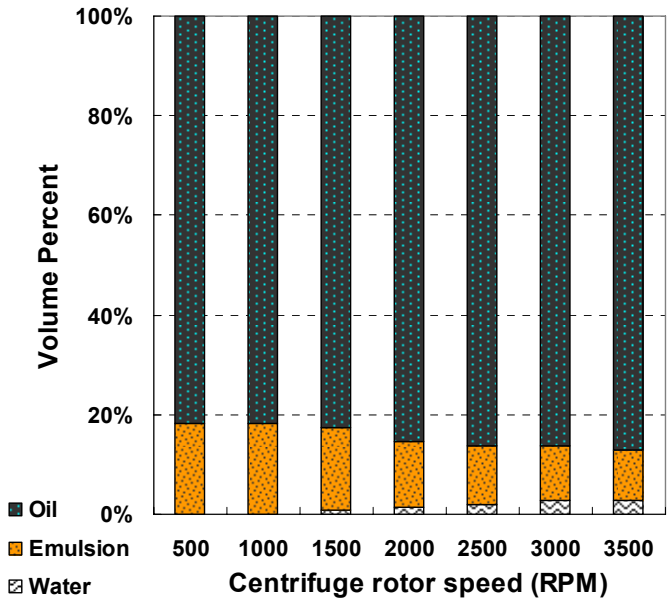

Figure 6.8 Stability of emulsions in an oil phase decanted from a diluted froth

6.2.4 Numerical Modeling of the Stepwise Centrifuge Tests

If the only mechanism of rag formation in stepwise centrifuge tests was hindered settling, the model would be expected to match the data obtained from experiments. Hence, the comparison of the data and the model can confirm the effects of other mechanisms in rag formation. This comparison was made with three sets of experimental data.

The input parameters for the model are shown in Table 6.1 and include the internal number, number of layers, and the time increment. The time increment was determined

by trial and error to achieve the fastest running time for the program that did not introduce numerical error. The height of the tube and centrifuge running time were the same as in the experiments.

Droplet numbers and solid particle numbers were chosen to fit measured volumes of water and solids. The volume of emulsified water was estimated from the change in height of the free water interface between 1000 and 4000 rpm. The volume of fine solids was assumed to be 50% of the final rag layer volume. The weight percentages of each component in the model are compared with the froth assays of Table 6.2. The model inputs are within the experimental error in the froth assay.

The diameters of the coarse solids and free water droplets were set smaller than measured values to allow for larger time steps but still fit the fast settling behavior observed in the experiments. Emulsified water droplet size was obtained from rag micrographs, and fine/coarse solid particle sizes were obtained from particle size measurements.

The density and viscosity of toluene and n-heptane diluted bitumen were measured (Romanova, 2006). The density of heptol 80/20 was calculated from the component densities assuming no volume change upon mixing. The viscosity of heptol 80/20 was assumed to be a volume average of the toluene and n-heptane viscosities. The density of solid particles was measured to be 1800 kg/m^3 using the Archimedes principle (Stasiuk, 2007).

Table 6.1 Input data for the numerical simulation

	n-Heptane	Heptol 80/20	Toluene
Internal number (number used in updating particle movements)	10000	10000	10000
Number of layers	50	50	50
Actual height, cm	12	12	12
Number of particle types	4	4	4
Free water droplet size, cm	0.00894	0.00894	0.00894
Emulsified water droplet size, cm	0.000506	0.000506	0.000506
Fine solid particle size, cm	0.000692	0.000692	0.000692
Coarse solid particle size, cm	0.00634	0.00634	0.00634
Free water droplet number in internal number	29	26	14
Emulsified water droplet number in internal number	9500	9064	9500
Fine solid particle number in internal number	441	883	471
Coarse solid particle number in internal number	30	27	15
Actual number of all particles / total volume, 1/cm³	5.49×10^{8}	5.49×10^{8}	5.49×10^{8}
Volume fraction of water in a free water layer	0.5	0.5	0.5
Density of medium, kg/m³	845	877	913
Viscosity of medium, Pa.s	0.0190	0.00993	0.0009
Density of solid particles, kg/m³	1800	1800	1800
Time increment, s	2	2	2
Centrifuge running time, min	40	40	40

Table 6.2 The overall weight percent of the components for the three model cases compared with the average assay for the LQOS3 froth.

	n-Heptane Model, wt%	Heptol 80/20 Model, wt%	Toluene Model, wt%	Average Assay LQOS3, wt%
Bitumen	8.1	11.3	5.0	9.7
Water	49.7	49.6	48.0	59.8
Solids	42.2	39.0	47.0	30.5

Figures 6.9 to 6.11 show the model results compared with the experimental data for three different solvents. At centrifuge speeds up to 2000 rpm, the model predictions are in qualitative agreement with the data for the heptane and heptol 80/20 diluted froths. This agreement suggests that hindered settling is the dominant mechanism at low centrifuge speeds. At moderate to high centrifuge speeds, the model over-predicts the rag layer volume. The most likely explanation is that, in the actual experiment, the emulsified water coalesced and passed through the interface. The model does not allow for coalescence and hence a larger rag volume is predicted.

The model predicts far more rapid settling than actually observed in the toluene diluted froth. A possible explanation is that the settling rate at the top of the interface is set by the smallest, least dense particles in the system. The model only accounts for the average sized particles. In heptane and heptol 80/20, some flocculation occurs and the average size of the individual droplets may be a good measure of the smaller aggregates. In toluene, there is little flocculation and the average size is not the best choice for modeling the movement of the top of the interface.

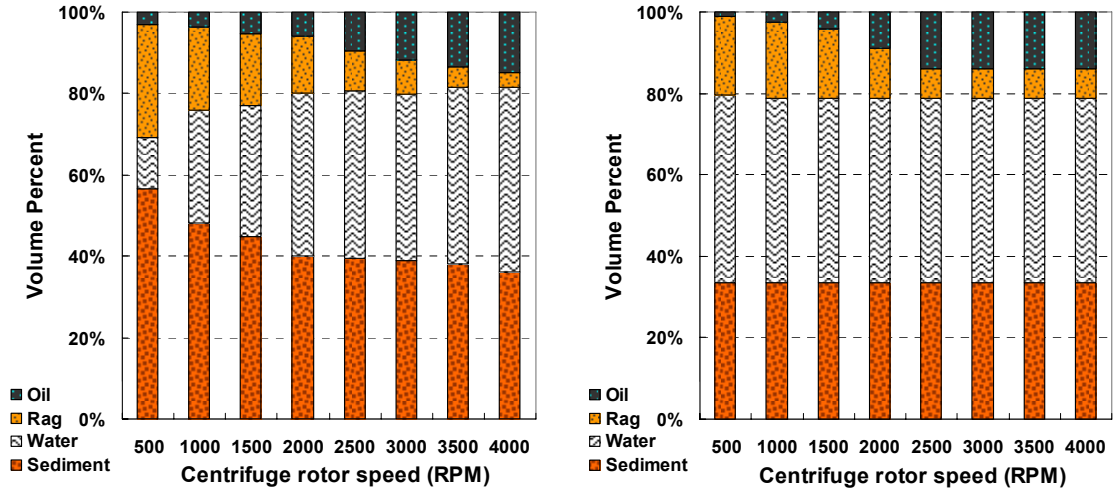

Figure 6.9 Experimental data (left) and the result of the model (right) for LQOS3 froth diluted with n-heptane. Data is the average of the experiments at 23°C at a solvent:bitumen ratio of 0.66 g/g.

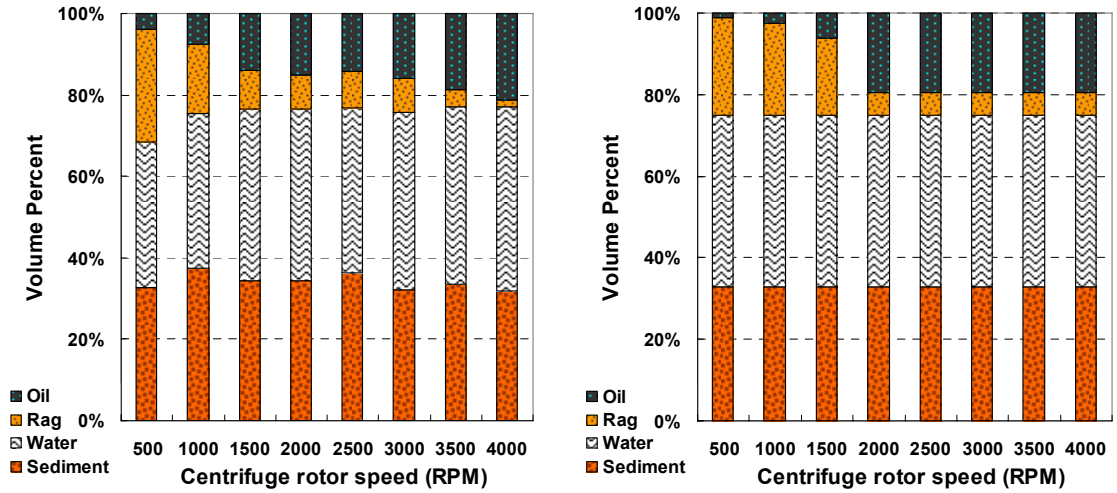

Figure 6.10 Experimental data (left) and the result of the model (right) for LQOS3 froth diluted with heptol 80/20. Data is the average of the experiments at 23°C at a solvent:bitumen ratio of 0.70 g/g.

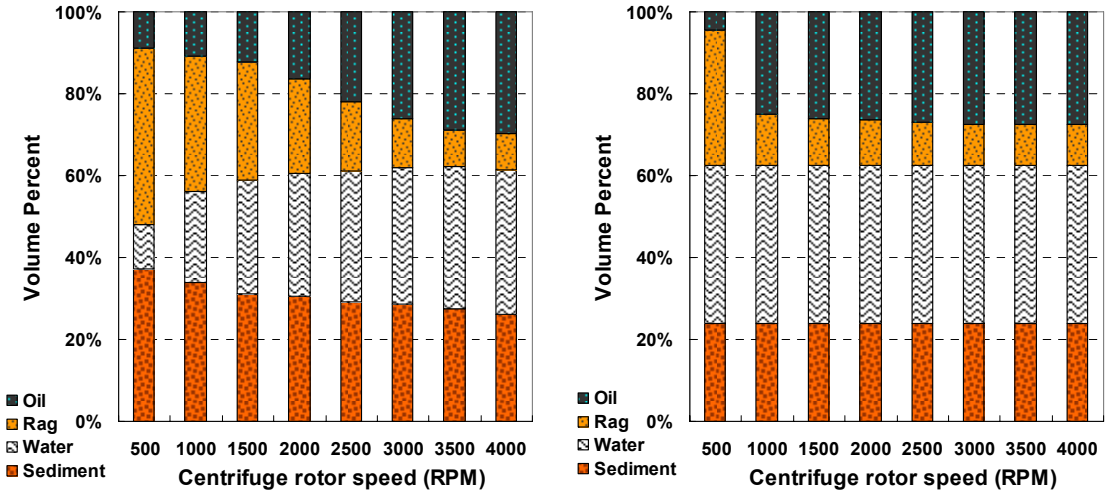

Figure 6.11 Experimental data (left) and the result of the model (right) for LQOS3 froth diluted with toluene. Data is the average of the experiments at 23 and 60 °C at a solvent:bitumen ratio of 4.11 g/g.

6.3 Summary

The experimental data and their comparison with the numerical model suggest that hindered settling, slow coalescence, and accumulation of oil-wet solids on the water/oil interface all contribute to the rag layer growth. Figure 6.12 summarizes a hypothesis on how the different mechanisms contribute to rag layer formation.

In the first seconds of centrifuging, coarse solids and large water droplets settle rapidly. If there is sufficient water volume, a water-oil interface rises above the sediment layer. The majority of the fine solids, emulsified water, and asphaltene particles remain dispersed in the early seconds of centrifuging. At these low centrifuge speeds and settling times, hindered settling is the dominant factor in rag formation, Figure 6.12a.

At higher speeds and times, fine solids and emulsified water accumulate at the water-oil interface and the pressure and contact is sufficient to start a slow coalescence. Above the compacted interfacial zone, fine solids and emulsified water continue to settle, Figure 6.12b. Flocculation may accelerate the settling rates. At still higher speeds and times, the

majority of the particles enter the interfacial zone and slow coalescence becomes the dominant effect. Some emulsion droplets coalesce and enter the water phase while some material still settles from above. Some precipitated asphaltenes, if present, and fine solids are also driven through the interface and join the sediment (Figure 6.12c).

At high speeds and times, only very small fine solids, asphaltenes, and possibly water droplets remain at the interface. These particles are so small that the centrifugal force cannot overcome the interfacial forces arising from their wettability. Hence, at the final stage, wettability dominates.

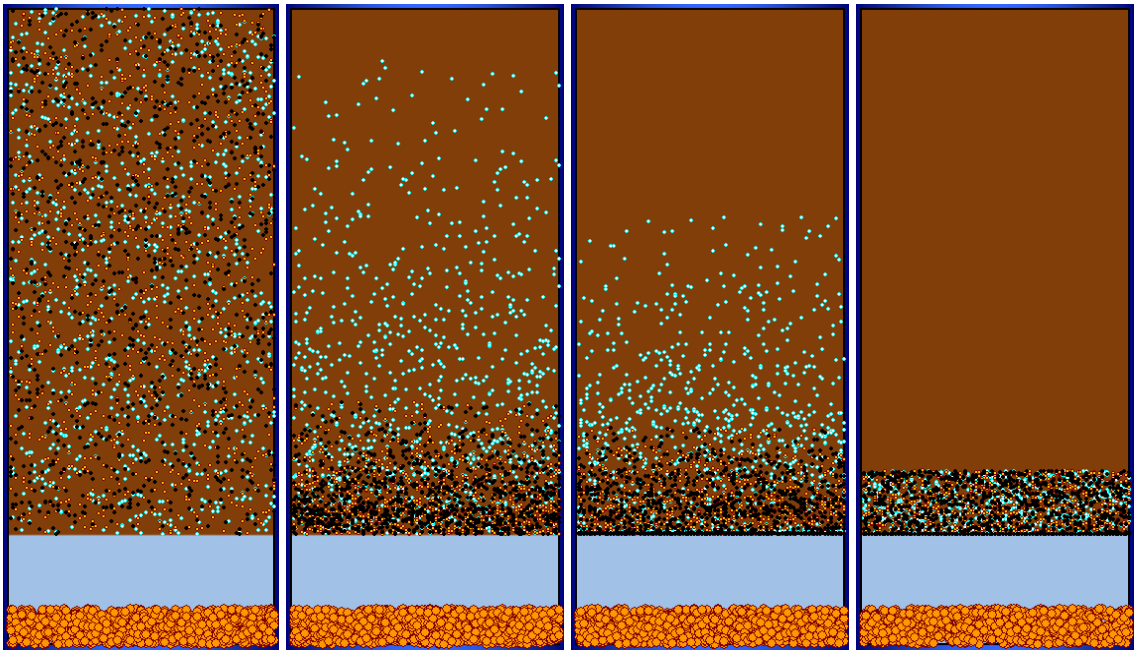

(a) (b) (c) (d)

Figure 6.12 Rag formation hypothesis: the early seconds of stepwise centrifuge tests at low rpms (a); low to intermediate rpms (b); intermediate rpms (c); high rpms (d)

Chapter 7

Effect of Processing Conditions

Key controllable process conditions in oil sands extraction and froth treatment are the extraction temperature, amount of NaOH added during extraction, the type and amount of solvent in froth treatment, and froth treatment temperature. The type and amount of solvent alter density, viscosity, and can cause asphaltene precipitation. Oil sand quality is also an important factor in processing efficiency. In this chapter, the effects of each of these factors on rag layer volumes are discussed.

One challenge with the step wise centrifuge tests was scatter in the data. While good repeatability was observed for a single froth sample, there was considerable variation between different samples. To overcome this problem, the largest number of similar trials was averaged wherever possible. In some cases, trials at different conditions such as treatment temperature were combined when that condition had been shown to have no effect on the rag layer volumes. After averaging, the variability at 500 rpm was approximately ±35%, ranging from ±0.09 to ±0.16 volume fraction units. The absolute deviation decreased as the centrifuge speed increased. The details are provided in Appendix C.

The results are presented in two formats, Figure 7.1: 1) rag layer volume per total volume, left hand plot; 2) rag layer volume per undiluted froth volume, right hand plot. Figure 7.1 does show that hindered settling effect, since it is scaled to the total volume which is proportional to the height. The latter plot is more useful for assessing coalescence or solids accumulation effects when different solvent dilution ratios are used, as it is scaled to the amount of these materials added to the system. In the case of Figure 7.1 and most of the following figures the two types of plots are similar because the average amount of undiluted froth is similar in each case.

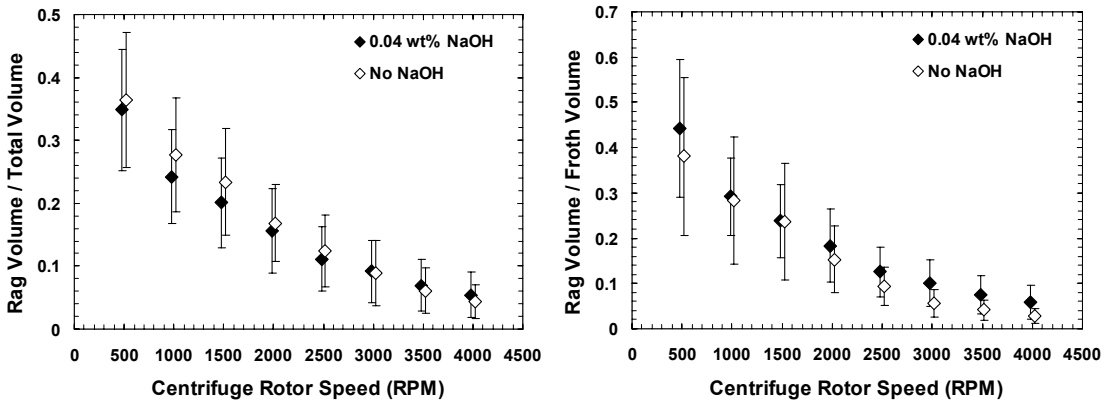

Figure 7.1 Effect of NaOH Addition on LQOS3 froth diluted with n-heptane. The zero and 0.04 wt% NaOH data were averages of 12 and 8 trials, respectively.

7.1 Extraction Conditions

The effect on rag layer volumes of two extraction conditions, namely NaOH addition and extraction temperature was studied. All the data in this section was collected only for LQOS3 froths. In summary, the solvent type had a pronounced effect on rag layer volumes while froth treatment temperature had little effect. Therefore, results are presented for each type of solvent but the trials at different froth treatment temperatures are combined into an average for each type of solvent.

7.1.1 NaOH Addition

For oil sands, adding sodium hydroxide during extraction increases the bitumen recovery. However, some oil sands do have a maximum oil recovery at zero NaOH addition, hence are not sensitive to NaOH addition. The processibility of the oil sand samples considered in this study was not sensitive to NaOH addition.

Figures 7.1 to 7.3 show the effect of NaOH addition on rag layer volumes from heptane, heptol 80/20, and toluene diluted froths, respectively. Due to the limited number of trials, the data was not divided beyond the solvent type. Therefore, the possibility remains that other factors are skewing the observed trends. With this proviso, NaOH addition has no significant effect on the rag layer volumes for any of the solvents. The results are not

surprising since NaOH addition had little impact on the extraction and similar froths were produced with and without NaOH. An oil sand for which NaOH addition improves recovery is required to determine if NaOH addition can affect rag layer formation.

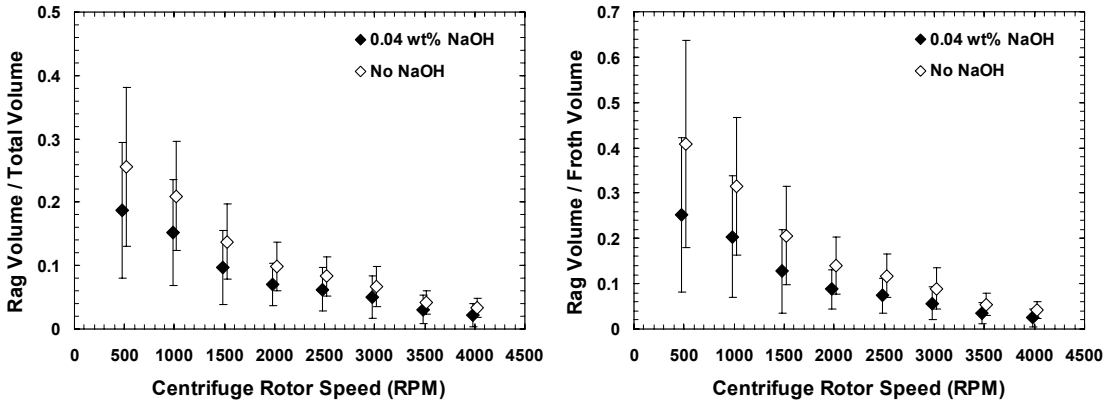

Figure 7.2 Effect of NaOH Addition on LQOS3 froth diluted with heptol 80/20. The zero and 0.04 wt% NaOH data were averages of 10 and 11 trials, respectively.

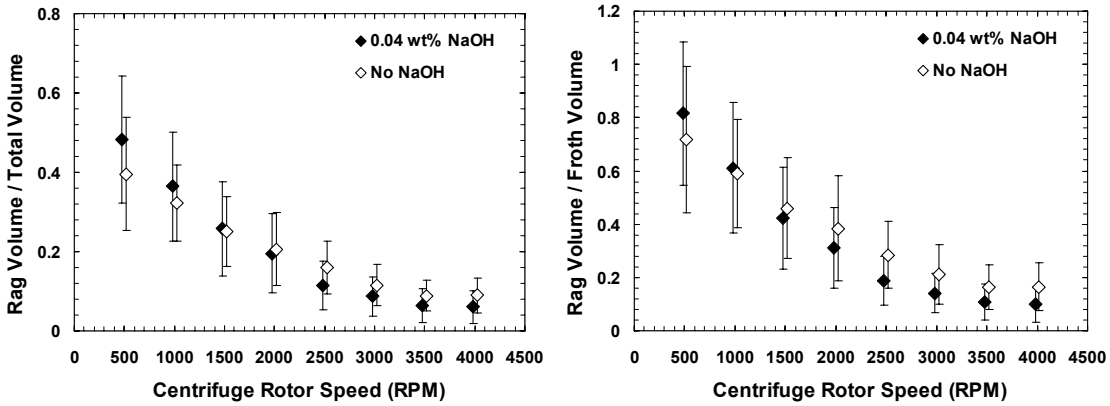

Figure 7.3 Effect of NaOH Addition on LQOS3 froth diluted with toluene. The zero and 0.04 wt% NaOH data were averages of 11 and 9 trials, respectively.

7.1.2 Extraction Temperature

Extraction temperatures of 23 and 80°C were studied. Figures 7.4 to 7.6 show the effect of extraction temperature on rag layer volumes for heptane, heptol 80/20, and toluene diluted froths, respectively. The data was only split by the solvent type. While there are

some differences between the data at 23 and 80°C, the differences are relatively small and the trends are inconsistent. It is likely that the differences reflect data scatter rather than a real effect.

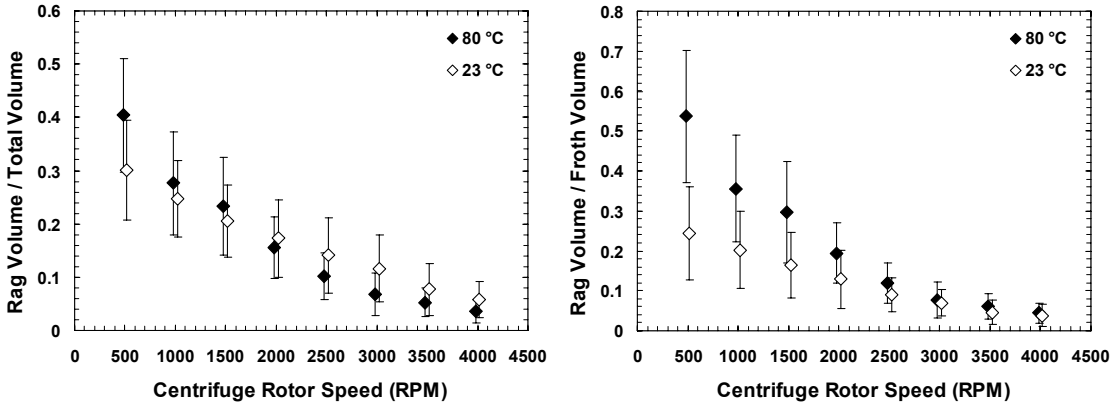

Figure 7.4 Effect of extraction temperature on LQOS3 froth diluted with n-heptane. The 23 and 80 °C data were averages of 9 and 11 trials, respectively.

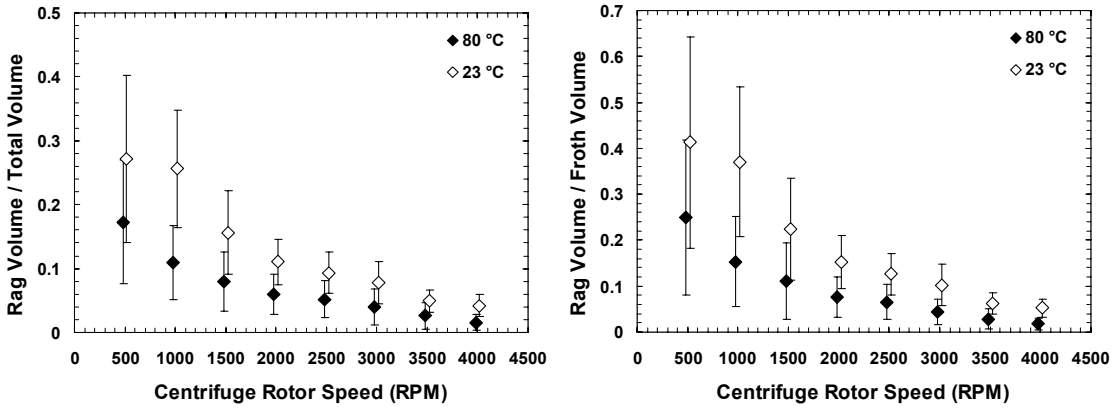

Figure 7.5 Effect of extraction temperature on LQOS3 froth diluted with heptol 80/20. The 23 and 80 °C data were averages of 10 and 11 trials, respectively.

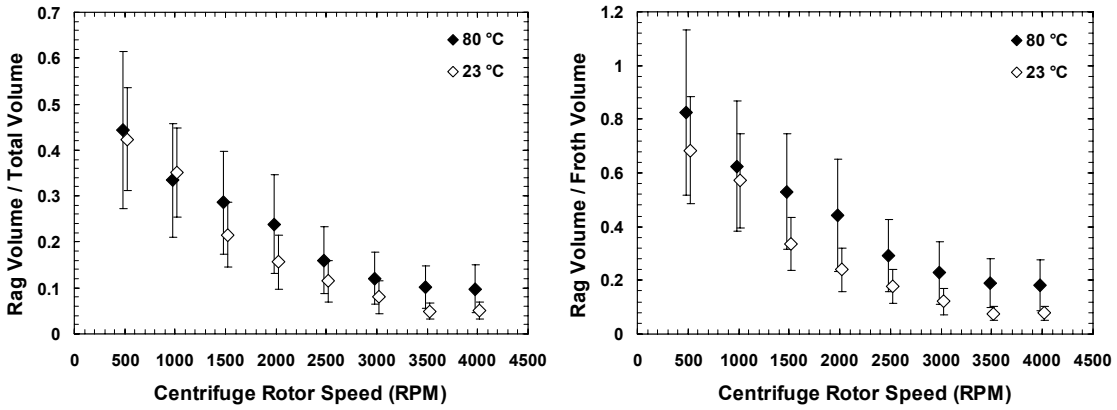

Figure 7.6 Effect of extraction temperature on LQOS3 froth diluted with toluene. The 23 and 80 °C data were averages of 9 and 11 trials, respectively.

7.2 Froth Treatment Conditions

The effects of solvent, asphaltene precipitation, and temperature on rag formation were studied. Since NaOH addition and extraction temperature had little effect on rag layer volumes, the trials at different extraction temperature and NaOH amounts were combined when averaging of the data. All of the data in this section are for LQOS3 froths.

7.2.1 Froth Treatment Temperature

Figures 7.7 to 7.9 show the effect of froth treatment temperature on rag layer volumes for heptane, heptol 80/20, and toluene diluted froths, respectively. Temperatures of 23 and 60 °C were used. Note, the froth treatment temperature had no significant effect on rag layer volumes.

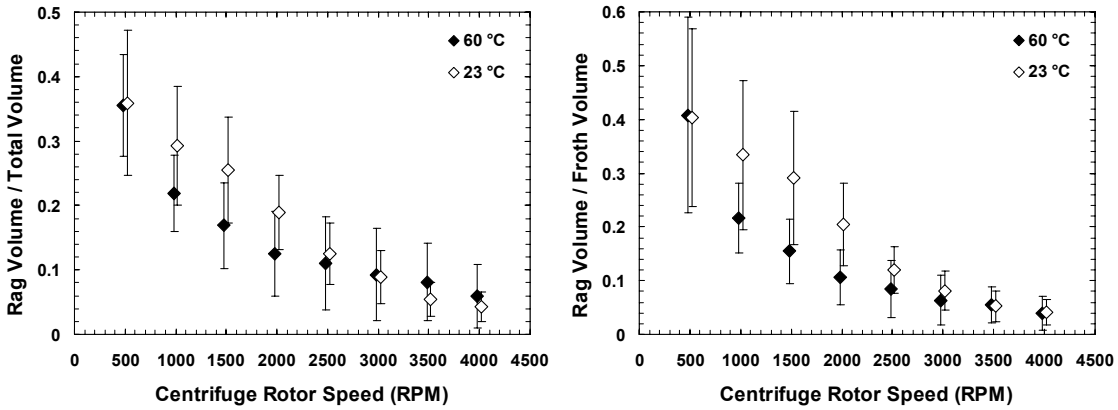

Figure 7.7 Effect of froth treatment temperature on LQOS3 froth diluted with n-heptane. The 23 and 60 °C data were averages of 12 and 8 trials, respectively.

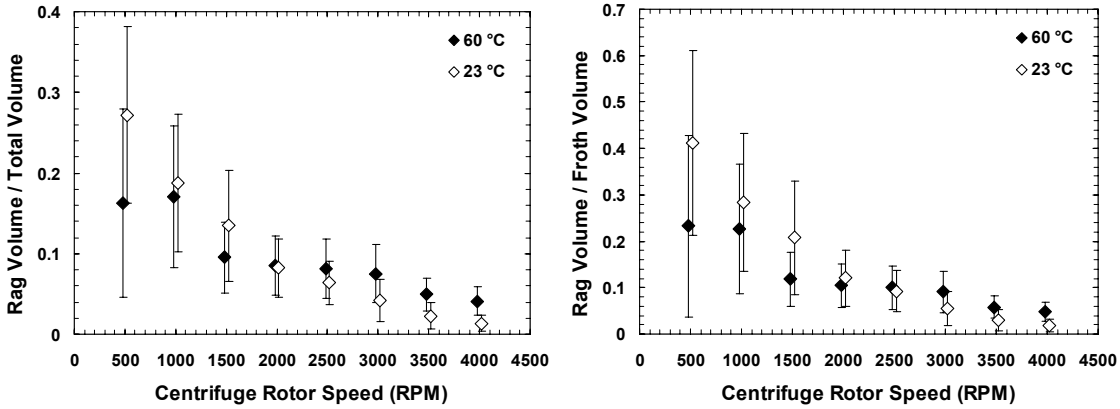

Figure 7.8 Effect of froth treatment temperature on LQOS3 froth diluted with heptol 80/20. The 23 and 60 °C data were averages of 11 and 10 trials, respectively.

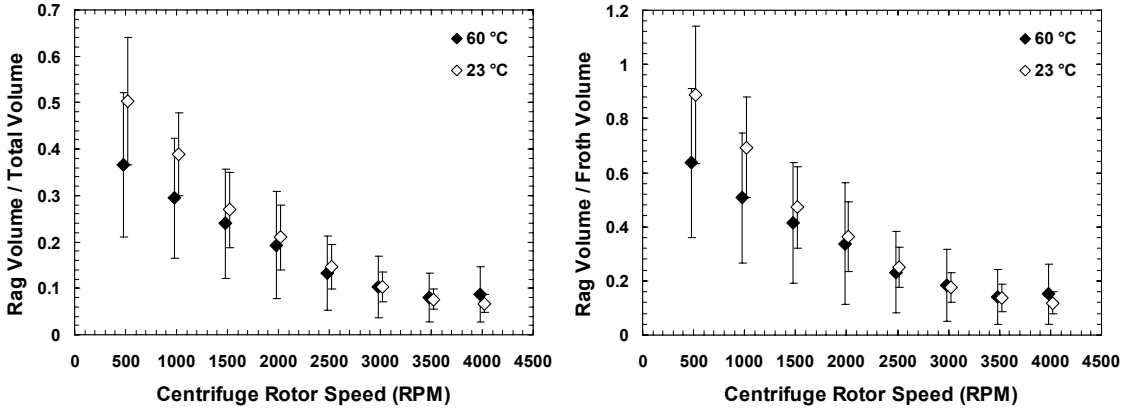

Figure 7.9 Effect of froth treatment temperature on LQOS3 froth diluted with toluene. The 23 and 60 °C data were averages of 10 and 10 trials, respectively.

7.2.2 Type of Solvent

Figure 7.10 shows rag layer volumes for three solvents: n-heptane, heptol 80/20, and toluene. Data from both froth treatment temperatures is combined and all of the data is below the onset of asphaltene precipitation. Below 2500 rpm, the rag layer volume is significantly larger in toluene than in the other solvents. Above 2500 rpm, the rag layer volumes are similar in all three solvents. The type of solvent has a strong effect in the region where hindered settling is dominant. A likely explanation is that heptane and heptol 80/20 promote flocculation, more rapid settling, and more compact rag layers. It is well known that heptane induces flocculation of asphaltenes and asphaltene coated water droplets (Rastegari *et al*., 2004; Long *et al*., 2007).

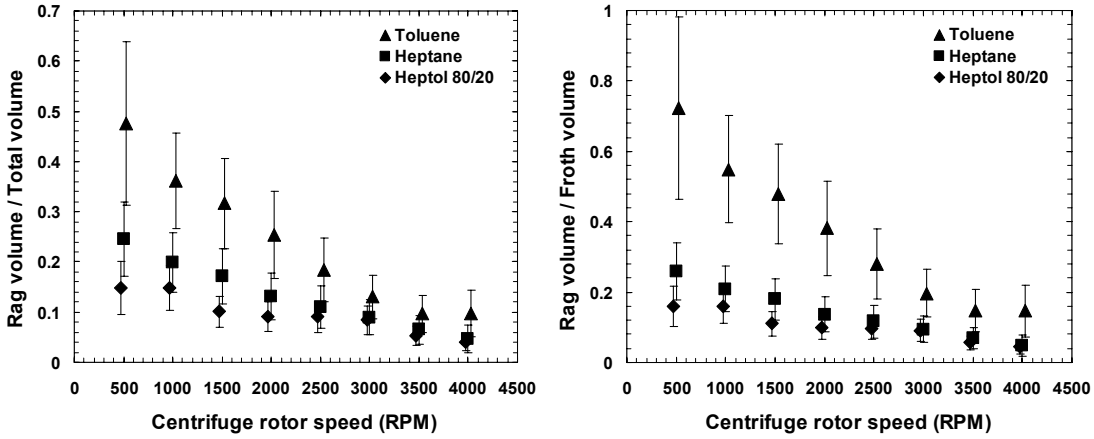

Figure 7.10 Rag layer volumes for the three different solvents. The data for toluene, heptane and heptol 80/20 were averages of 10, 10 and 11 trials, respectively.

Figure 7.11 shows the effect of the dilution ratio on rag layers formed in toluene. The initial rag layer volume is the same in both cases, left plot. Up to 1500 rpm, the rag layer volume decreases at the same rate up to 1500 rpm as expected in the hindered settling region. At 1500 rpm, the low dilution rag layer is larger. The right hand plot shows that from this point on, the rag layer volume is proportional to the amount of froth material. In other words, the rag layer volume is now controlled by the amount of emulsified water and solids in the system.

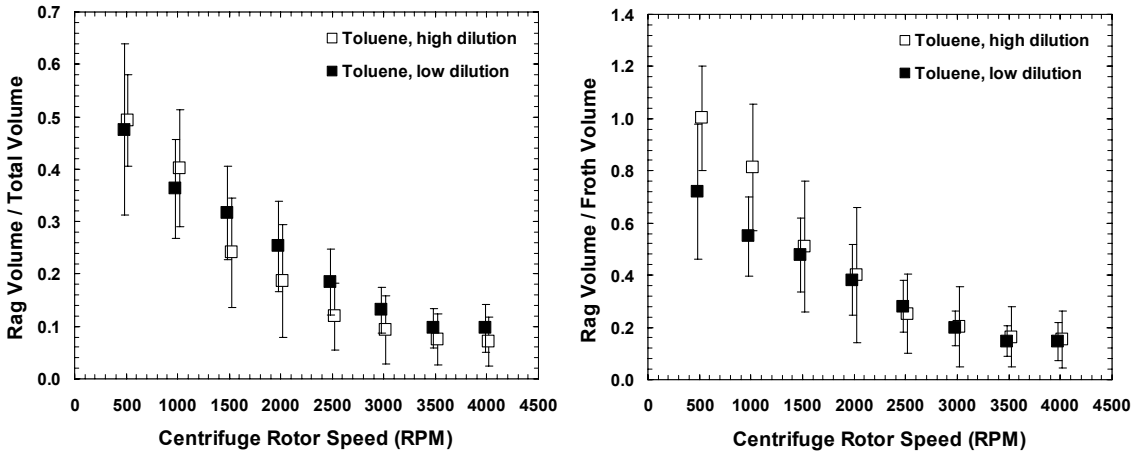

Figure 7.11 The effect of dilution ration on rag volumes in toluene. The data at high and low dilution ratios were averages of 9 and 11 trials, respectively.

7.2.3 Asphaltene Precipitation

Figures 7.12 and 7.13 show the effect of asphaltene precipitation on rag layer volumes for heptane and heptol 80/20 froths, respectively. In both cases, at low rpm, asphaltene precipitation significantly increases the rag volume. As expected, oil-wet asphaltene particles accumulate at the interface and contribute to the rag layer volume. These particles may contribute to a barrier at the interface or hinder coalescence. However, above 2500 rpm, the volume of the rag layers with precipitated asphaltenes are smaller than those without precipitation. At these centrifuge speeds, the asphaltenes may be forced through the interface releasing some trapped water at the same time.

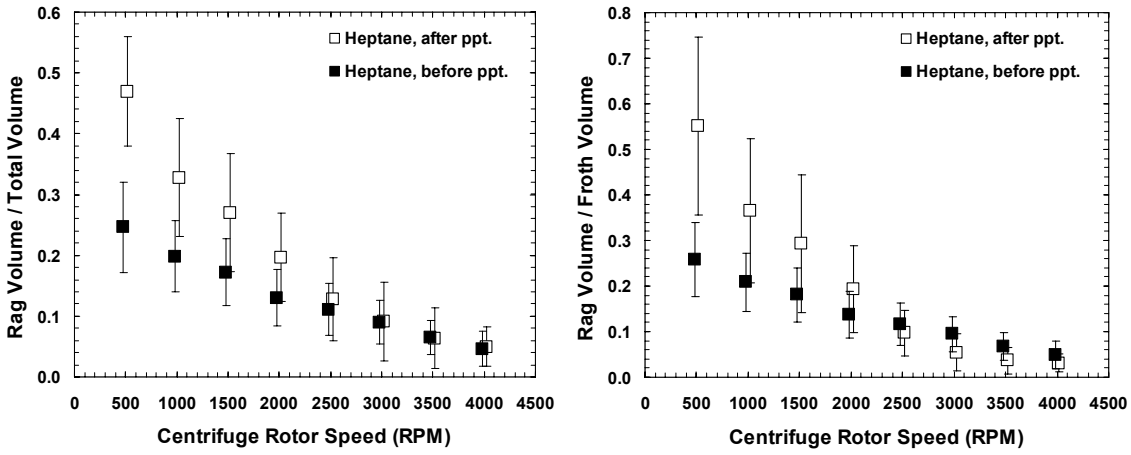

Figure 7.12 Rag volume and stability in n-heptane. The data above and below the asphaltene precipitation point were averages of 10 trials for each case.

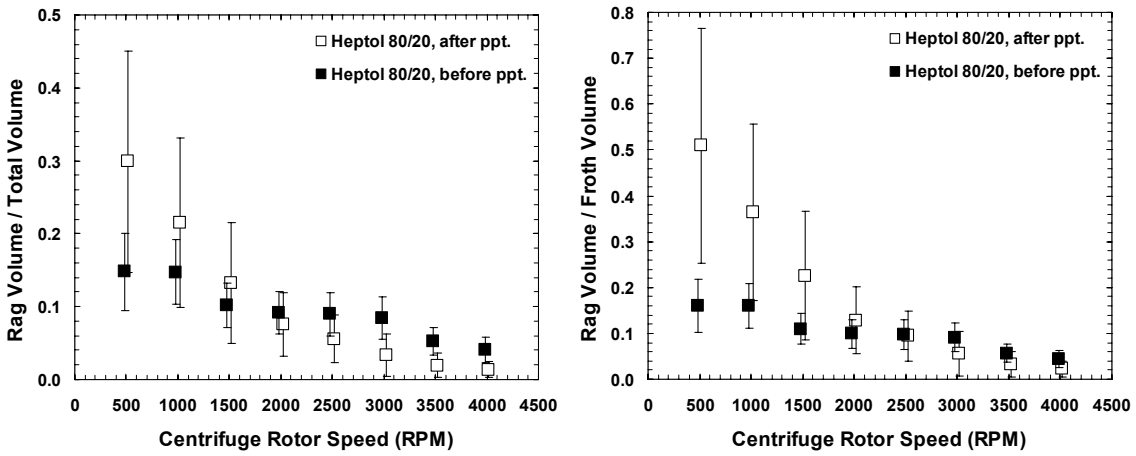

Figure 7.13 Rag volume and stability in heptol 80/20. The data above and below asphaltene precipitation point were averages of 10 and 11 trials, respectively.

7.3 Oil Sand Quality

Figure 7.14 compares rag layer volumes from the LQOS3 and AQOS2 froths diluted with toluene. All dilution ratios are included in the averaging. Note, there was so little water in the AQOS2 froth that RO water was added to raise the rag layer above the sediment (Appendix B).

Figure 7.14 shows that the rag layer volumes from AQOS2 froth are considerably lower than from the LQOS3 froth. The same trends were found with the other solvents. The reason for this major difference is not known. However, the LQOS3 oil sand contains more fine solids than the AQOS2 oil sand, 28.5 wt% versus 23.6%. The LQOS3 froth contains more total solids than the AQOS2 froth, 30.5wt% versus 25.9 wt%. Also, as shown in Chapter 5, the number frequency of fine solids in rag layers of each oil sand is different. The number mean diameter of the particles from the LQOS3 rag is 0.14 μm, much smaller than the mean diameter of 3.98 μm for the particles from the AQOS2 rag. It is likely that the larger quantity of very fine solids in the LQOS3 oil sand become part of the froth, contribute to emulsion stability, and to larger and more stable rag layers.

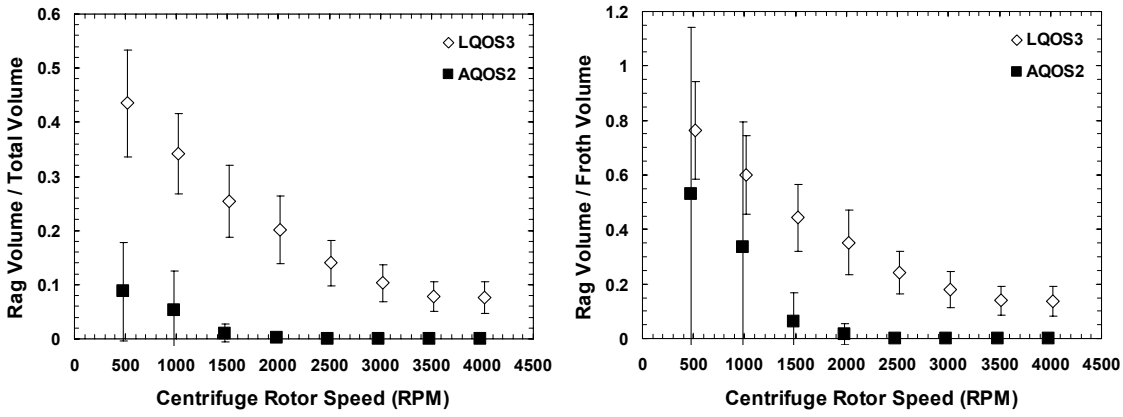

Figure 7.14 Comparing the rag formation in LQOS3 froth and AQOS2 froth diluted with toluene. The LQOS3 and AQOS2 data were averages of 9 and 2 trials, respectively.

7.4 Summary

Rag layer volume was found to be very sensitive to oil sand quality. The low quality oil sand produced much larger rag layers than the average quality oil sand. The low quality oil sand contains more very fine solids which may stabilize emulsions and consequently increase rag layer volumes.

Extraction conditions had little effect on rag layer formation for the oil sands used in this study. Rag layer volumes were not sensitive to froth treatment temperature but were sensitive to solvent type and dilution ratio. The rag layers were largest in toluene diluted froths. Heptane and heptol 80/20 produced more compact rag layers because they induced flocculation of the water droplets, solids, and precipitated asphaltenes. Note, Chapter 5 data show that the rag layers from heptane and heptol 80/20 froths also had higher water contents, consistent with a more compact rag layer.

Chapter 8

Conclusions and Recommendations

8.1 Thesis Conclusions

A variety of experiments were performed to understand the mechanisms that cause rag layer formation in oil sands froth treatment. The method used was step-wise centrifuge tests which is a comparison means for rag layer volumes from different oil sand samples and froth treatment methods. These tests were also used to assess the effects of operating conditions and oil sand quality on rag layer formation. The data was also used to calculate the initial rag layer compositions.

To understand the effect of wettability of fine solids a new method was developed based on the floatation technique and the wettability of fine solids in rag layer. Finally, a numerical model was developed to model the hindered settling effects on the build up of the rag layer.

The main conclusions of this study are as follows:

Rag Layer Composition:

- The material balance calculations based on the data from stepwise centrifuge tests suggest that rag layers at 500 rpm consist of 16–23 vol% of fine solids, 25–59 vol% water and 18–58 vol% diluted bitumen for froth obtained from LQOS3 and AQOS2 oil sands.
- The type of solvents affects rag layer composition. The rag layer that forms in bitumen froth diluted with toluene is loose and has high oil content. The rag layer that forms in bitumen froth diluted with heptol 80/20 or heptane is more compact.

Rag Layer Formation Mechanisms:

- The formation of rag in gravity force or low centrifuge forces at short settling times is mostly controlled by hindered settling.
- As more centrifugal force is used, the dominant mechanism shifts towards the slow coalescence of emulsions.
- Once enough force is applied to force coalescence, the remaining rag layer appears to consist of small oil-wet particles or asphaltene-coated water droplets; that is, wettability becomes the dominant mechanism.

Effect of Processing Conditions:

- Rag layer volume is sensitive to the type of solvent. Toluene produced the largest rag layer volumes. Heptol 80/20 and heptane produced much smaller volumes.
- Asphaltene precipitation increased the rag layer volume.
- The effect of froth treatment temperature on rag layer volume was small and inconsistent.
- Extraction temperature and sodium hydroxide addition had no effect on rag layer volumes. However, the effect of sodium, hydroxide addition has not yet been investigated for an oil sand whose processibility is sensitive to sodium, hydroxide addition.
- For lower quality oil sand a significantly larger rag layer than the average quality oil sand occurred.

8.2 Recommendations for Future Study

One conclusion from this study was that the choice of solvent has a significant effect on rag layer formation. It would be useful to assess the effects of different diluents on rag formation and the possibility of reducing the rag volume by the choice of diluent.

The amount of oil-wet solids in the system and the rag volume was not measured. It is recommended the experiments be performed with different amount of oil-wet solids to determine if there are threshold concentrations that maximize or minimize rag layer formation.

There is a possibility that the rag formation is related to the size and the type of clays. Research in this area might shed some light on the effect of different oil sands on rag formation.

In this study, three different oil sands were analyzed but not one of them was sensitive to the sodium hydroxide addition. It is recommended that data be gathered used an oil sand that is sensitive to NaOH.

References

Akbarzadeh, K., Alboudwarej, H., Svrcek, W.Y., and Yarranton, H.W., A Generalized Regular Solution Model for Asphaltene Precipitation from n-Alkane Diluted Heavy Oils and Bitumens, *Fluid Phase Equilibria*, 232 (1-2),159-170, **2005**.

Ali, M.F., and Alqam, M.H., *Fuel*, 79 (11), 1309-1316, **2000**.

Badamchizadeh, A., Maini, B., and Yarranton, H., Solubility and Viscosity Measurements for Athabasca Bitumen- Propane and Bitumen-Propane-CO2 Systems, *56th Canadian Chemical Engineering Conference*, Sherbrooke, Oct. 16-19, **2006**.

Baptista, M.V., and Bowman, C.W., The Flotation Mechanism of Solids from the Athabasca Oil Sands, *19th Canadian Chemical Engineering Conference, Edmonton, Alberta*, **1969**.

Barnea, E., and Mizrahi, J., A Generalized Approach to the Fluid Dynamics of Particulate Systems Part 1. General Correlation for Fluidization and Sedimentation in Solid Multiparticle Systems, *Chemical Engineering Journal*, 5 (2), 171-189, **1973**.

Barnea, E., and Mizrahi, J., Separation Mechanism of Liquid-Liquid Dispersions in Deep-Layer Gravity Settler: Part III – Hindered Settling and Drop-to-Drop Coalescence in the Dispersion Band, *Transactions of the Institution of Chemical Engineers*, 53 (2), 75-82, **1975**.

Bazhlekov, I.B., Chesters, A.K., and van de Vosse, F.N., The Effect of The Dispersed to Continuous-Phase Viscosity Ratio on Film Drainage Between Interacting Drops, *International Journal of Multiphase Flow*, 26 (3), 445-466, **2000**.

Berg, J.C., *Wettability*, Marcel Dekker, New York, 75-148, **1993**.

Bibette, J., Leal Calderon, F., and Poulin, P., Emulsions: Basic Principles, *Reports on Progress in Physics*, 62 (6), 969-1033, **1999**.

Bowman C.W., Molecular and Interfacial Properties of Athabasca Tar Sands, *Proceedings of the Seventh World Petroleum Congress*, *Mexico City*, 3, 583-604, **1967**.

Buerger, R., Bustos, M.C., and Concha, F., Settling Velocities of Particulate Systems: 9. Phenomenological Theory of Sedimentation Processes: Numerical Simulation of The Transient Behaviour of Flocculated Suspensions in an Ideal Batch or Continuous Thickener, *International Journal of Mineral Processing*, 55 (4), 267-282, **1999**.

Bulmer, J.T., and Starr, J., *Syncrude Analytical Methods of Oil Sands and Bitumen Processing*, AOSTRA, Edmonton, AB, Method 2.10, 62-68, **1979**.

Burrowes, A., Marsh, R., Ramdin, N., and Evans, C., *Alberta's Energy Reserves 2006 and Supply/Demand Outlook 2007-2016*, Alberta Energy and Utilities Board, **2007**.

Chen, F., Finch, J.A., Xu, Z., and Czarnecki, J., Wettability of Fine Solids Extracted from Bitumen Froth, *Journal of Adhesion Science and Technology*, 13 (10), 1209-1224, **1999**.

Chesters, A.K., Modelling of Coalescence Processes in Fluid-Liquid Dispersions: A Review of Current Understanding, *Chemical Engineering Research & Design*, 69 (4), 259-270, **1991**.

Clark, K.A., and Pasternack, D.S., Hot Water Separation of Bitumen from Alberta Bituminous Sand, *Industrial and Engineering Chemistry*, 24 (12), 1410-1416, **1932**.

Czarnecki, J., Moran, K., and Yang, X., On the so-called Rag Layer and Diluted Bitumen Dewatering, *57th Canadian Chemical Engineering Conference*, **2007**.

Dai, Q., and Chung, K.H., Hot Water Extraction Process Mechanism Using Model Oil Sands, *Fuel*, 75 (2), 220-226, **1996**.

Dean, J.A., *Lange's Handbook of Chemistry*, McGraw-Hill, 15th Edition, **1999**.

Donley, H.E., The Drag Force on a Sphere, *UMAP Journal*, 12 (1), 47-80, **1991**.

Durand, G, and Poirier J.E., *PCT Int Appl WO 014161*, **2000**.

Fang, H., Zhang, L., Luo, L., Zhao, S., An, J., Xu, Z., Yu, J., Ottova, A., and Tien, H.T., A Study of Thin Liquid Films as Related to the Stability of Crude Oil Emulsions, *Journal of Colloid and Interface Science*, 238 (1), 177-182, **2001**.

Freer, E.M., and Radke, C.J., Relaxation of Asphaltenes at the Toluene/Water Interface: Diffusion Exchange and Surface Rearrangement, *Journal of Adhesion*, 80 (6), 481-496, **2004**.

Frising, T., Noik, C., and Dalmazzone, C., The Liquid/Liquid Sedimentation Process: From Droplet Coalescence to Technologically Enhanced Water/Oil Emulsion Gravity Separators: A Review, *Journal of Dispersion Science and Technology*, 27 (7), 1035-1057, **2006**.

Gafonova, O.V., and Yarranton, H.W., The Stabilization of Water-in-Hydrocarbon Emulsions by Asphaltenes and Resins, *Journal of Colloid and Interface Science*, 241 (2), 469-478, **2001**.

Garside, J., and Al-Dibouni, M.R., Velocity Voidage Relationships for Fluidization and Sedimentation, *Industrial & Engineering Chemistry Process Design and Development*, 2, 206, **1977**.

Gu, G., Xu, Z., Nandakumar, K., and Masliyah, J.H., Influence of Water-Soluble and Water-Insoluble Natural Surface Active Components on the Stability of Water-in-Toluene-Diluted Bitumen Emulsion, *Fuel*, 81 (14), 1859-1869, **2002**.

Hepler, L.G., *Alberta oilsands: Industrial procedures for extraction and some recent fundamental research*, AOSTRA Technical publication No. 14, **1994**.

Hiemenz, P.C., Rajagopalan R., *Principles of Colloid and Surface Chemistry*, CRC Press Third edition, **1997**.

Jiang, T., Hirasaki, G., Miller, C., Moran, K., and Fleury, M., Diluted Bitumen Water-in-Oil Emulsion Stability and Characterization by Nuclear Magnetic Resonance (NMR) Measurements, *Energy and Fuels*, 21 (3), 1325-1336, **2007**.

Jiang, T., Hirasaki, G.J., and Miller, C.A., Multi-Scale Observations of the Separation of Solids-Stabilized Diluted Bitumen Emulsions, *57th Canadian Chemical Engineering Conference*, **2007**.

Khadim, M.A., and Sarbar, M.A., Role of Asphaltene and Resin in Oil Field Emulsions, *Journal of Petroleum Science and Engineering*, 23 (3-4), 213-221, **1999**.

Klaseboer, E., Chevaillier, J.Ph., Gourdon, C., and Masbernat, O., Film Drainage Between Colliding Drops at Constant Approach Velocity: Experiments and Modeling, *Journal of Colloid and Interface Science*, 229, 274-285, **2000**.

Kotlyar, L.S., Kodama, H., Sparks, B.D., and Grattan-Bellew, P.E., Non-Crystalline Inorganic Matter-Humic Complexes in Athabasca Oil Sand and their Relationship to Bitumen Recovery, *Applied Clay Science*, 2 (3), 253-271, **1987**.

Kotlyar, L.S., Sparks, B.D., Woods, J.R., Raymond, S., Le Page, Y., and Shelfantook, W., Distribution and Types of Solids Associated with Bitumen, *Petroleum Science and Technology*, 16 (1-2), 1-19, **1998**.

Leja, J., and Bowman, C.W., Application of Thermodynamics to the Athabasca Tar Sands, *Canadian Journal of Chemical Engineering*, 46, 479-481, **1968**.

Liu, J., Xu, Z., and Masliyah, J., Role of Fine Clays in Bitumen Extraction From Oil Sands, *AIChE Journal*, 50 (8), 1917-1927, **2004**.

Lobo, L., Ivanov, I., and Wasan, D., Dispersion Coalescence: Kinetic Stability of Creamed Dispersions. *AIChE Jornal*, 39 (2), 322-334, **1993**.

Long, J., Xu, Z., and Masliyah, J.H., Single Molecule Force Spectroscopy of Asphaltene Aggregates, *Langmuir*, 23 (11), 6182-6190, **2007**.

Long, Y., Dabros, T., and Hamza, H., Stability and Settling Characteristics of Solvent-Diluted Bitumen Emulsions, *Fuel*, 81 (15), 1945-1952, **2002**.

Long, Y., Dabros, T., and Hamza, H., Structure of Water/Solids/Asphaltenes Aggregates and Effect of Mixing Temperature on Settling Rate in Solvent-Diluted Bitumen, *Fuel*, 83 (7-8), 823-832, **2004**.

MacRitchie, F., *Chemistry at Interfaces*, Academic Press, San Diego, CA, **1990**.

Masliyah, J., Zhou, Z., Xu, Z., Czarnecki, J., and Hamza, H., Understanding Water-Based Bitumen Extraction from Athabasca Oil Sands, *Canadian Journal of Chemical Engineering*, 82 (4), 628-654, **2004**.

Masliyah, J.H., Hindered Settling in a Multi-Species Particle System, *Chemical Engineering Science*, 34 (9), 1166-1168, **1979**.

McCabe, W.L., Smith, J.C., and Harriott, P., *Unit Operations of Chemical Engineering*, McGraw-Hill International Editions, Fourth Edition, Singapore, **1985**.

McLean, J.D., and Kilpatrick, P.K., Effects of Asphaltene Solvency on Stability of Water-in-Crude-Oil Emulsions, *Journal of Colloid and Interface Science*, 189 (2), 242, **1997**.

Moran, K., personal communication, Syncrude Canada Ltd., Edmonton, **2006**.

Ozkan, A., and Yekeler, M., A New Microcolumn Flotation Cell for Determining the Wettability and Floatability of Minerals, *Journal of Colloid and Interface Science*, 261 (2), 476-480, **2003**.

Palermo, T., Coalescence Phenomena a Review, *Revue de l'Institut Francais du Petrole*, 46 (3), 325-360, **1991**.

Peach, T.J., Bitumen Recovery from Tar Sands, *Energy Processing Canada*, May-June, **1974**.

Pow, J. R., G. H. Fairbanks, and W. J. Zamora, *Descriptions and Reserve Estimates of the Oil Sands of Alberta,* Athabasca Oil Sands, K. A. Clark Volume: Research Council of Alberta, 1-14, **1963**.

Rastegari, K., Svrcek, W.Y., and Yarranton, H.W., Kinetics of Asphaltene Flocculation, *Industrial and Engineering Chemistry Research*, 43 (21), 6861-6870, **2004**.

Richardson, J.F., and Zaki, W.N., Sedimentation and Fluidization: Part I, *Process Safety and Environmental Protection: Transactions of the Institution of Chemical Engineers, Part B*, 75, S82-S100, **1997**.

Romanova, U.G., Yarranton, H.W., Schramm, L.L., and Shelfantook, W.E., Investigation of Oil Sands Froth Treatment, *Canadian Journal of Chemical Engineering*, 82 (4), 710-721, **2004**.

Romanova, U.G., Valinasab, M., Stasiuk, E.N., Yarranton, H.W., Schramm, L.L., and Shelfantook, W.E., The Effect of Oil Sands Bitumen Extraction Conditions on Froth Treatment Performance, *Journal of Canadian Petroleum Technology*, 45 (9), 36-45, **2006**.

Romanova, U.G., personal communication, Calgary, **2006**.

Rommel, W., Meon, W., and Blass, E., Hydrodynamic Modeling of Droplet Coalescence at Liquid-Liquid Interfaces, *Separation Science and Technology*, 27 (2), 129-159, **1992**.

Saboni, A., Alexandrova, S., Gourdon, C., and Chesters, A.K., Interdrop Coalescence with Mass Transfer: Comparison of the Approximate Drainage Models with Numerical Results, *Chemical Engineering Journal*, 88, (1-3), 127-139, **2002**.

Sanford, E.C., and Seyer, F.A., Processibility of Athabasca Tar Sand Using a Batch Extraction Unit: The Role of NaOH, *CIM Bulletin*, 72 (803), 164-169, **1979**.

Scales, M., Growing for Black Gold, *Canadian Mining Journal*, 128 (3), 15-21, **2007**.

Schramm, L.L., and Kwak, J.C.T., Rheological Properties of an Athabasca Bitumen and Some Bituminous Mixtures and Dispersions, *Journal of Canadian Petroleum Technology*, 27 (1), 26-35, **1988**.

Schramm, L.L., and Smith, R.G., Some Observations on the Ageing Phenomenon in the Hot Water Processing of Athabasca Oil Sands. Part 1. The nature of the phenomenon, *AOSTRA Journal of Research*, 3, 195-214, **1987**a.

Schramm, L.L., and Smith, R.G., Some Observations on the Ageing Phenomenon in the Hot Water Processing of Athabasca Oil Sands. Part 2. The Reversibility of the Phenomenon, *AOSTRA Journal of Research*, 3, 215-224, **1987**b.

Schramm, L.L., and Smith, R.G., Some Parametric Studies of Oil Sand Conditioning in the Hot Water Floatation Process, *AOSTRA Journal of Research*, 5, 87-107, **1989**.

Schramm, L.L., Smith, R.G., and Stone, J.A., The Influence of Natural Surfactant Concentration on the Hot Water Process for Recovering Bitumen from the Athabasca Oil Sands, *AOSTRA Journal of Research*, *1*, 5-14, **1984**.

Schramm, L.L., The Influence of Suspension Viscosity of Bitumen Rise Velocity and Potential Recovery in the Hot Water Floatation Process for Oil Sands, *Journal of Canadian Petroleum Technology*, 28, 73-80, **1989**.

Shelfantook, W.E., A Perspective on the Selection of Froth Treatment Processes, *Canadian Journal of Chemical Engineering*, 82 (4), 704-709, **2004**.

Shih, Y.T., Gidaspow, D., and Wasan, D.T., Hydrodynamics of Sedimentation of Multisized Particles, 50 (3), 201-215, **1987**.

Spiecker, P.M., Gawrys, K.L., Trail, C.B., and Kilpatrick, P.K., Effects of Petroleum Resins on Asphaltene Aggregation and Water-in-Oil Emulsion Formation, *Colloids and Surfaces A: Physicochemical and Engineering Aspects*, 220 (1-3), 9-27, **2003**.

Stasiuk, E.N., personal communication, Calgary, **2006**.

Sztukowski, D.M., and Yarranton, H.W., Characterization and Interfacial Behavior of Oil Sands Solids Implicated in Emulsion Stability, *Journal of Dispersion Science and Technology*, 25 (3), 299-310, **2004**.

Sztukowski, D.M., and Yarranton, H.W., Oilfield Solids and Water-in-Oil Emulsion Stability, *Journal of Colloid and Interface Science*, 285 (2), 821-833, **2005**b.

Sztukowski, D.M., *Asphaltene and solid-stabilized water-in-oil emulsions*, Ph.D. dissertation, Department of Chemical and Petroleum Engineering, University of Calgary, AB, **2005**.

Sztukowski, D.M., Jafari, M., Alboudwarej, H., and Yarranton, H.W., Asphaltene Self-Association and Water-in-Hydrocarbon Emulsions, *Journal of Colloid and Interface Science*, 265 (1), 179-186, **2003**.

Takamura, K., Microscopic Structure of Athabasca Oil Sand, *Canadian Journal of Chemical Engineering*, 60 (4), 538-545, **1982**.

Tobin, T., Muralidhar, R., Wright, H., and Ramkrishna, D., Determination of Coalescence Frequencies in Liquidliquid Dispersions: Effect of Drop Size Dependence, *Chemical Engineering Science*, 45 (12), 3491–3504, **1990**.

Tsouris, C., and Tavlarides, L.L., Breakage and Coalescence Models for Drops in Turbulent Dispersions, *AIChE Journal*, 40 (3), 395-406, **1994**.

Valinasab, M., *The Effect of Bitumen Extraction Conditions on Froth Treatment Effectiveness*, Master thesis, Department of Chemical and Petroleum Engineering, University of Calgary, AB, **2006**.

Varadaraj, R., and Brons, C., Molecular Origins of Crude Oil Interfacial Activity Part 3: Characterization of the Complex Fluid Rag Layer Formed at Crude Oil-Water Interfaces, *Energy and Fuels*, 21 (3), 1617-1621, **2007**.

Walter, C., and Rohner, R., *Fundamentals of the Volumetric Karl Fischer Titration, Mettler Toledo DL31/DL38 Titrators*, Application brochure 26, **2007**.

Wells, P.R.A., Oil Supply Challenges - 1: The Non-OPEC Decline, *Oil and Gas Journal*, 103 (7), 20-28, **2005**.

Yan Z., Elliott J.A.W., and Masliyah J.H., *Journal of Colloid and Interfacial Science*, 220 (2), 329, **1999**.

Yan, N., Gray, M.R., and Masliyah, J.H., On Water-in-Oil Emulsions Stabilized by Fine Solids, *Colloids and Surfaces A: Physicochemical and Engineering Aspects*, 193 (1-3), 97-107, **2001**.

Yan, Y., and Masliyah, J.H., Sedimentation of Solid Particles in Oil-in-Water Emulsions, *International Journal of Multiphase Flow*, 19 (5), 875-886, **1993**.

Yarar, B., and Kaoma, J., Critical Surface Tension of Sulfide Minerals, *Preprint - Society of Mining Engineers of AIME*, 276, 1875-1878, **1983**.

Yarranton, H.W., Asphaltene Self-Association, *Journal of Dispersion Science and Technology*, 26 (1), 5-8, **2005**.

Yarranton, H.W., Sztukowski, D.M., and Urrutia, P., Effect of Interfacial Rheology on Model Emulsion Coalescence. I. Interfacial Rheology, *Journal of Colloid and Interface Science*, 310 (1), 246-252, **2007**.

Yarranton, H.W., Urrutia, P., and Sztukowski, D.M., Effect of Interfacial Rheology on Model Emulsion Coalescence. II. Emulsion Coalescence, *Journal of Colloid and Interface Science*, 310 (1), 253-259, **2007**.

Zisman, W.A., *Contact Angle, Wettability and Adhesion*, *Adv. Chem. Ser*., 43, 1, American Chemical Society, Washington, DC, **1964**.

Appendix A

Tabular Experimental Data

Table A.1 Stepwise centrifuge tests data for froth diluted with toluene. Data with an asterisk beside their trial numbers were used for initial rag components calculations.

		Extraction			Froth Treatment			
Trial Number	Sample Number	Oil Sand Quality	Temperature °C	NaOH wt%	Temperature °C	Solvent/Froth ,g/g	Solvent/Bitumen ,g/g	Total Volume cm³
1	MS-85	LQOS3	23	0	23	0.0696	0.9765	8.5
2 *	MS-85	LQOS3	23	0	23	0.2919	4.0954	9.2
3 *	MS-86	LQOS3	23	0	23	0.5963	8.3661	8.8
4 *	MS-89	LQOS3	23	0.04	23	0.6115	6.9618	9.6
5 *	MS-90	LQOS3	23	0.04	23	0.2955	3.3637	8.9
6	MS-86	LQOS3	23	0	60	0.6043	8.4789	8.3
7 *	MS-90	LQOS3	23	0.04	60	0.6112	6.9583	9.2
8	MS-86	LQOS3	23	0	60	0.2907	4.0785	8.9
9 *	MS-90	LQOS3	23	0.04	60	0.3009	3.4250	9.3
10	MS-92	LQOS3	80	0	23	0.5331	4.1197	9.1
11 *	MS-96 & 97	LQOS3	80	0.04	23	0.5298	2.9076	9.5
12 *	MS-92	LQOS3	80	0	23	1.0973	8.4790	9.5
13 *	MS-97	LQOS3	80	0.04	23	1.1024	6.0504	9.7
14	MS-92	LQOS3	80	0	60	0.5306	4.0998	9.2
15 *	MS-96	LQOS3	80	0.04	60	0.3709	2.0359	9.0
16 *	MS-92	LQOS3	80	0	60	1.0940	8.4535	9.5
17	MS-96	LQOS3	80	0.04	60	1.0962	6.0166	9.2
18	MS-92 & 93	LQOS3	80	0	23	0.5288	4.0859	9.0
19	MS-93	LQOS3	80	0	60	0.5244	4.0523	8.7
20	MS-96	LQOS3	80	0.04	60	1.0899	5.9816	9.3
21	MS-100	AQOS2	80	0	23	1.8723	4.1349	9.6
22	MS-95	LQOS3	80	0	60	1.1078	8.5604	9.0
23	MS-100	AQOS2	80	0	23	3.7637	8.3120	9.7
24	MS-100	AQOS2	80	0	60	1.8432	4.0706	9.6
25	MS-100	AQOS2	80	0	60	3.8223	8.4416	9.8
26	MS-116	AQOS2	80	0	23	1.7091	3.9720	10.8
27	MS-116	AQOS2	80	0	60	1.7888	4.1572	10.4
28 *	MS-116	AQOS2	80	0	23	3.5499	8.2497	10.0
29 *	MS-116	AQOS2	80	0	60	3.7093	8.6203	10.0
30	MS-115	LQOS3	80	0	23	0.9117	8.5769	7.5
31	MS-115	LQOS3	80	0	23	0.9030	8.4952	10.0

Table A.1 Cont'd

Trial Number	Oil Volume, cm³								Rag Volume, cm³							
	500 RPM	1000 RPM	1500 RPM	2000 RPM	2500 RPM	3000 RPM	3500 RPM	4000 RPM	500 RPM	1000 RPM	1500 RPM	2000 RPM	2500 RPM	3000 RPM	3500 RPM	4000 RPM
1	0.0	0.0	0.0	0.1	0.1	0.4	0.5	0.5	0.0	0.0	0.0	0.1	0.1	0.1	0.1	0.1
2 *	0.1	0.1	0.1	0.5	0.7	1.1	1.6	1.6	4.3	3.6	3.1	2.7	2.5	1.7	1.0	1.0
3 *	0.8	0.9	2.3	2.6	3.1	3.6	3.6	3.6	4.3	4.1	1.9	1.3	1.0	0.5	0.5	0.5
4 *	0.9	0.9	3.1	3.1	3.1	3.6	3.7	3.7	4.4	4.1	1.0	1.0	1.0	0.5	0.4	0.4
5 *	0.2	0.5	0.5	0.5	1.6	1.6	2.1	2.1	4.5	3.4	3.0	2.6	1.5	1.5	0.5	0.6
6	0.5	1.1	2.5	2.9	3.1	3.2	3.2	3.2	4.3	3.4	1.5	0.6	0.4	0.3	0.3	0.3
7 *	0.2	1.0	1.9	2.5	3.1	3.4	3.7	3.7	5.8	4.7	2.5	1.5	0.9	0.5	0.2	0.2
8	0.4	0.5	0.5	1.1	1.4	1.5	1.8	1.8	2.7	1.9	1.7	1.0	1.0	0.8	0.5	0.5
9 *	0.4	0.5	0.5	0.8	1.7	1.9	2.0	2.1	4.1	3.3	2.8	1.9	1.0	0.6	0.5	0.5
10	1.4	1.4	1.4	1.6	2.1	3.4	3.6	3.6	3.2	3.2	3.2	3.1	2.7	1.2	1.0	1.0
11 *	0.7	0.8	1.4	2.6	4.0	4.0	4.0	4.5	7.3	5.7	4.6	3.0	1.1	1.0	1.0	0.5
12 *	3.0	3.0	3.7	3.8	5.0	5.0	5.2	5.5	5.4	4.1	3.4	3.2	1.4	1.4	1.3	1.0
13 *	2.9	2.9	4.7	5.4	5.4	5.8	6.0	6.0	5.2	4.5	2.8	1.6	1.1	0.9	0.8	0.8
14	0.7	1.4	1.4	1.9	1.9	2.7	3.2	2.9	2.0	3.8	3.8	3.3	2.8	2.1	1.7	2.3
15 *	0.7	1.2	1.2	1.2	2.5	3.3	3.5	3.5	7.3	4.8	4.8	4.6	3.0	2.2	2.0	2.0
16 *	2.0	2.4	2.5	2.5	4.0	4.3	5.0	5.0	5.2	4.8	4.8	4.8	3.1	2.9	2.1	2.1
17	3.4	5.0	5.0	5.0	5.0	5.0	5.0	5.0	1.8	0.0	0.0	0.0	0.0	0.0	0.0	0.0
18	1.0	1.0	1.8	2.7	2.7	2.9	3.3	3.5	8.0	3.4	1.9	0.8	1.1	0.7	0.5	0.3
19	3.1	3.3	3.3	3.3	3.3	3.3	3.3	3.5	0.0	0.0	0.0	0.0	0.0	0.0	0.0	0.0
20	5.1	5.3	5.2	5.2	5.3	5.3	5.5	5.8	0.0	0.0	0.0	0.0	0.0	0.0	0.0	0.0
21	7.5	7.5	7.5	7.5	7.9	7.9	7.9	7.9	0.0	0.0	0.0	0.0	0.0	0.0	0.0	0.0
22	0.7	1.0	1.5	2.2	3.5	3.8	4.5	4.7	6.4	6.1	4.9	4.1	2.8	2.2	1.5	1.3
23	8.4	8.2	8.7	8.7	8.7	8.8	8.8	8.8	0.0	0.0	0.0	0.0	0.0	0.0	0.0	0.0
24	7.3	8.1	8.1	8.1	8.1	8.1	8.1	8.1	0.0	0.0	0.0	0.0	0.0	0.0	0.0	0.0
25	8.8	8.8	8.8	8.8	9.0	9.0	9.0	9.0	0.0	0.0	0.0	0.0	0.0	0.0	0.0	0.0
26	6.8	6.8	6.8	6.8	6.8	7.0	7.0	7.0	0.0	0.0	0.0	0.0	0.0	0.0	0.0	0.0
27	6.9	6.9	6.9	6.9	6.9	6.9	6.9	7.1	0.5	0.0	0.0	0.0	0.0	0.0	0.0	0.0
28 *	7.2	7.3	7.7	8.0	8.0	8.0	8.0	8.0	1.3	1.2	0.3	0.0	0.0	0.0	0.0	0.0
29 *	7.0	7.5	8.3	8.3	8.3	8.3	8.3	8.3	1.7	0.9	0.1	0.1	0.0	0.0	0.0	0.0
30	4.7	5.2	5.2	5.2	5.2	5.2	5.2	5.2	0.0	0.0	0.0	0.0	0.0	0.0	0.0	0.0
31	0.5	0.7	0.9	0.9	2.5	3.5	4.1	4.5	7.0	6.8	6.3	6.0	3.7	2.5	1.4	1.0

Table A.1 Cont'd

	Water Volume, cm³								Sediment Volume, cm³							
Trial Number	500 RPM	1000 RPM	1500 RPM	2000 RPM	2500 RPM	3000 RPM	3500 RPM	4000 RPM	500 RPM	1000 RPM	1500 RPM	2000 RPM	2500 RPM	3000 RPM	3500 RPM	4000 RPM
1	2.5	3.6	4.0	4.7	4.8	4.6	5.0	5.0	6.0	4.9	4.5	3.6	3.5	3.5	3.1	3.1
2 *	0.8	2.0	3.0	3.0	3.3	3.7	3.9	3.9	4.0	3.5	3.0	3.0	2.7	2.7	2.7	2.7
3 *	0.2	0.7	1.5	1.8	2.2	2.2	2.2	2.2	3.5	3.1	3.1	3.1	2.5	2.5	2.5	2.5
4 *	1.4	2.3	3.2	3.2	3.2	3.2	3.2	3.2	2.9	2.3	2.3	2.3	2.3	2.3	2.3	2.3
5 *	1.2	2.4	2.8	3.2	3.3	3.3	3.8	3.9	3.0	2.5	2.5	2.5	2.5	2.5	2.5	2.3
6	0.5	0.8	1.3	2.3	2.3	2.3	2.3	2.3	3.0	3.0	3.0	2.5	2.5	2.5	2.5	2.5
7 *	1.2	1.5	2.6	3.0	3.0	3.1	3.1	3.1	2.0	2.0	2.2	2.2	2.2	2.2	2.2	2.2
8	1.0	2.8	3.2	3.3	3.5	3.5	3.5	3.5	4.8	3.7	3.5	3.5	3.0	3.0	3.0	3.0
9 *	1.3	2.5	3.0	3.6	3.6	3.6	3.6	4.0	3.5	3.0	3.0	3.0	3.0	3.0	3.0	2.5
10	0.5	1.6	2.0	2.0	2.0	2.3	2.4	2.5	4.0	2.9	2.5	2.4	2.3	2.2	2.1	2.0
11 *	0.4	1.5	2.0	2.0	2.1	2.5	2.5	2.7	1.1	1.5	1.5	1.9	2.3	2.0	2.0	1.8
12 *	0.1	0.9	0.9	1.0	1.1	1.3	1.5	1.5	1.0	1.5	1.5	1.5	2.0	1.8	1.5	1.5
13 *	0.2	1.0	1.2	1.4	1.7	1.7	1.7	1.9	1.4	1.3	1.0	1.3	1.5	1.3	1.2	1.0
14	0.5	1.2	1.8	1.8	2.5	2.6	2.7	2.2	6.0	2.8	2.2	2.2	2.0	1.8	1.6	1.8
15 *	0.4	1.2	1.2	1.4	1.5	1.5	1.5	1.5	0.6	1.8	1.8	1.8	2.0	2.0	2.0	2.0
16 *	0.8	0.8	1.0	1.0	1.2	1.4	1.5	1.5	1.5	1.5	1.2	1.2	1.2	0.9	0.9	0.9
17	0.5	1.0	1.3	2.2	2.7	2.8	3.0	3.0	3.5	3.2	2.9	2.0	1.5	1.4	1.2	1.2
18	0.0	1.1	2.3	2.5	2.7	2.9	3.0	3.2	0.0	3.5	3.0	3.0	2.5	2.5	2.2	2.0
19	1.8	2.2	2.2	2.2	2.4	2.4	2.4	2.7	3.8	3.2	3.2	3.2	3.0	3.0	3.0	2.5
20	1.0	1.1	1.3	1.3	1.3	1.5	1.8	1.7	3.2	2.9	2.8	2.8	2.7	2.5	2.0	1.8
21	0.0	0.0	0.9	0.9	0.6	0.6	0.6	0.6	2.1	2.1	1.2	1.2	1.1	1.1	1.1	1.1
22	0.4	0.4	1.2	1.3	1.3	1.6	1.6	1.6	1.5	1.5	1.4	1.4	1.4	1.4	1.4	1.4
23	0.0	0.0	0.0	0.0	0.5	0.4	0.4	0.4	1.3	1.5	1.0	1.0	0.5	0.5	0.5	0.5
24	0.0	0.0	0.0	0.0	0.6	0.6	0.6	0.7	2.3	1.5	1.5	1.5	0.9	0.9	0.9	0.8
25	0.0	0.0	0.0	0.0	0.2	0.2	0.2	0.3	1.0	1.0	1.0	1.0	0.6	0.6	0.6	0.5
26	2.0	2.0	2.0	2.0	2.2	2.3	2.3	2.3	2.0	2.0	2.0	2.0	1.8	1.5	1.5	1.5
27	2.1	2.5	2.5	2.5	2.5	2.5	2.6	2.7	0.9	1.0	1.0	1.0	1.0	1.0	0.9	0.6
28 *	1.0	1.0	1.2	1.2	1.2	1.2	1.2	1.2	0.5	0.5	0.8	0.8	0.8	0.8	0.8	0.8
29 *	0.9	0.9	0.9	0.9	1.2	1.2	1.2	1.2	0.4	0.7	0.7	0.7	0.5	0.5	0.5	0.5
30	0.0	0.0	0.0	0.0	0.5	0.5	0.5	0.5	2.8	2.3	2.3	2.3	1.8	1.8	1.8	1.8
31	0.7	0.7	1.0	1.6	1.6	2.0	2.5	2.5	1.8	1.8	1.8	1.5	2.2	2.0	2.0	2.0

Table A.2 Stepwise centrifuge tests data for froth diluted with n-heptane. Data with an asterisk beside their trial numbers were used for initial rag components calculations.

		Extraction			Froth Treatment			
Trial Number	Sample Number	Oil Sand Quality	Temperature °C	NaOH wt%	Temperature °C	Solvent/Froth ,g/g	Solvent/Bitumen ,g/g	Total Volume cm³
1 *	MS-83	LQOS3	23	0	23	0.1857	2.6060	12.0
2 *	MS-83	LQOS3	23	0	60	0.1857	2.6060	11.8
3	MS-83	LQOS3	23	0	23	0.0482	0.6760	9.6
4 *	MS-88	LQOS3	23	0.04	23	0.2336	2.6594	10.8
5 *	MS-88	LQOS3	23	0.04	23	0.0581	0.6617	10.7
6	MS-84	LQOS3	23	0	60	0.0486	0.6815	10.3
7 *	MS-89	LQOS3	23	0.04	60	0.2323	2.6450	10.7
8	MS-89	LQOS3	23	0.04	60	0.0659	0.7501	11.7
9	MS-84	LQOS3	23	0	23	0.0483	0.6784	10.2
10	MS-92	LQOS3	80	0	23	0.0867	0.6702	8.3
11 *	MS-96	LQOS3	80	0.04	23	0.1185	0.6505	8.9
12 *	MS-92	LQOS3	80	0	23	0.3381	2.6128	8.7
13	MS-96	LQOS3	80	0.04	23	0.4906	2.6929	9.0
14 *	MS-92	LQOS3	80	0	60	0.1183	0.9143	10.4
15	MS-96	LQOS3	80	0.04	60	0.1213	0.6658	8.5
16 *	MS-92	LQOS3	80	0	60	0.4904	3.7897	8.8
17 *	MS-96	LQOS3	80	0.04	60	0.4782	2.6248	10.6
18	MS-95	LQOS3	80	0	23	0.3463	2.6763	8.7
19	MS-95	LQOS3	80	0	23	0.3430	2.6507	8.5
20	MS-95	LQOS3	80	0	23	0.3440	2.6585	5.9
21	MS-95	LQOS3	80	0	23	0.3433	2.6531	8.6
22	MS-95	LQOS3	80	0	23	0.3566	2.7560	11.0
23	MS-100	AQOS2	80	0	23	0.3018	0.6666	9.2
24	MS-100	AQOS2	80	0	23	1.1959	2.6411	9.7
25	MS-100	AQOS2	80	0	60	0.3028	0.6688	9.5
26	MS-100	AQOS2	80	0	60	1.2006	2.6516	9.6
27	MS-110	AQOS2	80	0	23	1.1418	2.6145	10.6
28	MS-110	AQOS2	80	0	23	1.1601	2.6563	10.5
29	MS-116	AQOS2	80	0	23	0.2798	0.6503	10.5
30 *	MS-116	AQOS2	80	0	60	0.2842	0.6606	10.5
31 *	MS-116	AQOS2	80	0	23	1.1451	2.6612	11.0
32 *	MS-116	AQOS2	80	0	60	1.1417	2.6532	10.6
33	MS-115	LQOS3	80	0	23	0.2838	2.6702	10.3
34	MS-115	LQOS3	80	0	23	0.2850	2.6807	9.3
35	MS-115	LQOS3	80	0	23	0.0702	0.6604	10.5
36	MS-115	LQOS3	80	0	23	0.0719	0.6760	9.5
37	MS-115	LQOS3	80	0	23	0.2862	2.6920	6
38	MS-115	LQOS3	80	0	23	0.2861	2.6912	9.7

Table A.2 Cont'd

Trial Number	Oil Volume, cm³								Rag Volume, cm³							
	500 RPM	1000 RPM	1500 RPM	2000 RPM	2500 RPM	3000 RPM	3500 RPM	4000 RPM	500 RPM	1000 RPM	1500 RPM	2000 RPM	2500 RPM	3000 RPM	3500 RPM	4000 RPM
1 *	0.0	0.0	0.1	0.2	0.3	1.3	2.5	2.5	6.5	4.5	3.9	3.9	3.9	3.0	1.4	1.2
2 *	0.2	0.2	0.4	0.4	0.4	0.4	1.1	1.7	4.9	4.2	3.7	3.5	3.5	3.5	2.8	1.6
3	0.0	0.0	0.0	0.2	0.3	0.6	0.7	0.7	0.7	0.6	0.5	0.3	0.2	0.2	0.1	0.1
4 *	0.1	0.2	0.5	0.7	2.1	2.1	2.6	2.6	4.7	4.1	3.5	3.1	1.5	1.0	0.1	0.1
5 *	0.0	0.0	0.0	0.2	0.7	0.7	0.7	0.7	3.2	2.9	2.9	2.2	1.7	1.5	1.5	1.4
6	0.0	0.0	0.1	0.6	0.6	0.6	0.6	0.6	1.8	1.3	0.9	0.2	0.1	0.1	0.1	0.1
7 *	1.2	1.4	1.8	2.2	2.7	2.8	2.8	2.9	4.0	2.8	1.9	1.2	0.5	0.3	0.3	0.2
8	0.0	0.1	0.5	0.7	0.7	0.7	0.7	0.7	2.7	2.4	2.0	1.7	1.7	1.5	1.2	1.0
9	0.0	0.0	0.0	0.0	0.0	0.1	0.5	0.7	1.7	1.7	1.2	1.2	1.2	0.8	0.4	0.2
10	0.4	0.5	0.7	0.8	0.8	1.1	1.3	1.3	1.6	1.0	0.8	0.5	0.5	0.4	0.2	0.2
11 *	0.4	0.4	0.7	0.7	1.1	1.4	1.7	1.9	4.5	3.5	2.9	2.4	1.8	1.5	1.0	0.8
12 *	0.5	0.5	0.7	2.2	2.9	3.2	3.2	3.2	5.2	4.4	4.0	1.9	0.9	0.3	0.3	0.3
13	3.3	3.5	3.8	4.0	4.3	4.3	4.3	4.3	1.0	0.8	0.7	0.5	0.2	0.0	0.0	0.0
14 *	0.1	0.1	0.1	0.7	0.7	1.4	1.4	0.0	4.0	3.1	2.8	1.9	1.9	1.0	1.0	0.0
15	0.0	0.0	0.1	0.5	0.6	1.0	1.5	1.9	2.5	2.0	1.9	1.5	1.5	1.5	0.8	0.4
16 *	3.0	3.0	3.8	3.9	4.3	4.3	4.3	0.0	3.8	1.4	0.6	0.6	0.2	0.0	0.0	0.0
17 *	4.1	4.1	4.6	4.9	5.1	5.1	0.0	0.0	5.7	1.1	0.4	0.0	0.0	0.0	0.0	0.0
18	0.2	0.5	2.2	2.2	2.5	2.9	3.7	3.8	5.0	4.2	2.5	1.9	1.6	0.8	0.3	0.1
19	0.8	1.0	2.1	3.0	2.6	2.7	2.5	2.9	4.2	3.5	1.9	0.9	0.5	0.3	0.3	0.0
20	2.9	3.0	3.0	3.0	3.0	3.0	3.0	3.0	0.0	0.0	0.0	0.0	0.0	0.0	0.0	0.0
21	0.1	0.3	0.6	2.3	3.1	3.2	3.2	3.4	5.5	4.5	4.2	2.3	0.8	0.2	0.2	0.2
22	0.0	0.3	0.3	0.3	0.9	2.5	3.2	3.2	7.0	5.7	5.0	4.7	3.8	1.7	0.6	0.6
23	6.0	5.9	5.9	5.7	5.7	5.7	5.7	5.7	0.0	0.0	0.0	0.0	0.0	0.0	0.0	0.0
24	5.5	7.2	7.2	7.2	7.2	7.2	7.2	7.2	0.0	0.0	0.0	0.0	0.0	0.0	0.0	0.0
25	6.0	6.0	6.0	6.0	5.3	5.3	5.3	5.3	0.0	0.0	0.0	0.0	0.0	0.0	0.0	0.0
26	6.6	7.2	7.2	7.4	7.4	7.4	7.4	7.4	0.0	0.0	0.0	0.0	0.0	0.0	0.0	0.0
27	3.1	3.6	3.6	4.3	4.3	4.3	4.3	4.3	1.8	1.4	1.4	0.0	0.0	0.0	0.0	0.0
28	3.7	4.3	4.3	4.5	4.4	4.4	4.5	4.5	1.3	0.5	0.5	0.0	0.0	0.0	0.0	0.0
29	3.5	3.7	3.7	3.7	3.7	3.7	3.7	3.7	0.0	0.0	0.0	0.0	0.0	0.0	0.0	0.0
30 *	2.5	2.5	2.5	3.0	3.0	3.0	3.0	3.0	1.5	1.5	1.5	0.0	0.0	0.0	0.0	0.0
31 *	5.0	5.9	5.9	6.4	6.4	6.4	6.4	6.4	3.5	2.0	2.0	0.0	0.0	0.0	0.0	0.0
32 *	6.1	6.1	6.1	6.1	6.1	6.1	6.1	6.1	1	1	0	0	0	0	0	0
33	0.3	0.3	2.2	3	3.3	3.5	3.8	3.8	6.5	5.5	3.2	2.2	1	0.5	0.2	0.1
34	0.3	0.3	1	1.3	1.8	2.2	2.6	2.7	5.7	4.7	3.8	3	2	1.6	1.1	0.7
35	0	0	0	0.9	1.3	1.3	1.8	2	4.3	3	2.7	1.4	1.2	1.1	0.5	0
36	0	0	0	0	0.6	0.6	0.5	0.7	1.3	1	1	0.9	0.3	0.3	0.2	0
37	2.3	3	3	3	3	3	3	3	0	0	0	0	0	0	0	0
38	0.4	0.7	1.3	2.2	2.5	2.9	3	3	5.1	4.3	2.9	1.9	1.2	0.3	0.2	0.2

Table A.2 Cont'd

Trial Number	Water Volume, cm³								Sediment Volume, cm³							
	500 RPM	1000 RPM	1500 RPM	2000 RPM	2500 RPM	3000 RPM	3500 RPM	4000 RPM	500 RPM	1000 RPM	1500 RPM	2000 RPM	2500 RPM	3000 RPM	3500 RPM	4000 RPM
1 *	1.0	3.0	4.0	4.0	4.0	4.1	4.5	4.7	4.5	4.0	3.5	3.5	3.5	3.5	3.5	3.5
2 *	1.6	2.8	3.5	3.9	3.9	3.9	3.9	4.5	5.1	4.5	4.1	3.9	3.9	3.9	3.9	3.9
3	2.4	2.6	3.6	3.9	4.3	4.2	4.2	4.5	6.5	6.4	5.5	5.3	4.9	4.8	4.8	4.5
4 *	3.5	4.5	5.0	5.3	5.5	5.6	5.6	5.6	2.5	2.0	1.8	1.7	1.7	2.1	2.5	2.5
5 *	2.5	3.8	4.1	4.6	4.6	5.0	5.0	5.1	5.0	4.0	3.7	3.7	3.7	3.5	3.5	3.5
6	2.0	3.0	4.0	4.2	4.3	4.8	5.0	5.0	6.5	6.0	5.3	5.3	5.3	4.8	4.6	4.6
7 *	3.5	4.2	4.7	5.0	5.2	5.3	5.3	5.3	2.0	2.3	2.3	2.3	2.3	2.3	2.3	2.3
8	4.5	5.7	5.9	6.5	6.5	7.0	7.6	7.8	4.5	3.5	3.3	2.8	2.8	2.5	2.2	2.2
9	2.1	2.7	3.5	3.5	4.5	4.8	4.8	4.8	6.4	5.8	5.5	5.5	4.5	4.5	4.5	4.5
10	1.0	2.1	2.9	3.6	3.6	3.6	3.6	3.8	5.3	4.7	3.9	3.4	3.4	3.2	3.2	3.0
11 *	1.1	2.3	2.3	2.8	3.0	3.0	3.2	3.2	2.9	2.7	3.0	3.0	3.0	3.0	3.0	3.0
12 *	1.0	1.6	1.8	2.4	2.7	2.7	2.7	2.7	2.0	2.2	2.2	2.2	2.2	2.5	2.5	2.5
13	1.0	1.2	1.7	1.9	1.9	2.1	2.1	2.5	3.7	3.5	2.8	2.6	2.6	2.6	2.6	2.2
14 *	1.3	2.4	3.5	3.5	3.8	4.0	4.2	0.0	5.0	4.8	4.0	4.3	4.0	4.0	3.8	0.0
15	1.5	2.2	2.7	3.0	3.1	3.2	3.7	3.7	4.5	4.3	3.8	3.5	3.3	2.8	2.5	2.5
16 *	0.8	1.4	1.6	1.6	1.8	2.0	2.0	0.0	1.2	3.0	2.8	2.7	2.5	2.5	2.5	0.0
17 *	0.2	2.1	2.1	2.2	2.5	3.0	0.0	0.0	0.6	3.3	3.5	3.5	3.0	2.5	0.0	0.0
18	0.5	1.3	1.3	1.9	1.9	2.5	2.2	2.5	3.0	2.7	2.7	2.7	2.7	2.5	2.5	2.3
19	0.3	1.3	1.8	1.8	2.5	2.3	2.2	2.2	3.2	2.7	2.7	2.9	3.0	3.2	3.5	3.4
20	0.0	0.1	0.1	0.3	0.4	0.5	0.5	0.5	3.0	2.8	2.8	2.6	2.5	2.4	2.4	2.4
21	0.8	1.3	2.0	2.2	2.5	2.7	2.7	2.8	2.2	2.5	1.8	1.8	2.2	2.5	2.5	2.2
22	1.5	2.5	3.5	3.8	4.1	4.3	4.5	4.5	2.5	2.5	2.2	2.2	2.2	2.5	2.7	2.7
23	0.0	0.0	0.0	1.0	0.9	0.9	1.2	1.5	3.2	3.3	3.3	2.5	2.6	2.6	2.3	2.0
24	0.0	0.0	0.0	0.5	0.5	0.5	0.5	0.5	4.2	2.5	2.5	2.0	2.0	2.0	2.0	2.0
25	0.0	0.0	0.0	0.4	1.1	1.2	1.2	1.2	3.5	3.5	3.5	3.1	3.1	3.0	3.0	3.0
26	0.0	0.0	0.0	0.0	0.0	0.0	0.0	0.0	3.0	2.4	2.4	2.2	2.2	2.2	2.2	2.2
27	3.9	4.6	4.6	5.5	5.5	5.5	5.5	5.5	1.8	1.0	1.0	0.8	0.8	0.8	0.8	0.8
28	2.0	4.2	4.4	4.7	5.0	5.0	4.8	4.8	3.5	1.5	1.3	1.3	1.1	1.1	1.2	1.2
29	4.0	4.3	4.3	4.3	4.3	4.3	4.3	4.3	3.0	2.5	2.5	2.5	2.5	2.5	2.5	2.5
30 *	3.0	3.0	3.5	5.0	5.0	5.0	5.0	5.0	3.5	3.5	3.0	2.5	2.5	2.5	2.5	2.5
31 *	1.6	2.1	2.1	3.0	3.0	3.0	3.0	3.0	0.9	0.9	0.9	1.5	1.5	1.5	1.5	1.5
32 *	2.1	2.1	2.5	2.7	2.7	2.7	3	3	1.4	1.4	2	1.8	1.8	1.8	1.5	1.5
33	1	2.5	3	3.1	3.6	3.7	3.7	3.708	2.5	2	1.9	2	2.4	2.6	2.6	2.692
34	0.8	2.1	2.5	2.8	3.3	3.3	3.3	3.3	2.5	2.2	2	2.2	2.2	2.2	2.3	2.6
35	0.9	3	4	4.6	5	5.1	5.2	5.5	5.3	4.5	3.8	3.6	3	3	3	3
36	1.2	3	3.4	4.3	4.4	4.4	4.8	5.1	7	5.5	5.1	4.3	4.2	4.2	4	3.7
37	0	0	0.2	1	1	1	1	1	3.7	3	2.8	2	2	2	2	2
38	1.5	2.2	2.5	2.6	2.8	3.2	3.2	3.5	2.7	2.5	3	3	3.2	3.3	3.3	3

Table A.3 Stepwise centrifuge tests data for froth diluted with heptol 80/20. Data with an asterisk beside their trial numbers were used for initial rag components calculations.

		Extraction			Froth Treatment			
Trial Number	Sample Number	Oil Sand Quality	Temperature °C	NaOH wt%	Temperature °C	Solvent/Froth ,g/g	Solvent/Bitumen ,g/g	Total Volume cm³
1	MS-87	LQOS3	23	0	23	0.0543	0.7621	7.4
2	MS-91	LQOS3	23	0.04	23	0.0616	0.7011	8.7
3 *	MS-87	LQOS3	23	0	23	0.3515	4.9292	8.0
4 *	MS-91	LQOS3	23	0.04	23	0.4412	5.0252	8.3
5	MS-87	LQOS3	23	0	60	0.0595	0.8347	7.5
6	MS-91	LQOS3	23	0.04	60	0.0630	0.7178	7.9
7 *	MS-87 & 84	LQOS3	23	0	60	0.3528	4.9481	8.0
8	MS-91	LQOS3	23	0.04	60	0.4332	4.9335	8.0
9	MS-84	LQOS3	23	0	60	0.0528	0.7410	5.4
10	MS-91	LQOS3	23	0.04	60	0.0619	0.7055	7.5
11 *	MS-92	LQOS3	80	0	23	0.0912	0.7048	8.2
12 *	MS-96	LQOS3	80	0.04	23	0.1180	0.6478	9.1
13	MS-92	LQOS3	80	0	23	0.6487	5.0135	9.2
14	MS-96	LQOS3	80	0.04	23	0.8962	4.9187	9.6
15	MS-96	LQOS3	80	0.04	23	0.1250	0.6861	9.0
16	MS-96	LQOS3	80	0.04	23	0.9046	4.9651	9.2
17	MS-92	LQOS3	80	0	60	0.0904	0.6983	8.4
18	MS-96	LQOS3	80	0.04	60	0.1184	0.6496	8.6
19	MS-92	LQOS3	80	0	60	0.6494	5.0182	9.0
20	MS-96	LQOS3	80	0.04	60	0.9077	4.9818	9.7
21 *	MS-92	LQOS3	80	0	23	0.6504	5.0259	9.2
22	MS-100	AQOS2	80	0	23	0.3221	0.7114	9.5
23	MS-100	AQOS2	80	0	23	2.3155	5.1138	9.7
24	MS-100	AQOS2	80	0	60	0.3189	0.7043	9.3
25	MS-100	AQOS2	80	0	60	2.2789	5.0330	9.8
26 *	MS-116	AQOS2	80	0	23	0.3016	0.7010	9.5
27	MS-116	AQOS2	80	0	60	0.2984	0.6934	9.3
28 *	MS-116	AQOS2	80	0	23	2.1725	5.0488	10.1
29 *	MS-116	AQOS2	80	0	60	2.1614	5.0230	10.0

Table A.3 Cont'd

	Oil Volume, cm³								Rag Volume, cm³							
Trial Number	500 RPM	1000 RPM	1500 RPM	2000 RPM	2500 RPM	3000 RPM	3500 RPM	4000 RPM	500 RPM	1000 RPM	1500 RPM	2000 RPM	2500 RPM	3000 RPM	3500 RPM	4000 RPM
1	0.0	0.1	0.2	0.4	0.4	0.5	0.6	0.6	0.7	0.6	0.5	0.3	0.3	0.2	0.1	0.1
2	0.3	0.3	0.3	0.5	0.6	0.7	1.0	1.1	1.2	0.9	0.7	0.7	0.6	0.5	0.2	0.1
3 *	0.5	0.7	1.0	1.8	2.3	2.5	2.7	2.9	4.2	3.3	2.5	1.7	1.2	1.0	0.5	0.3
4 *	0.3	0.4	1.3	2.7	3.3	3.7	0.0	0.0	4.5	3.9	3.0	1.1	0.5	0.1	0.0	0.0
5	0.0	0.0	0.0	0.0	0.0	0.0	0.4	0.4	0.2	2.2	1.4	1.2	1.2	1.1	0.7	0.7
6	0.0	0.0	0.0	0.0	0.0	0.0	0.7	0.7	0.6	2.2	1.7	1.5	1.5	1.4	0.7	0.7
7 *	0.5	0.8	1.7	1.9	1.9	1.9	2.4	2.4	4.5	3.4	1.4	1.0	1.0	1.0	0.5	0.3
8	0.8	1.2	2.5	2.5	2.7	3.0	2.9	2.9	4.0	2.8	0.8	0.8	0.6	0.3	0.2	0.2
9	0.0	0.0	0.2	0.2	0.2	0.2	0.2	0.2	0.7	0.4	0.2	0.2	0.2	0.2	0.2	0.2
10	0.0	0.1	0.4	0.5	0.5	0.5	0.5	0.5	0.9	0.6	0.3	0.3	0.3	0.3	0.3	0.3
11 *	0.4	0.4	0.7	0.7	0.8	0.8	0.9	1.2	2.3	2.0	1.2	1.2	0.9	0.9	0.6	0.3
12 *	0.3	0.9	1.6	1.9	0.0	0.0	0.0	0.0	3.3	1.4	0.7	0.4	0.0	0.0	0.0	0.0
13	3.4	3.4	4.4	4.6	4.6	4.8	4.9	5.0	3.6	1.7	0.8	0.5	0.4	0.1	0.0	0.0
14	5.4	5.6	5.6	5.6	5.6	5.9	5.9	6.0	0.0	0.0	0.0	0.0	0.0	0.0	0.0	0.0
15	0.3	0.7	1.4	1.4	1.7	2.0	2.4	2.5	1.7	1.0	0.6	0.6	0.6	0.5	0.1	0.0
16	5.4	5.4	5.4	5.4	5.4	5.4	5.6	5.7	0.0	0.0	0.0	0.0	0.0	0.0	0.0	0.0
17	0.4	0.4	0.4	0.4	0.7	0.8	0.9	0.9	0.7	0.7	0.7	0.7	0.6	0.6	0.5	0.5
18	0.8	0.8	0.8	0.8	0.8	1.1	1.6	2.1	1.1	1.1	1.1	1.1	1.1	1.1	0.8	0.3
19	5.0	4.7	4.7	4.7	4.7	4.7	4.6	4.6	0.0	0.0	0.0	0.0	0.0	0.0	0.0	0.0
20	5.7	5.7	5.7	5.7	5.6	5.6	5.6	5.6	0.0	0.0	0.0	0.0	0.0	0.0	0.0	0.0
21 *	2.9	2.9	2.9	4.2	4.5	4.7	4.7	4.7	4.3	2.8	2.6	1.2	0.9	0.2	0.2	0.2
22	6.0	6.0	6.0	6.0	6.0	6.2	6.3	6.3	0.0	0.0	0.0	0.0	0.0	0.0	0.0	0.0
23	7.5	7.9	8.2	8.2	8.2	8.2	8.4	8.4	0.0	0.0	0.0	0.0	0.0	0.0	0.0	0.0
24	5.8	5.8	5.8	5.8	5.8	5.8	5.8	5.8	0.0	0.0	0.0	0.0	0.0	0.0	0.0	0.0
25	8.0	8.2	8.2	8.3	8.3	8.3	8.3	8.3	0.0	0.0	0.0	0.0	0.0	0.0	0.0	0.0
26 *	3.5	3.5	3.5	3.5	3.5	3.5	3.5	3.5	0.5	0.5	0.0	0.0	0.0	0.0	0.0	0.0
27	3.6	3.6	3.6	3.6	3.6	3.6	3.6	3.6	1.2	0.0	0.0	0.0	0.0	0.0	0.0	0.0
28 *	6.6	6.6	7.1	7.1	7.1	7.1	7.3	7.3	1.5	1.5	0.5	0.0	0.0	0.0	0.0	0.0
29 *	6.0	7.0	7.0	7.0	7.2	7.2	7.2	7.2	2.0	1.0	0.5	0.2	0.0	0.0	0.0	0.0

Table A.3 Cont'd

Trial Number	Water Volume, cm³								Sediment Volume, cm³							
	500 RPM	1000 RPM	1500 RPM	2000 RPM	2500 RPM	3000 RPM	3500 RPM	4000 RPM	500 RPM	1000 RPM	1500 RPM	2000 RPM	2500 RPM	3000 RPM	3500 RPM	4000 RPM
1	1.7	2.2	2.7	2.7	3.0	3.0	3.2	3.7	5.0	4.5	4.0	4.0	3.7	3.7	3.5	3.0
2	3.2	3.5	4.0	4.3	4.5	5.0	5.0	5.0	4.0	4.0	3.7	3.2	3.0	2.5	2.5	2.5
3 *	1.3	2.0	2.5	2.7	2.7	2.7	2.8	2.6	2.0	2.0	2.0	1.8	1.8	1.8	2.0	2.2
4 *	2.0	2.5	2.5	2.7	2.7	2.7	0.0	0.0	1.5	1.5	1.5	1.8	1.8	1.8	0.0	0.0
5	2.8	1.6	3.1	3.6	3.6	3.7	3.9	3.9	4.5	4.0	3.3	3.0	3.0	3.0	2.8	2.8
6	2.1	1.7	3.0	3.4	3.7	3.8	3.9	3.9	5.2	4.3	3.5	3.3	3.0	3.0	2.9	2.9
7 *	1.1	1.8	2.3	2.5	2.5	2.5	2.5	3.2	1.9	1.9	2.5	2.5	2.5	2.5	2.5	1.8
8	0.8	2.0	2.2	2.2	2.2	2.2	2.6	2.8	2.4	2.0	2.5	2.5	2.5	2.5	2.2	2.0
9	1.9	2.5	2.5	2.8	3.0	3.2	3.3	3.3	2.8	2.5	2.5	2.2	2.0	1.8	1.7	1.7
10	1.6	2.2	2.7	3.2	3.4	3.7	3.9	3.9	5.0	4.5	4.0	3.5	3.3	3.0	2.8	2.8
11 *	2.0	2.3	2.8	2.8	3.0	3.5	3.5	3.5	3.5	3.5	3.5	3.5	3.5	3.0	3.2	3.2
12 *	3.5	3.8	4.3	4.3	0.0	0.0	0.0	0.0	2.0	3.0	2.5	2.5	0.0	0.0	0.0	0.0
13	0.3	1.7	1.7	2.2	2.2	2.3	2.3	2.7	1.9	2.4	2.3	1.9	2.0	2.0	2.0	1.5
14	1.9	1.9	2.1	2.1	2.3	2.3	2.3	2.4	2.3	2.1	1.9	1.9	1.7	1.4	1.4	1.2
15	4.0	4.0	4.0	4.0	4.0	4.0	4.0	4.3	3.0	3.3	3.0	3.0	2.7	2.5	2.5	2.2
16	1.0	1.5	1.8	1.8	1.8	1.8	1.8	2.0	2.8	2.3	2.0	2.0	2.0	2.0	1.8	1.5
17	2.0	2.0	2.6	3.0	3.5	3.5	3.5	3.5	5.3	5.3	4.7	4.3	3.6	3.5	3.5	3.5
18	1.0	1.7	2.5	2.7	3.2	3.2	3.2	3.2	5.7	5.0	4.2	4.0	3.5	3.2	3.0	3.0
19	0.7	1.3	1.8	1.8	1.8	2.3	2.4	2.4	3.3	3.0	2.5	2.5	2.5	2.0	2.0	2.0
20	1.0	1.2	1.7	1.7	1.8	2.1	2.1	2.1	3.0	2.8	2.3	2.3	2.3	2.0	2.0	2.0
21 *	0.5	1.3	1.5	1.6	1.8	2.3	2.3	2.3	1.5	2.2	2.2	2.2	2.0	2.0	2.0	2.0
22	0.0	0.0	0.0	1.0	1.0	1.0	0.9	1.2	3.5	3.5	3.5	2.5	2.5	2.3	2.3	2.0
23	0.0	0.0	0.0	0.0	0.0	0.0	0.1	0.1	2.2	1.8	1.5	1.5	1.5	1.5	1.2	1.2
24	0.0	0.0	1.0	1.0	1.0	1.0	1.4	1.4	3.5	3.5	2.5	2.5	2.5	2.5	2.1	2.1
25	0.0	0.0	0.0	0.0	0.0	0.0	0.5	0.5	1.8	1.6	1.6	1.5	1.5	1.5	1.0	1.0
26 *	3.0	3.3	4.0	4.2	4.3	4.3	4.5	4.5	2.5	2.2	2.0	1.8	1.7	1.7	1.5	1.5
27	3.5	4.2	4.2	4.2	4.2	4.2	4.2	4.2	1.0	1.5	1.5	1.5	1.5	1.5	1.5	1.5
28 *	1.5	1.5	1.8	2.3	2.3	2.3	2.3	2.3	0.5	0.5	0.7	0.7	0.7	0.7	0.5	0.5
29 *	1.5	1.5	1.9	1.9	1.9	1.9	1.9	1.9	0.5	0.5	0.6	0.9	0.9	0.9	0.9	0.9

Appendix B

Effect of Height of Water-Oil Interface in Step Wise Tests

During the initial experiments conducted on LQOS3 froth and AQOS2 froth, a significant difference between these two samples was observed. Distinct rag layers formed from the LQOS3 froth, while no rag layer was observed for the AQOS2 froth in any of the experiments. In fact, as explained below, rag layers were forming but could not be observed because the water-oil contact was in the sediment layer.

B.1 Removing Free Water from LQOS3 Froth

In this experiment before diluting the LQOS3 froth and doing the usual stepwise centrifuge test, the froth sample was centrifuged for 5 minutes at 4000 rpm and the free water was decanted from the test tube. Figure B.1 compares the result of this experiment (right hand side) with the average of two normal cases which can be considered the base case. In all cases LQOS3 froth was diluted with n-heptane to the solvent-to-bitumen ratio beyond the required for the onset of asphaltene precipitation. While at a first glance of the data shown in Figure B.1, it might be concluded that removing free water from froth has prevented the rag formation, it is also possible that the rag layer has settled on top of the sediment.

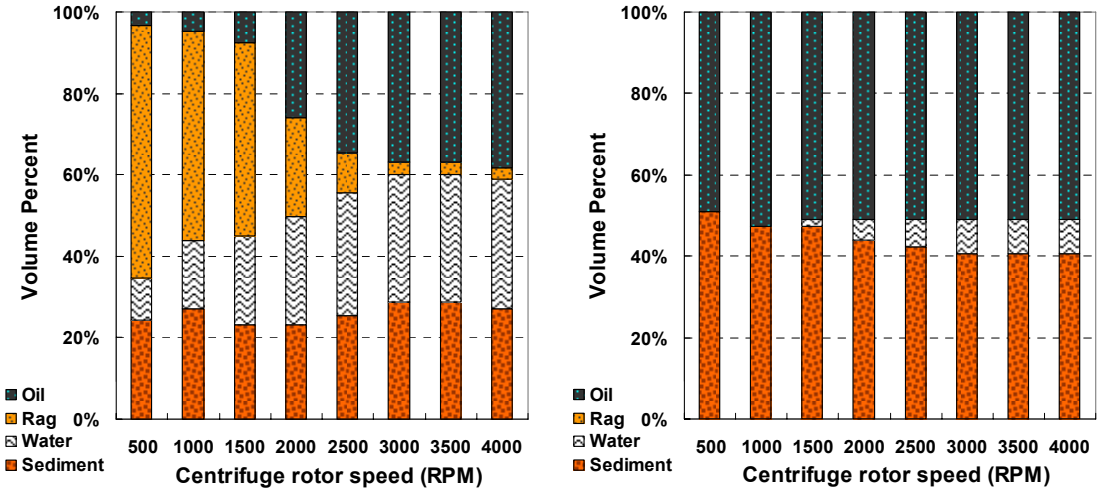

Figure B.1 Comparing the rag formation in LQOS3 froth diluted with n-heptane (left) with the case of removing the free water from froth sample before its dilution (right). Data in the left plot is the average of the two experiments. All the experiments were conducted at 23°C and Solvent/Bitumen = 2.66, g/g.

B.2 Adding Free Water to AQOS2 Froth

Removing free water from LQOS3 froth before its dilution apparently led to a pattern of no rag formation. To investigate this effect more, free water was added to a sample of AQOS2 froth to test the possibility of rag formation. Interestingly, although as stated previously, all the preliminary experiments of AQOS2 froth showed no rag layer formation in this sample, however the addition of free water led to rag formation in virtually all the cases.

In this experiment, process water obtained from bitumen extraction of the same oil sand was added to undiluted froth. The mixture was dispersed in a shaker table for 5 minutes. Water was added in the same water-to-froth ratio of LQOS3 froth to make the overall froth composition similar to the LQOS3 sample. After this step, the stepwise centrifuge test was conducted on the sample. Figure B.2 shows that, after adding free water to this sample, a rag layer could be observed.

This experiment shows that, if the top of the free water in the test tube lies below the top of the sediment, any rag layer that forms will settle to the upper part of the sediment layer. In such a case the formation of rag might not be observable. Adding water to the test tube acts allows the rag layer to be detected.

In all the rag layer related experiments conducted on the AQOS3 froth, water was added to the test tube to make the rag layer observable.

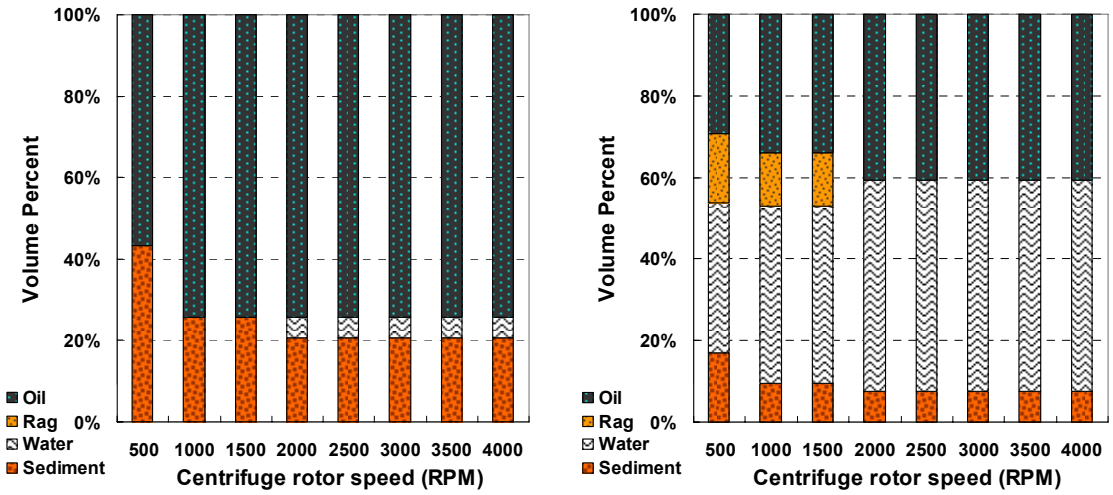

Figure B.2 Comparing the rag formation in AQOS2 froth diluted with n-heptane (left) with the case of adding free water to froth sample before its dilution (right). All the experiments were conducted at 23°C and Solvent/Bitumen = 2.66, g/g.

Although adding free water to a froth sample seems to be a good method of observing the rag formation, it produces several questions too. For example the process water that was used in the previous experiment contained an abundance of fine solids and chemical surfactants. To better understand the effect of free water on rag formation, the following questions needed to be answered:

- Is the rag formation in the previous experiment just the result of adding free water or it is related to the presence of fine solids and surfactants in the process water?
- Adding water before or after froth dilution might affect the froth quality. Does the sequence of adding free water to undiluted froth change the rag formation?

- Does the added free water volume change the rag volume?

The following experiments were conducted to answer these questions.

B.3 Effect of Fine Solids Contents of Process Water on Rag Formation

To check if fine solids in process water can contribute to the rag formation in AQOS2, the previous experiment was repeated using the same process water filtered to 0.1 μm. The process water was centrifuged first at 6000 rpm for 5 minutes. A sediment and an overlying free water layer were formed in the test tube. The free water layer was decanted and filtered using a Stainless steel pressure filter holder, Model 302400 by Advantec MFS, Inc., USA. The filtration was under 40 psi air pressure and up to 0.1 μm. The filtering process repeated at least twice to ensure the effective removing of fine solids greater than 0.1 μm.

Adding the filtered process water to AQOS2 froth resulted in formation of the same volumes of rag in the test tube. Therefore, the formation of the rag layer by adding process water to the AQOS2 froth does not relate to the fine solids content of the process water.

B.4 Effect of RO Water Versus Process Water in Rag Formation

The previous experiment showed that rag formed by adding process water to AQOS2 froth does not relate to fine solids content of it. However, the effect of chemical surfactants present in the process water could not be determined from this experiment.

Using the same procedure of adding free water to AQOS2 froth, RO water was used instead of process water to observe the possible difference in rag formation. No difference in rag formation or volume was observed by using RO water instead of process water.

B.5 Effect of Sequence of Adding Free Water in Rag Formation

Two identical samples of AQOS2 froth were used in this experiment. RO water was mixed with froth before its dilution with the solvent, and in the other sample RO water was added to the test tube after the dilution. The rag layer volumes from the two cases were almost identical.

B.6 Effect of Free Water Volume on Rag Volume

In all the experiments described so far in this section, water was added to AQOS2 froth samples in the proper weight to increase the water weight percent of AQOS2 froth to its value for LQOS3 froth (24 and 59 wt% respectively). In order to understand the possible effect of amount of water added to the froth on rag volume, several different weight percents of water were added to the AQOS2 froth and the volumes of the rag layers were compared. Figure B.3 shows the results of these experiments. Although the data in this plot are scattered, the figure shows that once enough water is added so that water-oil interface lies above the sediment (approximately 0.4 wt% water), the rag layer can be observed and the rag layer volume pre volume of froth is independent of the amount of added water.

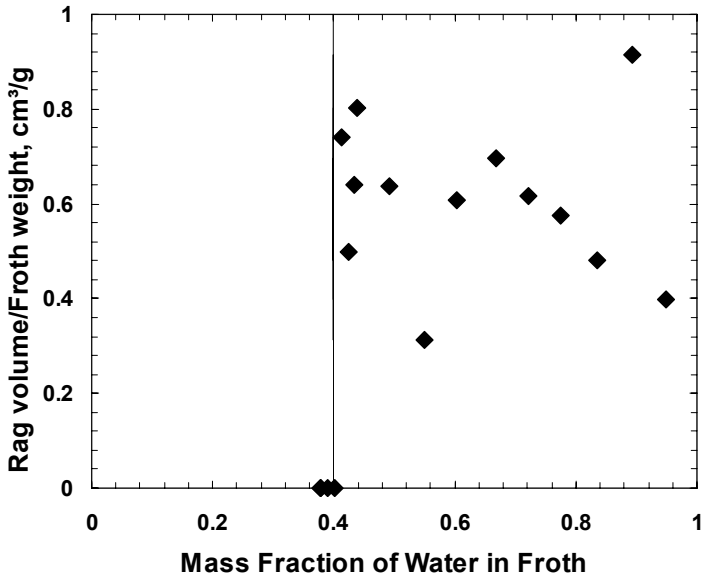

Figure B.3 Relation between the mass fractions of water added to AQOS2 froth prior to dilution and the volume of the rag layer formed in the test tube.

In summary, there are two interesting results from these experiments:

- To observe rag, there must have enough water in froth to form a water/oil interface above the sediment layer.
- The only effect of adding RO water, process water or filtered process water is to raise the water/oil interface and make the rag observable. It does not increase the rag volume.

Appendix C

Variability Analysis

The confidence intervals of the data were calculated from the mean, standard deviation and *t-distribution* for each set of measurements. In the first step the mean is calculated by:

$$\bar{x} = \frac{1}{n}\sum_{i=1}^{n} x_i \qquad \textbf{(C.1)}$$

where n is the number of repeat measurements and x_i is a measured value. The standard deviation is calculated from the following relation:

$$s = \sqrt{\frac{1}{n-1}\sum_{i=1}^{n}(x_i - \bar{x})^2} \qquad \textbf{(C.2)}$$

In the second step, the critical value of the *t-distribution* is calculated. The *t-distribution* is the suitable statistical distribution for determination of the confidence interval based on the standard deviation. The confidence interval is calculated from:

$$\bar{x} - t_{(\alpha/2,v)}\frac{s}{\sqrt{n}} \le \mu \le \bar{x} + t_{(\alpha/2,v)}\frac{s}{\sqrt{n}} \qquad \textbf{(C.3)}$$

where μ is the correct mean, $v = n-1$ and $\alpha = 1-(\%conf/100)$; for example for 90% confidence, $\alpha/2 = 0.05$ and for 5 measurements $n = 5$ and $v = 4$. Therefore, from table C.1 $t_{(\alpha/2=0.05,v=4)} = 2.13$. This is used with equation C.3 to calculate the confidence interval of the 5 measurements.

Table C.1 Percentile values for student *t-distribution* (Dean, J.A., 1999).

v	$t_{0.995}$	$t_{0.99}$	$t_{0.975}$	$t_{0.95}$	$t_{0.90}$	$t_{0.80}$	$t_{0.75}$	$t_{0.70}$	$t_{0.60}$	$t_{0.55}$
1	63.66	31.82	12.71	6.31	3.08	1.376	1	0.727	0.325	0.158
2	9.92	6.96	4.3	2.92	1.89	1.061	0.816	0.617	0.289	0.142
3	5.84	4.54	3.18	2.35	1.64	0.978	0.765	0.584	0.277	0.137
4	4.6	3.75	2.78	2.13	1.53	0.941	0.741	0.569	0.271	0.134
5	4.03	3.36	2.57	2.02	1.48	0.92	0.727	0.559	0.267	0.132
6	3.71	3.14	2.45	1.94	1.44	0.906	0.718	0.553	0.265	0.131
7	3.5	3	2.36	1.9	1.42	0.896	0.711	0.549	0.263	0.13
8	3.36	2.9	2.31	1.86	1.4	0.889	0.706	0.546	0.262	0.13
9	3.25	2.82	2.26	1.83	1.38	0.883	0.703	0.543	0.261	0.129
10	3.17	2.76	2.23	1.81	1.37	0.879	0.7	0.542	0.26	0.129
11	3.11	2.72	2.2	1.8	1.36	0.876	0.697	0.54	0.26	0.129
12	3.06	2.68	2.18	1.78	1.36	0.873	0.695	0.539	0.259	0.128
13	3.01	2.65	2.16	1.77	1.35	0.87	0.694	0.538	0.259	0.128
14	2.98	2.62	2.14	1.76	1.34	0.868	0.692	0.537	0.258	0.128
15	2.95	2.6	2.13	1.75	1.34	0.866	0.691	0.536	0.258	0.128
16	2.92	2.58	2.12	1.75	1.34	0.865	0.69	0.535	0.258	0.128
17	2.9	2.57	2.11	1.74	1.33	0.863	0.689	0.534	0.257	0.128
18	2.88	2.55	2.1	1.73	1.33	0.862	0.688	0.534	0.257	0.127
19	2.86	2.54	2.09	1.73	1.33	0.861	0.688	0.533	0.257	0.127
20	2.84	2.53	2.09	1.72	1.32	0.86	0.687	0.533	0.257	0.127
21	2.83	2.52	2.08	1.72	1.32	0.859	0.686	0.532	0.257	0.127
22	2.82	2.51	2.07	1.72	1.32	0.858	0.686	0.532	0.256	0.127
23	2.81	2.5	2.07	1.71	1.32	0.858	0.685	0.532	0.256	0.127
24	2.8	2.49	2.06	1.71	1.32	0.857	0.685	0.531	0.256	0.127
25	2.79	2.48	2.06	1.71	1.32	0.856	0.684	0.531	0.256	0.127
26	2.78	2.48	2.06	1.71	1.32	0.856	0.684	0.531	0.256	0.127
27	2.77	2.47	2.05	1.7	1.31	0.855	0.684	0.531	0.256	0.127
28	2.76	2.47	2.05	1.7	1.31	0.855	0.683	0.53	0.256	0.127
29	2.76	2.46	2.04	1.7	1.31	0.854	0.683	0.53	0.256	0.127
30	2.75	2.46	2.04	1.7	1.31	0.854	0.683	0.53	0.256	0.127
40	2.7	2.42	2.02	1.68	1.3	0.851	0.681	0.529	0.255	0.126
60	2.66	2.39	2	1.67	1.3	0.848	0.679	0.527	0.254	0.126
120	2.62	2.36	2.98	1.66	1.29	0.845	0.677	0.526	0.254	0.126
∞	2.58	2.33	1.96	1.645	1.28	0.842	0.674	0.524	0.253	0.126

C.1 Data Averaging

While the repeatability of the experiments was reasonable for a single froth sample, the stepwise centrifuge tests data which is used in this study were scattered when different froth samples (and sometimes different conditions) were compared. To obtain meaningful trends, the average of the subsets of the data was used in most cases. Figure C.1 shows the scatter for the one subset of data used for Figure 7.12.

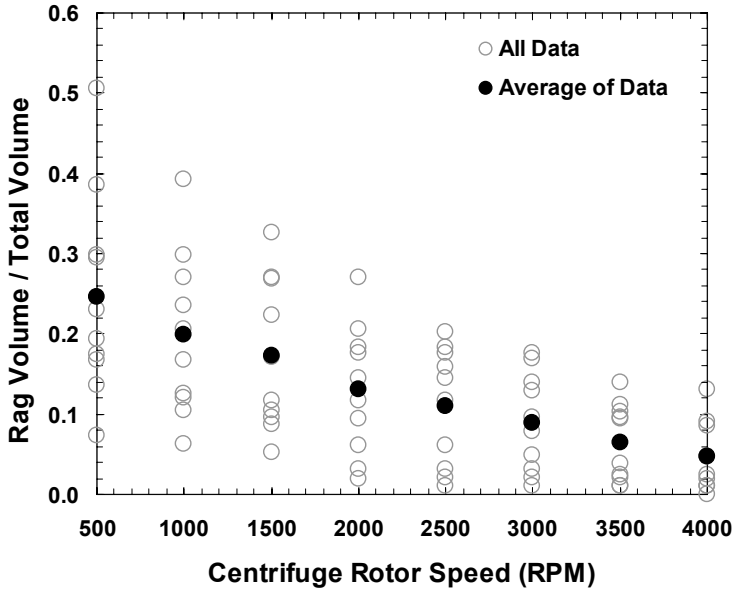

Figure C.1 Data scatter for rag volume in n-heptane. The 10 trials of data shown here are all below the asphaltene precipitation point.

C.2 Error Analysis for the Stepwise Centrifuge Test Data

The error for the stepwise centrifuge data was calculated as described above. As an example, the errors for the cases of Figures 7.11 to 7.13 are shown in Tables C.2 to C.13.

Table C.2 Error analysis for the data of rag volume over total volume for heptane diluted LQOS3 froth below the onset of asphaltene precipitation (90% confidence interval).

RPM	# data	data (avg)	S.D.	±
500	10	0.246	0.128	0.07
1000	10	0.198	0.102	0.06
1500	10	0.172	0.094	0.05
2000	10	0.130	0.081	0.05
2500	10	0.111	0.073	0.04
3000	10	0.090	0.062	0.04
3500	10	0.065	0.049	0.03
4000	9	0.046	0.046	0.03
		Average =	0.079	

Table C.3 Error analysis for the data of rag volume over total volume for heptane diluted LQOS3 froth above the onset of asphaltene precipitation (90% confidence interval).

RPM	# data	data (avg)	S.D.	±
500	10	0.470	0.156	0.09
1000	10	0.328	0.166	0.10
1500	10	0.270	0.168	0.10
2000	10	0.197	0.125	0.07
2500	10	0.127	0.118	0.07
3000	10	0.090	0.112	0.06
3500	9	0.063	0.080	0.05
4000	8	0.050	0.049	0.03
		Average =	0.122	

Table C.4 Error analysis for the data of rag volume over froth volume for heptane diluted LQOS3 froth below the onset of asphaltene precipitation (90% confidence interval).

RPM	# data	data (avg)	S.D.	±
500	10	0.258	0.140	0.08
1000	10	0.208	0.112	0.06
1500	10	0.180	0.102	0.06
2000	10	0.137	0.087	0.05
2500	10	0.116	0.079	0.05
3000	10	0.094	0.066	0.04
3500	10	0.068	0.052	0.03
4000	9	0.049	0.048	0.03
		Average =	0.086	

Table C.5 Error analysis for the data of rag volume over froth volume for heptane diluted LQOS3 froth above the onset of asphaltene precipitation (90% confidence interval).

RPM	# data	data (avg)	S.D.	±
500	10	0.552	0.337	0.20
1000	10	0.365	0.274	0.16
1500	10	0.294	0.261	0.15
2000	10	0.193	0.163	0.09
2500	10	0.097	0.087	0.05
3000	10	0.054	0.070	0.04
3500	9	0.037	0.047	0.03
4000	8	0.031	0.031	0.02
		Average =	0.159	

Table C.6 Error analysis for the data of rag volume over total volume for heptol 80/20 diluted LQOS3 froth below the onset of asphaltene precipitation (90% confidence interval).

RPM	# data	data (avg)	S.D.	±
500	11	0.148	0.097	0.05
1000	11	0.147	0.082	0.04
1500	11	0.101	0.056	0.03
2000	11	0.091	0.053	0.03
2500	10	0.090	0.051	0.03
3000	10	0.084	0.050	0.03
3500	10	0.053	0.032	0.02
4000	10	0.041	0.030	0.02
		Average =	0.056	

Table C.7 Error analysis for the data of rag volume over total volume, LQOS3, Heptol 80/20, above the onset of asphaltene precipitation and for 90% Confidence Interval.

RPM	# data	data (avg)	S.D.	±
500	10	0.299	0.261	0.15
1000	10	0.215	0.201	0.12
1500	10	0.132	0.142	0.08
2000	10	0.076	0.076	0.04
2500	10	0.055	0.056	0.03
3000	10	0.033	0.050	0.03
3500	9	0.019	0.027	0.02
4000	9	0.014	0.017	0.01
		Average =	0.104	

Table C.8 Error analysis for the data of rag volume over froth volume for heptol 80/20 diluted LQOS3 froth below the onset of asphaltene precipitation (90% confidence interval).

RPM	# data	data (avg)	S.D.	±
500	11	0.160	0.105	0.06
1000	11	0.159	0.088	0.05
1500	11	0.110	0.062	0.03
2000	11	0.099	0.057	0.03
2500	10	0.098	0.057	0.03
3000	10	0.091	0.055	0.03
3500	10	0.057	0.034	0.02
4000	10	0.044	0.034	0.02
		Average =	0.062	

Table C.9 Error analysis for the data of rag volume over froth volume for heptol 80/20 diluted LQOS3 froth above the onset of asphaltene precipitation (90% confidence interval).

RPM	# data	data (avg)	S.D.	±
500	10	0.510	0.442	0.26
1000	10	0.363	0.332	0.19
1500	10	0.225	0.242	0.14
2000	10	0.128	0.127	0.07
2500	10	0.094	0.095	0.06
3000	10	0.056	0.082	0.05
3500	9	0.032	0.044	0.03
4000	9	0.023	0.028	0.02
		Average =	0.174	

Table C.10 Error analysis for the data of rag volume over total volume for toluene diluted LQOS3 froth at low dilution ratios (90% confidence interval).

RPM	# data	data (avg)	S.D.	±
500	10	0.432	0.281	0.16
1000	10	0.329	0.165	0.10
1500	10	0.288	0.154	0.09
2000	10	0.230	0.149	0.09
2500	10	0.168	0.109	0.06
3000	10	0.119	0.075	0.04
3500	10	0.088	0.065	0.04
4000	10	0.088	0.080	0.05
		Average =	0.135	

Table C.11 Error analysis for the data of rag volume over total volume for toluene diluted LQOS3 froth at high dilution ratios (90% confidence interval).

RPM	# data	data (avg)	S.D.	±
500	8	0.493	0.131	0.09
1000	8	0.402	0.166	0.11
1500	8	0.241	0.155	0.10
2000	8	0.187	0.161	0.11
2500	8	0.119	0.095	0.06
3000	8	0.093	0.096	0.06
3500	8	0.075	0.072	0.05
4000	8	0.071	0.069	0.05
		Average =	0.118	

Table C.12 Error analysis for the data of rag volume over froth volume for toluene diluted LQOS3 froth at low dilution ratios (90% confidence interval).

RPM	# data	data (avg)	S.D.	±
500	10	0.722	0.448	0.26
1000	10	0.549	0.263	0.15
1500	10	0.479	0.243	0.14
2000	10	0.382	0.232	0.13
2500	10	0.279	0.171	0.10
3000	10	0.197	0.116	0.07
3500	10	0.147	0.103	0.06
4000	10	0.147	0.127	0.07
		Average =	0.213	

Table C.13 Error analysis for the data of rag volume over froth volume for toluene diluted LQOS3 froth at high dilution ratios (90% confidence interval).

RPM	# data	data (avg)	S.D.	±
500	8	1.003	0.300	0.20
1000	8	0.814	0.362	0.24
1500	8	0.508	0.374	0.25
2000	8	0.402	0.387	0.26
2500	8	0.252	0.229	0.15
3000	8	0.203	0.229	0.15
3500	8	0.163	0.173	0.12
4000	8	0.154	0.165	0.11
		Average =	0.277	